# REPUBLIC OF TURKEY YILDIZ TECHNICAL UNIVERSITY GRADUATE SCHOOL OF NATURAL AND APPLIED SCIENCES

# MODELING AND CHARACTERIZATION OF ORGANIC LIGHT EMITTING DIODES FOR AUTOMOTIVE LIGHTING APPLICATIONS

#### Arda GÜNEY

DOCTOR OF PHILOSOPHY THESIS

Department of Electronics and Communications Engineering

Program of Electronics

Advisor Assoc. Prof. Dr. Nihan KAHRAMAN

Co-Advisor
Assoc. Prof. Dr. Mustafa Berke YELTEN

December, 2020

# REPUBLIC OF TURKEY YILDIZ TECHNICAL UNIVERSITY GRADUATE SCHOOL OF NATURAL AND APPLIED SCIENCES

## MODELING AND CHARACTERIZATION OF ORGANIC LIGHT EMITTING DIODES FOR AUTOMOTIVE LIGHTING APPLICATIONS

A thesis submitted by Arda GÜNEY in partial fulfillment of the requirements for the degree of **DOCTOR OF PHILOSOPHY** is approved by the committee on 02.12.2020 in Department of Electronics and Communications Engineering, Program of Electronics.

Assoc. Prof. Dr. Nihan KAHRAMAN Yildiz Technical University Advisor Assoc. Prof. Dr. Mustafa Berke YELTEN Istanbul Technical University Co-Advisor

# Assoc. Prof. Dr. Nihan KAHRAMAN, Advisor Yildiz Technical University Prof. Dr. Tülay YILDIRIM, Member Yildiz Technical University Prof. Dr. Serdar ÖZOĞUZ, Member İstanbul Technical University Dr. Sadiye Nergis TURAL POLAT, Member Yildiz Technical University Assoc. Prof. Dr. Serkan TOPALOĞLU, Member Yeditepe University

I hereby declare that I have obtained the required legal permissions during data collection and exploitation procedures, that I have made the in-text citations and cited the references properly, that I haven't falsified and/or fabricated research data and results of the study and that I have abided by the principles of the scientific research and ethics during my Thesis Study under the title of Modeling and Characterization of Organic Light Emitting Diodes for Automotive Lighting Applications supervised by my supervisor, Assoc. Prof. Dr. Nihan KAHRAMAN. In the case of a discovery of false statement, I am to acknowledge any legal consequence.

Arda GÜNEY

Signature



#### ACKNOWLEDGEMENTS

First of all, I would like to thank my advisor Assoc. Prof. Dr. Nihan KAHRAMAN for her personal kindness and scientific enthusiasm that has always been motivating me. She has mentored and molded me both consciously and unconsciously with her supervision, advice, and guidance to strive for deeper understanding. I would also like to thank Assoc. Prof. Dr. Mustafa Berke YELTEN who is my co-advisor for his valuable insight and advice in this work.

I would like to express my sincere thanks to the members of my dissertation committee, Prof. Dr. Tülay YILDIRIM, and Prof. Dr. Serdar ÖZOĞUZ not only for their time, but for their brilliant comments and suggestions. I also would like to thank the members of the examining committee, Dr. Sadiye Nergis TURAL POLAT, and Assoc. Prof. Dr. Serkan TOPALOĞLU for letting my defense be an enjoyable moment. I am truly thankful to Assoc. Prof. Dr. Onur FERHANOĞLU from the Electro-Optic Devices Laboratory (EDL) at Istanbul Technical University. I appreciate all his contributions of time, ideas, extraordinary understanding and support in various ways throughout during initial phase of the experimental research at EDL.

I would like to thank my brother Mert GÜNEY and former colleagues Erhan BAĞBANCI, and Muhammet ÖZCAN from VLE Elektronik, for their support in the mechanical design phase of the OLED holder and heat-sinks. I would also like to convey thanks to Emre USTA, and Köksal AYDIN from Odelo Slovenija for great collaboration and providing us the OLED samples. I would like to thank my colleague Volkan FENERCİOĞLU from Tübitak and Sadık İLİK from Istanbul Technical University for valuable feedback and guidance during the measurement phase of the experiments. I am also thankful to Ali Rıza YILMAZ for his kind friendship and support during the writing periods of the thesis in LaTex.

I would like to express my deepest gratitude to my mother Ayşe GÜNEY, my father Yıldırım GÜNEY, for all their unconditional love, faith, and constant support. Last but not least, I would like to thank my wife Arzem GÜNEY who is always supporting me all the years.

Arda GÜNEY

#### TABLE OF CONTENTS

LI	ST O	F SYMB	COLS	vii
LI	ST O	F ABBR	EVIATIONS	X
LI	ST O	F FIGUI	RES	xii
LI	ST O	F TABLI	ES	xiv
Αŀ	3STR	ACT		XV
Ö	ZET			xvii
1	INT	RODUC	CTION	1
	1.1	Literat	ture Review	4
	1.2	Object	rive of the Thesis	12
	1.3	Hypot	hesis	12
2	STA	ГЕ-ОГ-Т	THE-ART ON OLED AND AUTOMOTIVE LIGHTING	14
	2.1	Organ	ic Semiconductors	15
		2.1.1	Basic Structure and Operation Principles of OLEDs	18
		2.1.2	Energy Levels and Quantum Efficiency	20
		2.1.3	Degradation Mechanisms of OLEDs	22
		2.1.4	Comparison Between LEDs and OLEDs	23
	2.2	Auton	notive Exterior Lighting	24
		2.2.1	Automotive Requirements	25
		2.2.2	OLEDs in Automotive Lighting	27
		2.2.3	Driving Methods: Current/ Voltage Mode	29
3	EXP	ERIME	NTAL MEASUREMENTS	31
	3.1		LED Sample	31
	3.2	Test S	etup	32
4	CHA		ERIZATION AND MODELLING OF THE OLED DEVICE	35
	4.1		ical and Optical Characterization	
	4.2	The Pi	roposed Model	42

	4.3	Parameter Extraction and Modeling Results	43
	4.4	Application Circuit: OLED Based Stop/Tail Light	51
5	EFF	ECTS OF THE ELECTRICAL STRESS	57
	5.1	Aging on Electrical and Optical Characteristics on the OLED	57
6	RES	ULTS AND DISCUSSION	62
RI	EFERI	ENCES	66
ΡĮ	JBLIC	ATIONS FROM THE THESIS	75

#### LIST OF SYMBOLS

 $V_{AC}$  AC Value of The Voltage Signal

A Active Area of The Device

 $\beta$  Aging Parameter

*T<sub>a</sub>* Ambient Temperature

*IBV* Breakdown Current

BV Breakdown Voltage

 $V_{bi}$  Built-in Voltage

 $au_0$  Characteristics Time

 $\gamma$  Charge Carrier Balance

 $Z_{OLED}$  Complex Impedance of The OLED

 $L_c$  Critical Size

J Current Density

 $V_{DC}$  DC Value of The Voltage Signal

 $C_D$  Diffusion Capacitance

 $P_D$  Dissipated Electrical Power

*P<sub>h</sub>* Dissipated Heat Power

 $\lambda_{dom}$  Dominant Wavelength

 $R_{ITO}$  Electrode Resistance

 $\eta_{ext}$  External Quantum Efficiency

FC Forward Capacitance Coefficient

*TT* Forward Transit Time

 $C_{geo}$  Geometric Capacitance

n Ideality Factor

 $L_0$  Initial Luminance

 $\eta_{int}$  Internal Quantum Efficiency

M Junction Capacitance Grading Exponent

 $T_i$  Junction Temperature

 $R_p$  Leakage Resistance

L(t) Luminance Degradation Over Time

E Luminous Efficacy

 $\Theta_V$  Luminous Flux

 $\mu$  Mobility

 $N_u$  Nusselt Number

 $I_{OLED}$  OLED Current

 $V_{OLED}$  OLED Voltage

 $\eta_{out}$  Out-coupling Efficiency

 $C_p$  Parallel Capacitance

 $R_p$  Parallel Resistance

 $\epsilon_0$  Permittivity of Free Space

 $\Phi_p$  Photo-luminescence Efficiency

 $\epsilon_r$  Relative Dielectric Constant

*I<sub>S</sub>* Saturation Current

 $R_s$  Series Resistance

 $\eta_{ST}$  Spin Factor

 $\sigma$  Steffen-Boltzmann Constant

 $\epsilon$  Surface Emissivity

 $\lambda_T$  Temperature Coefficient

 $(V_K, I_K)$  The Knee Point

 $(V_M, I_M)$  The Maximum Operating Point

 $(V_Q, I_Q)$  The Rated Operating Point

 $k_{air}$  Thermal Conductivity of The Air

 $V_T$  Thermal Voltage

 $R_{\theta_{aluminium}}$  Thermal Resistances for Aluminium

 $R_{\theta_{rro}}$  Thermal Resistances for Electrode

 $R_{\theta_{conv}}$  Thermal Resistances for Convection

 $R_{\theta_{\mathit{elass}}}$  Thermal Resistances for Glass

 $R_{\theta_{organic}}$  Thermal Resistances for Organic Layer

 $R_{\theta_{rad}}$  Thermal Resistances for Radiation

 $R_{\theta_{i-a}}$  Thermal Resistances From The Junction to Ambient

L Thickness of The Active Layers

d Thickness of The Organic Layers

t Time

 $A_{OLED}$  Total Surface Area

*CJ*0 Zero–Bias Junction Capacitance

#### LIST OF ABBREVIATIONS

ACTFEL Alternating-Current Thin-Film Electroluminescent

AEC-Q Automotive Electronics Council Qualified

BOM Bill of Materials

CHMSL Center High Mounted Brake Light

CIE Commission Internationale de l'Eclairage

C-f Capacitance-Frequency

C-V Capacitance-Voltage

DRL Daytime Running Light

DUT Device Under Test

ECE Economic Commission for Europe

EL Electroluminescence

EMC Electromagnetic Compatibility

EMI Electromagnetic Interference

EQE External Quantum Efficiency

ESD Electrostatic Discharge

ESL Equivalent Series Inductance

HI High-Injection

HOMO Highest Occupied Molecular Orbital

IC Integrated Circuit

IQE Internal Quantum Efficiency

IS Impedance Spectroscopy

I-V Current-Voltage

J-V Current Density-Voltage

LED Light Emitting Diode

LI Low-Injection

LOMO Lowest Occupied Molecular Orbital

OEM Original Equipment Manufacturers

OLED Organic Light Emitting Diode

PCB Printed Circuit Board

PET Photo-Electro-Thermal

PLED Polymer Light-Emitting Device

PWL Piece-Wise Linear

PWM Pulse Width Modulation

RoHS Restriction of Hazardous Substances Directive

SAE Society of Automotive Engineers

SMU Source-Meter Unit

SPICE Simulation Package with Integrated Circuit Emphasis

SSL Solid-State-Lighting

TADF Thermally Assisted Delayed Fluorescence

TEC Thermoelectric Coolers

TVS Transient-Voltage-Suppression

VPWL Voltage-Controlled Piece-wise Linear

#### LIST OF FIGURES

Figure 1.1	Some examples of oled applications: (a) foldable mobile device	
	[14], (b) agriculture [15], (c) tv display [16]	2
Figure 1.2	The first proposed electrical model of the multi-layer oled [27]	5
Figure 1.3	Equivalent circuit model of the oled [28]	6
Figure 1.4	Double-diode oled model [33]	6
Figure 1.5	Proposed equivalent circuit model for pled [34]	7
Figure 1.6	Proposed hardware equivalent model [38]	7
Figure 1.7	Proposed vpwl and pwl based equivalent circuit model [47]	9
Figure 1.8	Oled thermal resistive model [49]	10
Figure 2.1	Luminous efficacy development history of traditional and ssl	
	sources (adapted from [66])	15
Figure 2.2	MacAdam ellipses plotted on the Cie coordinates (the ellipses are	
	ten times magnified)	16
Figure 2.3	(a) Flexible organic device examples [75, 76] (b) cross section view	
	of flexible devices	17
Figure 2.4	Typical multi-layer oled structure	18
Figure 2.5	The visible light spectrum	19
Figure 2.6	Different types of oled structures: (a) top-emitting (b)	
	bottom-emitting (c) transparent configuration	20
Figure 2.7	Energy levels and light out-coupling process: (1) charge injection	
	(2) charge transportation (3) recombination	21
Figure 2.8	Oled-based rear lamp components: mechanical, optical, and	
	electrical systems (adapted from [97])	24
Figure 2.9	Oled-based automotive tail lamps: (a) Bmw m4 [101], (b)	
	Mercedes s-class coupe [104], (c)Audi a8 [105], and (d)Tt rs coupe	
	[106]	28
Figure 2.10	Automotive lighting market forecast for 2023 (adapted from [103])	28
Figure 2.11	A typical circuit schematic diagram of a multi-segment oled-based	
	tail lamp	30
Figure 3.1	Photograph of the investigated oled sample	31
Figure 3.2	The test setup covered with black foam block	32

Figure 3	3.3	The heat-sinks and thermoelectric cooler	33
Figure 3	3.4	The experimental test setup: (1) cmos camera, (2) imaging lens,	
		(3) spectrometer, (4) the oled under test, (5) source-meter unit	34
Figure 4	<b>l.1</b>	The forward current-voltage characteristic of the oled sample	36
Figure 4	<b>l.2</b>	The reverse current-voltage characteristic of the oled sample	37
Figure 4	<b>l.</b> 3	The impedance and phase response of the oled sample	39
Figure 4	<b>l.</b> 4	Capacitance versus applied voltage for the different frequencies	40
Figure 4	<b>l.</b> 5	Capacitance-frequency characteristic of the oled sample under 5 $\it V$	
		bias condition	40
Figure 4	ŀ.6	Spectral radiance characteristic of the oled	41
Figure 4	<b>1.</b> 7	Pixel values and histogram of the oled	42
Figure 4	<b>l.8</b>	The proposed oled model	43
Figure 4	ŀ.9	The forward I-V characteristic plotted in linear and semi-	
		logarithmic scale	45
Figure 4	<b>l.10</b>	Reverse voltage characteristic of the oled shows that the reverse	
		voltage is not destructive until the $V_{b\nu}$	46
Figure 4	l.11	Comparison of the simulated and measured reverse voltage	
		characteristics	46
Figure 4	<b>l.12</b>	The measured and simulated C-V plots	48
Figure 4	l.13	(a) The model card and (b) schematic symbol of the oled sample .	51
Figure 4	l.14	The schematic view of the application circuit: tail/stop light	54
Figure 4	l.15	The simulation result of the application circuit	56
Figure 5	5.1	A typical light measurement equipment [121]	58
Figure 5	5.2	Spectral emission variation (the inset shows the luminance decay)	59
Figure 5	5.3	Cie 1931 chromaticity diagram for the oled samples with the	
		MacAdam ellipses (ten times magnified)	59
Figure 5	5.4	Dominant wavelength variation	60
Figure 5	5.5	Impedance characteristic change before and after electrical stress .	60
Figure 5	5.6	Current-voltage characteristic with the electrical aging effect	61

#### LIST OF TABLES

Table 2.1	Wavelengths of the visible spectrum	19
Table 2.2	Comparison of thermal resistance	23
Table 2.3	The Sae requirements for the rear lamp functions [98, 99]	25
Table 4.1	Operation points of the oled sample	37
Table 4.2	The Iso $16750 - 2:2012$ reverse voltage parameters [113]	38
Table 4.3	The main characteristics of the oled sample	42
Table 4.4	The model parameters	49
Table 4.5	Comparison of the proposed oled model with the previously reported	
	models	50
Table 4.6	The bill of material (bom) of the application circuit	55

#### Modeling and Characterization of Organic Light Emitting Diodes for Automotive Lighting Applications

#### Arda GÜNEY

Department of Electronics and Communications Engineering
Doctor of Philosophy Thesis

Advisor: Assoc. Prof. Dr. Nihan KAHRAMAN Co-advisor: Assoc. Prof. Dr. Mustafa Berke YELTEN

In this thesis, we aim to propose a SPICE compatible new and accurate electrical model of an Automotive Electronics Council-Qualified (AEC-Q) organic light-emitting diode (OLED), and investigate the reliability of the OLEDs for automotive exterior lighting applications. The proposed model smoothly provides the current-voltage relation in the forward and reverse operating regions, and also dynamic capacitive behaviour of OLED is included in the model. The AEC-Q OLED samples that are currently used in a rear stop lamps have been electrically stressed with a current density of  $J=11.5mA/cm^2$  (25% more than the nominal current density value) at room temperature. The model was presented through theoretical equations for forward and reverse current-voltage characteristics and impedance behaviour of OLED. The simulated and experimental results are in close agreement with each other.

We characterize the complex impedance, operational voltage and current, wavelength, and luminance variation of OLED aged under electrical stress for 7040 hours. We utilize a simple setup that is based on image processing and a CMOS camera to monitor variations in light intensity of the tested device. Under pure electrical stress, the dominant wavelength was slightly red-shifted by  $3.3 \ nm$ , the threshold voltage of OLED is increased from  $4.2 \ V$  to  $5.25 \ V$ , and luminance decayed to 88% of the peak luminance with stress time whereas spectral shape was not affected.

**Keywords:** Automotive exterior lighting, modeling, organic light emitting diode (OLED), reliability, reverse bias characteristic

### YILDIZ TECHNICAL UNIVERSITY GRADUATE SCHOOL OF NATURAL AND APPLIED SCIENCES

#### Otomotiv Aydınlatma Uygulamaları İçin Organik Işık Yayan Diyotların Modellenmesi ve Karakterizasyonu

#### Arda GÜNEY

Elektronik ve Haberleşme Mühendisliği Anabilim Dalı Doktora Tezi

Danışman: Doç. Dr. Nihan KAHRAMAN Eş-Danışman: Doç. Dr. Mustafa Berke YELTEN

Bu tez çalışmasında, Otomotiv Elektroniği Konseyi-Onaylı (AEC-Q) organik ışık yayan diyot (OLED) için SPICE uyumlu yeni ve doğru bir elektriksel model önerilmiş ve otomotiv dış aydınlatma uygulamaları için OLED'lerin güvenilirliği araştırılmıştır. Önerilen model ileri ve ters çalışma bölgelerinde OLED'in akım-gerilim ilişkisini sorunsuz bir şekilde sağlamaktadır ve ayrıca OLED'in dinamik kapasitif davranışı da modele dâhil edilmiştir. Günümüzde bir arka stop lambasında aktif olarak kullanılan AEC-Q OLED numunelerine oda sıcaklığında,  $J=11.5mA/cm^2$  (nominal akım yoğunluğundan %25 daha fazlasına denk gelmektedir.) akım yoğunluğu ile elektriksel stres uygulanmıştır. Önerilen model OLED'in ileri ve geri çalışma bölgesindeki akım-gerilim karakteristikleri ve empedans davranışlarını temel alan teorik denklemler aracılığıyla sunulmuştur. Benzetim ve deneysel sonuçlar, birbirleri ile yakın uyum içerisindedir.

OLED'in empedansı, çalışma gerilimi ve akımı, dalga boyu ve parlaklık değişimi, 7040 saatlik operasyon süresi boyunca elektriksel stres altında karakerize edilmiştir. Numunelerin ışık yoğunluğundaki değişimleri izlemek için, imge işleme ve CMOS kamera temelli bir test düzeneği hazırlanmıştır. Saf elektriksel stres altında; baskın dalga boyunun, kırmızı renk spektrum sınırları içerisinde 3.3 *nm* kaydığı, eşik geriliminin 4.2 *V*'den 5.25 *V*'ye yükseldiği ve ışık şiddetinin başlangıç değerinin %88'ine düştüğü gözlenirken, ışık spektrumunun şeklinde bir değişim gözlenmemiştir.

Anahtar Kelimeler: Otomotiv dış aydınlatma, modelleme, organik ışık yayan diyot

(OLED), g	üvenilirlik, ters kutup	lama karakter	istiği	
_				
	YILI	DIZ TEKNİK ÜN	iversitesi	
	FEN BİLİMLERİ ENSTİTÜSÜ			

## 1 INTRODUCTION

Light consists of massless and uncharged subatomic particles called photons. Like all particles, photons also exhibit wave properties. Therefore they have a wavelength and a frequency. After the photons emerge from their sources, if there is no obstacle in front of them, they propagate in a straight line and without any deviation. When they hit an object, they reflect or break, depending on whether the object is transparent or not. Luminescence is created by the transfer of electrons in a substance from a high energy point to a lower point. Multiple types of luminescence have been reported: chemiluminescence, a result of a chemical reaction, electroluminescence (EL), light produced when an electric current is passed through a substance, or bio-luminescence, is produced by living microscopic organisms [1]. The first studies on the conductivity of organic molecules appear in the early 1900s [2]. However, it has been found that a practical application of this technology is not possible because of the extremely high operating voltage ( $\approx 100 \ V$ ) at that time. The first effective, bi-layer organic light emitting diode (OLED) is described in 1987 by Tang et al., which is generally recognized as the most significant step towards the practical applications of OLEDs technology [3].

The flexible structure, easy availability, and abundant production of organic semiconductor materials have led to new horizons, especially in organic electronics applications. In the last decade, there has been a rapid and powerful transition from traditional light sources such as incandescent and fluorescent lamps to solid-state-lighting (SSL) which is based on new technologies such as light emitting diodes (LEDs) and OLEDs. Organic LEDs appear in different types of applications such as indoor and street lighting, wearable devices, TV displays, mobile devices, embedded antennas, visible light communication, and agriculture [4–9]. Figure 1.1 shows some examples of the OLED applications for SSL devices. This novel technology has significant advantages over conventional lighting technologies such as high efficiency, long lifetime and design flexibility. At the same time, it makes an important transition to innovative products in the lighting industry. In the light of this information, it is



**Figure 1.1** Some examples of oled applications: (a) foldable mobile device [14], (b) agriculture [15], (c) tv display [16]

expected that the OLED lighting concepts to come to an important point.

The automotive lighting market is one of the most attractive markets for OLEDs, and they can be the next technological development after the point-sourced LED technology [10–12]. Like the point-sourced LED sister technology, light is emitted as a function of the current through the device. OLED's current-voltage behavior is very similar to LEDs. However, the multi-layer organic structure and the bigger light emitting area produce a critical capacitive behavior compared to their inorganic counterparts [13]. OLED technology is slowly being introduced in the shape of automotive rear lighting, but they are still very expensive and not suitable for mass production. It means that it is likely only to be used for premium car models in the next few years.

The most important challenges for OLEDs in automotive lighting systems are lifetime and reliability. With increasing demand for illumination flux for automotive rear lighting system, electrical, optical and thermal behavior of OLEDs are crucial for the lifetime and reliability of the system. Unlike other lighting industries, automotive exterior lighting requirements are more challenging.

A typical automotive rear lamp consists of mechanical, optical, and electrical subsystems enclosed in a plastic housing. Maximum temperature includes the temperature rise in the housing caused by self-heating within an enclosed lamp. OLEDs are extremely sensitive to ambient temperature, and the lifetime of OLEDs decreases with an increased junction temperature. Automotive applications need to

withstand a wide range of temperature ( $-40^{\circ}C$  to  $125^{\circ}C$ ). High ambient temperatures present the challenge in OLED rear lamps: controlling the junction temperature of the OLED. For automotive rear lamp applications, a different types of thermal designs such as heat sinks, air cooling, heat pipes are used to keep the junction temperature within prescribed limits. Unlike LED based systems, OLEDs' base materials and large surfaces provide an effective heat transfer mechanism and low thermal resistance. For this reason, electrical current distribution rather than junction temperature is more effective in the deterioration of light intensity in OLEDs in automotive lighting applications.

During maintenance or service, the battery of the car is typically detached and reconnected. There is a probability of connecting the wires to the wrong terminals of the battery. In case of a reverse polarity condition, there could be significant damage to the electronic components. Due to the automotive operation standards, OLEDs are sometimes subject to reverse bias potentials, which they should properly withstand. Every electronic subsystem of a vehicle has to follow the requirements of original equipment manufacturers (OEMs) and ISO 16750-2 DC reverse voltage standard. Consequently, the reverse bias region is critical to be captured by an electrical model especially for the automotive applications even though the OLED does not emit light in the reverse bias region.

Accurate modeling and characterization are important topics for OLED based lighting systems. In order to understand the OLED's characteristics, different types of equivalent models have been proposed in the literature. However, in many models, the larger parasitic capacitive value of OLED compared to LEDs has been accepted as constant, and the reverse bias characteristic, which is very important especially for automotive applications, is not included in these models.

Under these premises, the main motivation of the thesis is to understand the automotive qualified OLED's operation and characterize its electrical and photo-metric dynamic behaviors under pure electrical stress. In order to investigate the OLED's reliability for automotive lighting applications electrical stress has been applied on the OLED sample. Optical and electrical characteristic changes over time have been observed for a duration of 7040 - hours. Thereby, a specific test setup is developed for this purpose to minimize the influence of external factors such as temperature variations, electro-optical interference, self-heating. In addition, this thesis is also dealing with new and more accurate SPICE compatible electrical model of the automotive qualified OLED. Both forward and reverse bias current-voltage regions and also capacitance behavior are included in the proposed model to describe the OLED's behavior. The variation in some important optical and electrical parameters

of the sample were examined depending on the aging of the OLED device.

The dissertation is organized as follows: a general information and preliminary investigation of the electrical models of OLEDs in the literature are presented in this chapter. The objectives of this thesis and hypothesis will also be discussed at the end of this chapter. The operation principles of OLEDs and automotive exterior lighting are discussed in Chapter 2. Chapter 3 explains the experimental setup. Chapter 4 presents the electrical and optical characterization of the OLED samples. The SPICE compatible model is presented and the model parameters are extracted in Chapter 4. After that, the application circuit is presented and the corresponding simulation results are given in the same chapter. Chapter 5 contains the effects of electrical stress on the OLED sample. Finally, the dissertation is concluded with the major results and concluding remarks in Chapter 6.

#### 1.1 Literature Review

In this section, the appropriate models related to the subject have been investigated in the literature. Different models, including empirical and physical models, have been developed in the literature. As the empirical model represent only the relationship between current and voltage, the parameters used in these models have no physical meaning. On the other hand, as physical models have been created due to physical equations based on the working principle of the device, all parameters of the model have physical meanings and the model can be applied a wide range of temperatures and device sizes. The physical representations are also helpful for understanding the physical phenomena such as carrier injection, occupied molecular orbital energy levels (HOMO and LUMO), recombination process, and light emission in OLEDs.

The main advantages and disadvantages of the related OLED models are reviewed in this section. The influence of aging effects, some thermal, electrical and optical problems and OLED-based automotive lighting applications will be analyzed in the following sections.

In order to improve the efficiency and reliability of OLEDs, the electrical, thermal and optical properties of OLEDs are important in OLED-based lighting systems. The performance of OLEDs is influenced by internal and external factors such as humidity, operational voltage/current level, temperature. Therefore, modelling is an important topic for SSL devices. There are several models in the previous research, several of which are simple and depend solely on data-sheet information. Some others are more elaborated and take into account the experimental results [17]. Such models are especially useful for OLED based lighting systems especially

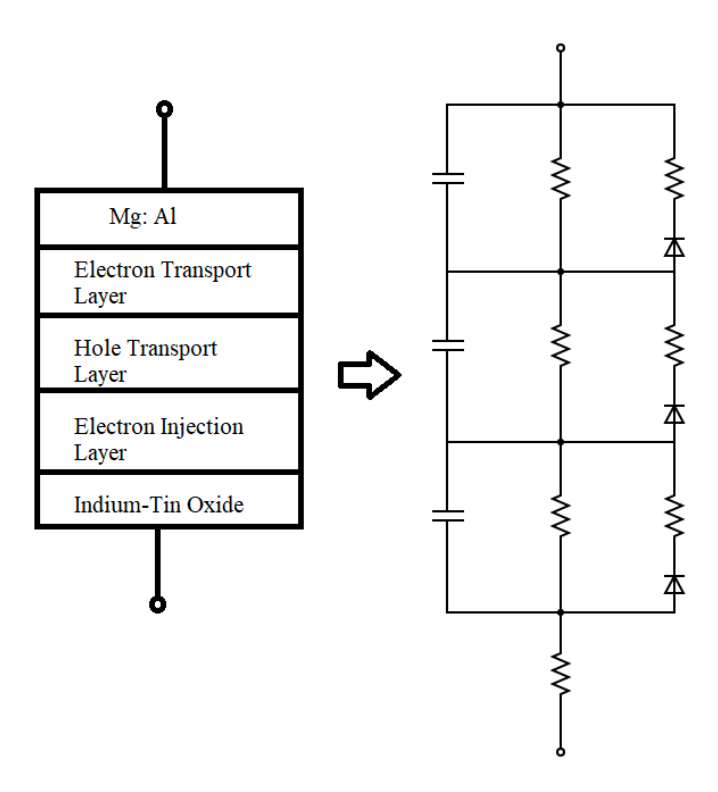


Figure 1.2 The first proposed electrical model of the multi-layer oled [27]

for driver circuits, while addressing some novel issues including thermal effects [18], layer thickness effect [19], and luminance degradation [20]. As for practical lighting applications, factors such as the model accuracy, complexity, and applicability on SPICE simulators should be carefully considered. Since the early 1970s, electroluminance applications for display technologies were used in thin films with alternating current electroluminescent thin-film (ACTFEL) systems [21]. This type of device consists of an emitting layer of phosphorus, sandwiched between two insulating layers and two electrodes. AC current allows capacitive coupling between the electrodes and phosphorus to obtain electroluminescence. The first model for ACTFEL devices is developed by Chen and Krupka [22]. After the invention of two-layer OLED device in 1986, OLEDs have attracted the attention of many researchers. Different structures have been proposed in order to develop efficient and inexpensive OLED based applications [23–26].

The first electrical model for OLEDs have been proposed by Bender, inspired by the similarities between the ACTFEL and OLED technologies [27]. Thus in this model, as shown in Figure 1.2, each organic layer, is represented by a capacitance with a diode and series connected a resistance in parallel branches. These diodes have been used to model the rectifying nature of each layer. The capacitances used for the physical capacitance value of the individual layers. The shunt resistors represent the large bulk series resistances resulting from the low mobility of the layers. An extra sheet

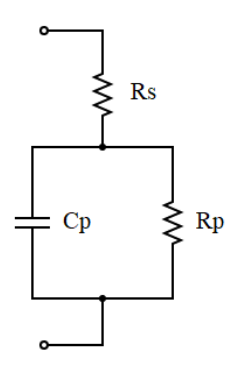


Figure 1.3 Equivalent circuit model of the oled [28]

resistance is connected in series with whole stacked circuit to describe the indium-tin oxide (ITO) layer. Bender has also shown that a simpler model could describe the behavior of OLED as precisely as the multi-diode model. In this mono-diode model, the parallel combination of the diode, resistor and the capacitor is placed in series with a ITO resistance. In [28], a small signal model of an OLED is proposed. The authors fabricated the OLED device with the  $Alq_3$  emissive layer between ITO anode and Alcathode, and investigated frequency-dependent response of the device at two different bias voltages; one above and one below the turn-on voltage. Equivalent circuit model of the OLED is given in Figure 1.3 where  $R_s$  represents the contact resistance  $C_p$ represents intrinsic capacitance and  $R_p$  represents intrinsic resistance. According to the experimental results  $R_s$ , and  $C_p$  is almost constant around 90  $\Omega$  and 10 nFrespectively in the measured frequency range. However, the  $R_p$  value decreases in the higher frequency range. Some other models are able to describe the OLED's design parameters regarding the bias voltage and frequency, considering charge injection and light generation mechanisms in OLEDs [29-32]. In [33], a double-diode OLED model is presented, as shown in Figure 1.4. Two diodes represent the OLED's current-voltage characteristic at low and high voltage levels. The accuracy of this dual diode model is quite low, the error between the simulated and measured currents reaches almost 8% at high current levels with high brightness issues. This is encountered as an accuracy problem, especially at high brightness levels.

Kanicki et al. have highlighted the need to use three diodes in parallel (corresponding

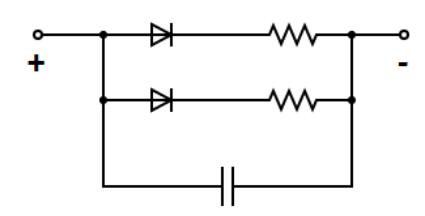


Figure 1.4 Double-diode oled model [33]

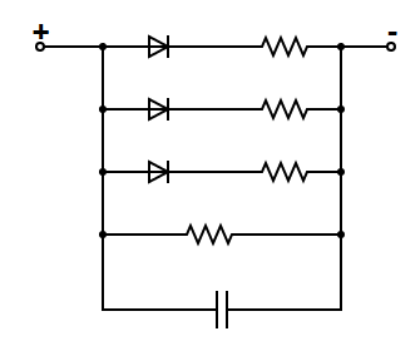


Figure 1.5 Proposed equivalent circuit model for pled [34]

to the hetero junctions of the structure) to adjust the simulated current density-voltage (J-V) curve with the experimental J-V curve of their polymer LED (PLED) device that is fabricated on a plastic substrate, as shown in Figure 1.5 [34]. A parallel connected capacitor is added to perform the transient simulations. The capacitance values of red, green, and blue PLEDs are 1.22 nF, 1.17 nF, and 1.12 nF, respectively. The authors are also presented a simple SPICE equivalent model to simulate the current-density-voltage characteristics of the PLED. Some other models in the literature are based on the carrier transport phenomena [35–37]. The parameters used in these models depend on the operating voltage and frequency and take into account the charge injection and light emission mechanisms in OLEDs.

Buso et al. have proposed an electrical equivalent device for the OLED driver topology as shown in Figure 1.6 [38]. The authors demonstrate the similarity between the light output waveform and  $V_1$ . Therefore, instead of using a photo-detector, the light output can be measured by the voltage on the resistor. Impedance spectroscopy (IS) is another method to characterize and model OLEDs [39–42]. In IS method, a small AC signal  $(V_{AC}(t) = V_1 \sin \omega t)$  is applied to the OLED with a constant DC voltage as follows:

$$V_{OLED} = V_{DC} + V_1 \sin \omega t \tag{1.1}$$

The complex impedance  $(Z_{OLED} = \frac{V_{OLED}}{I_{OLED}})$  is defined as the ratio of the voltage to

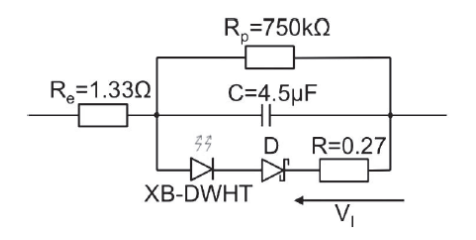


**Figure 1.6** Proposed hardware equivalent model [38]

current amplitude of the OLED. The measured impedance data generated by IS can be represented in various ways. The most important of these formats are the capacitance-voltage and capacitance-frequency (C-V and C-f) curves that can be found in OLEDs to describe the charge and charge-injection. These characteristics is further discussed in this thesis. According to Lee et.al, an impedance change in OLEDs can be observed to understand the degradation mechanism [43]. They have fabricated three different OLED structures and observed the impedances before and after an electrical stress. The authors use the IS technique to measure the OLED impedance related to the frequency range and observe the OLED response using the small-signal equivalent circuit, as shown in Figure 1.3. An analytical model based on the band diagrams of different layers is proposed in [19]. The authors examine the OLED's operation region in two main parts, a low and high-injection (LI and HI) regions. They introduce the band diagram theory for the bi-layer OLED.

Some OLED models also consider the thermal behaviour of the device. Automotive applications need to withstand a wide range of temperatures. High ambient temperatures present the challenge in OLED rear lamps which is the control of the junction temperature of the OLED. OLEDs are extremely sensitive to temperature, and temperature has a great impact on the electrical properties of OLEDs. In [44], the authors show that a deviation of  $\pm 10^{\circ}C$  in the operating temperature of an OLED operating around  $\pm 40^{\circ}C$  could change the operating voltage of the OLED between  $\pm 2.5$  % and  $\pm 5$  %. A rise in junction temperature results in the forward voltage of OLED to decrease and therefore it can change the dynamic stability [45]. The voltage drop in OLED operation causes an increase in OLED's operation current, so that it should be carefully controlled by the OLED driver system [46].

In [47], in order to define voltage-current properties of OLEDs at different ambient temperatures between  $\pm 10^{\circ}C$  and  $\pm 40^{\circ}C$ , an equivalent OLED circuit model with a temperature coefficient, forming an electro-thermal model, is presented. A four-parameter Taylor series based equivalent circuit is proposed to create voltage-controlled piece-wise linear (VPWL) and piece-wise linear (PWL) based behavior model, as shown in Figure 1.7. Lin et al. provided a Shockley function by using a Taylor series as follows:

$$I_{OLED(T_a)} = I_{SAT(T_a)} \sum_{j=0}^{\infty} \frac{\left(\frac{V_{OLED(20^{\circ}C)} + (T_a - 20^{\circ}C) \cdot \lambda_T - r_s \cdot I_{OLED(T_a)}}{n_{(T_a)} \cdot V_{T(T_a)}}\right)^j}{j!}$$
(1.2)

$$r_{s} = \frac{V_{M} - V_{Q}}{I_{M} - I_{Q}} \tag{1.3}$$

$$\lambda_T = \frac{V_{Q(40^{\circ}C)} - V_{Q(20^{\circ}C)}}{T_a - 20^{\circ}C} \tag{1.4}$$

$$n_{(T_a)} = \frac{V_K - V_M - r_s \cdot (I_K - I_M)}{V_{T(T_a)} \cdot \ln(\frac{I_K}{I_M})}$$
(1.5)

$$I_{SAT(T_a)} = \frac{I_K}{e^{\left(\frac{V_K(20^{\circ}C) + (T_a - 20^{\circ}C) \cdot \lambda_T - r_s \cdot I_K}{n_{(T_a)} \cdot V_T(T_a)}\right)}}$$
(1.6)

where the parameters are defined as:

•  $(V_M, I_M)$ : the maximum operating point,

•  $(V_Q, I_Q)$ : the rated operating point,

•  $(V_K, I_K)$ : the knee point.

They obtain these parameters from the experimental measurements. They measure the error less than 2% with the 75th (j=75) order in the voltage-current characteristics for ambient temperatures between  $10^{\circ}C$  to  $40^{\circ}C$ . The authors also take into account the OLED's capacitance variations. They measure the voltage-charge (V-Q) values and prepare the PWL lookup table of the V-Q curve for the OLED's parasitic capacitor.

In [48], a photo-electro-thermal (PET) model has been proposed to characterize OLEDs in view of electrical photo-metric, chromatic and thermal aspects. The authors demonstrate that OLEDs' larger surface and contact areas are effective heat transfer paths regarding inorganic LEDs. They also show that the deterioration in the luminance uniformity is not caused by the heat distribution. The current distribution leads to obtain the better luminance uniformity.

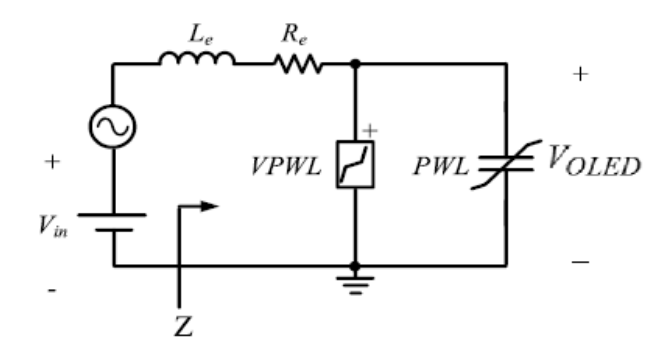


Figure 1.7 Proposed vpwl and pwl based equivalent circuit model [47]

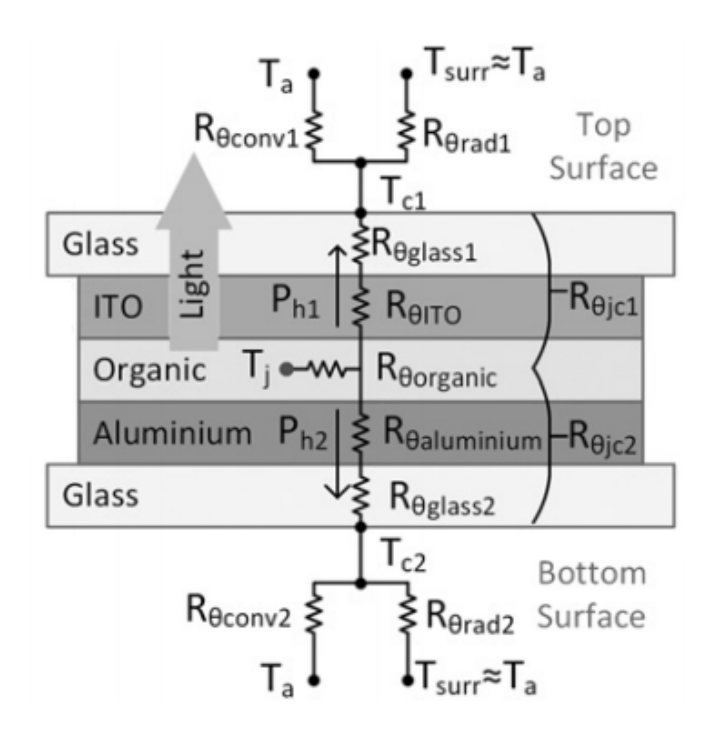


Figure 1.8 Oled thermal resistive model [49]

One another PET model is presented in [49]. The authors use the datasheet information and experimental results. The proposed model consists of scale, photo-metrical, electrical and thermal domain variables. Interaction between these domains is explained on the OLED's operation. The model is built on the usage of voltage, light and heat dependent sources. Bender et al. consider the heat transfer from the junction to the ambient through thermal resistances of each organic layer  $(R_{\Theta_{organic}})$ , glass substrates  $(R_{\Theta_{glass}})$ , electrodes and aluminium  $(R_{\Theta_{ITO}}, R_{\Theta_{aluminium}})$ , as shown in Figure 1.8. They assume that the temperature is distributed uniformly throughout the OLED panel. The authors provide the thermal resistance equations for the heat radiation  $(R_{\Theta_{rad}})$ , and convection  $(R_{\Theta_{conv}})$  are obtained as:

$$R_{\theta_{rad}} = \frac{1}{4\epsilon\sigma T_a^3 A_{OLED}} \tag{1.7}$$

$$R_{\theta_{conv}} = \frac{L_c}{k_{air} N_u A_{OLED}} \tag{1.8}$$

where the parameters are defined as:

- $\epsilon$ : surface emissivity of the OLED,
- $\sigma$ : Steffen-Boltzmann constant,

•  $T_a$ : ambient temperature,

•  $A_{OLED}$ : total surface area,

•  $L_c$ : the critical size that is a function of the orientation,

•  $k_{air}$ : the thermal conductivity of the air,

•  $N_u$ : Nusselt number.

The 1.7 and 1.8 show that  $R_{\theta_{rad}}$  and  $R_{\theta_{conv}}$  are strongly depend on the OLED device surface. The authors calculate the OLED thermal resistance from the junction to ambient  $(R_{\theta_{i-a}})$  as follows:

$$R_{\theta_{j-a}} = \frac{(R_{\theta_{j-c1}} + R_{\theta_{c-a1}})(R_{\theta_{j-c2}} + R_{\theta_{c-a2}})}{R_{\theta_{i-c1}} + R_{\theta_{c-a1}} + R_{\theta_{i-c2}} + R_{\theta_{c-a2}}}$$
(1.9)

The junction temperature  $(T_i)$  of the OLED can be obtained as:

$$T_i = T_a + R_{\theta_{i-a}} P_h \tag{1.10}$$

As seen from 1.10 the maximum allowed ambient temperature can be determined by given internal temperature and power dissipation of OLED. The junction temperature directly affects the lifetime and efficiency during the operation of OLEDs [50]. Therefore, thermal management is one of the key design parameters for the efficient operation of OLEDs. In automotive environment, the OLED's input power cannot be converted fully into photon energy. The output energy can be examined in two parts: optical energy and energy consumed as heat dissipation. The luminous efficacy (E) and flux $(\Theta_V)$  are also functions of the junction temperature as explained in the following equations [51].

$$E = E_{(25^{\circ}C)} e^{\frac{-(T_j - 25^{\circ}C)}{T_1}}$$
 (1.11)

$$\Theta_V = P_D E \tag{1.12}$$

where  $T_1$  is the characteristic temperature, and  $P_D$  is the dissipated electrical power of the OLED. The luminance degradation is one of the most important parameters to define the OLEDs lifetime and reliability. Many studies have been conducted on the lifetime estimation and the luminance decay models of OLEDs [52–57]. One

of the well-known mathematical models for the luminance degradation is Arrhenius equation [58] that can be explained as:

$$L(t) = L_0 e^{-\beta t} \tag{1.13}$$

where the parameter  $L_0$  is the initial luminance of the OLED, L(t) is the parameter that shows the luminance degradation over time (t), and  $\beta$  is the aging parameter. 1.13 assumes that the aging rate is constant and the luminance decays exponentially with time. Zhang et al. demonstrate that the luminance degradation data well fitted to this exponential model under three constant stress groups [59]. Another model is the stretched exponential decay (SED) [60] model given as:

$$L(t) = L_0 e^{-(\frac{t}{\tau_0})^{\beta}} \tag{1.14}$$

where  $\tau_0$  corresponds the characteristics time where the luminance decays to 63.2% of the  $L_0$ . These proposed OLED models in the literature can assist the designer for the OLED-based lighting systems and the following parameters can be determined before starting the design: the maximum operating temperature, luminous flux, operating voltage and current values.

#### 1.2 Objective of the Thesis

The main objective of this thesis is to introduce a new and accurate SPICE compatible OLED model for automotive lighting applications. This thesis also presents the outcome of investigations on the electrical stress effects on the AEC-Q OLED's optical and electrical characteristic changes over time for the automotive lighting applications. The investigations are obtained by performing experimental research. A specific test setup developed for this purpose to minimize the influence of external factors such as temperature variations, electro-optical interference and self-heating. Both forward and reverse current-voltage regions and also capacitance behaviors are included in the proposed model to describe thoroughly the OLED's behavior.

#### 1.3 Hypothesis

The typical one diode based model [61] has the advantage of simplicity but it suffers from the accuracy. Some SPICE compatible electrical OLED models [19],[62] only take into account the forward current-voltage behavior but reverse characteristic or

capacitance behavior are not included. Some others [13], [38] include capacitance behavior as well but they generally assume that the OLED's intrinsic capacitance is constant and not voltage dependent. As investigated in the following chapters, this assumption is not able to represent the device dynamics.

The mentioned demands for OLEDs require a precise and reliable model that can cover all the operation voltage range and the impedance behavior of the OLED. In the following chapters of the thesis, it is aimed to propose a precise and SPICE compatible model that can provide all the operation range including dynamic capacitive behavior.

#### 2 STATE-OF-THE-ART ON OLED AND AUTOMOTIVE LIGHTING

In this chapter, we briefly introduce the lighting technologies. Then we explain basic structure and operation principle of the OLEDs. Finally, we summarize the automotive exterior lighting, and driving methods of the OLED in automotive environment.

Traditional lighting technologies such as incandescent, halogen, and fluorescent have made significant progress over the years in terms of energy efficiency and light quality. However, it has been observed that these technologies can not keep up with the technological demands. As a result of the rapid developments in the semiconductor technology, the efficiency factors of SSL technology are constantly increasing. Light sources that use semiconductor material instead of standard filament, gas or arc tubes to generate light are in the SSL group. LED, OLED and PLED technologies can be shown as examples of solid state lighting.

Solid state lighting solutions have emerged as good alternatives to traditional lighting with its high efficiency. Solid state lighting applications are energy efficient, long-lasting, environmentally friendly, small in size, reliable and low cost [63]. The main reason for using the SSL source in lighting is that it provides energy efficiency.

Lighting consumes 15 - 20% of the total electricity of the world, so more energy efficient lighting sources have recently become more in demand. In fact, the switch to innovative lighting systems such as LEDs, OLEDs may reduce electricity usage by 50% [64].

In 1907, Henry Joseph Round conducted experiments to investigate the usability of silicon carbide in different fields. Round obtained yellow colored light by passing current through silicon carbide in his experiments, and with this invention, the first LED concept emerged [65]. In 1962, Holonyak invented a red emitting GaAsP inorganic LED. The luminous output was  $0.1 \, lm/W$ . In 1980, he changed the material as AlGaAs/GaAs and increased the efficacy to  $2 \, lm/W$ , approximately the same as first

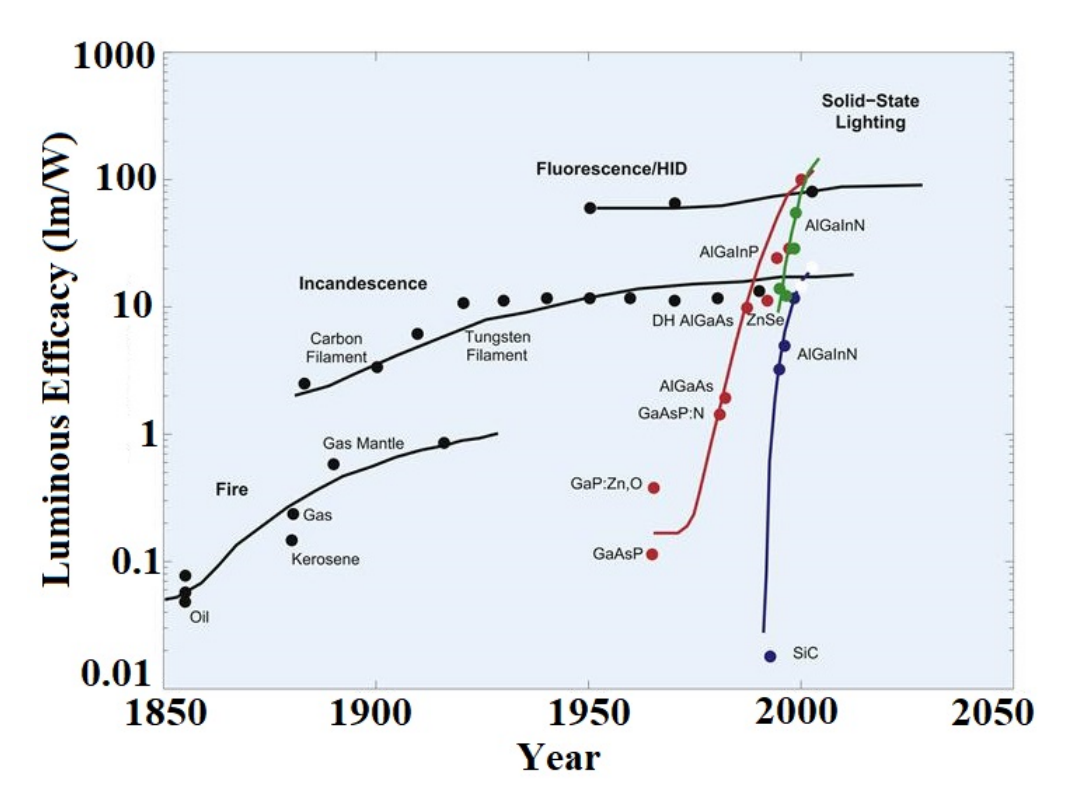


**Figure 2.1** Luminous efficacy development history of traditional and ssl sources (adapted from [66])

light filament bulb in 1879 invented by Thomas Edison. A  $100 \, lm/W$  luminous output were reached in 2000s. Figure 2.1 illustrates this lighting history and the luminous efficacy for different lighting sources.

In the last decade, tremendous researches have been made in solid-sate lighting. OLEDs open up a whole new world of opportunities for working with light. Distinctive features of OLEDs have attractive features such as; low thickness, bendable structure, aesthetic view even in off-state [67]. These features make OLEDs more attractive for the lighting applications. Additionally, OLEDs based lighting can help to reduce electricity consumption up to 70% than conventional light sources [68]. OLED devices have considered to be the main applicant for the next light source generation.

#### 2.1 Organic Semiconductors

Silicon constitutes the basic building block of electronic components and is an inorganic semiconductor. Silicon is also constitutes the raw material of most of the electronic components currently produced. Although it is abundant in nature, the researches have focused on obtaining other materials due to the difficulty of obtaining pure silicon and the high operating cost. At this point, organic semiconductors with advantages such as low infrastructure cost, application to wide and flexible surfaces,

easy and fast production methods and application-specific synthesizable material properties, they have the superior than silicon in certain areas. Organic electronics is a branch of electronics using carbon compounds with semiconductor properties, thus differentiating itself from traditional electronics based on inorganic compounds such as Silicon, and Germanium. There are two types of carbon chain compounds according to their molecular weight: small molecules and macro molecules consisting of the repeated sequence of the same pattern. The first studies on the conductivity of organic molecules appear in the early 1900s. These first devices in organic electroluminescent agents have no practical use because the operating voltage of the device reaches several hundred volts, with very low efficiency. The decisive stages took place at the end of the 1980s. It gained momentum with the discovery of the first multi-layer OLED in 1987 [3]. Since this date, many studies have been carried out to increase the efficiency of OLEDs and to reduce their degradation processes. Thermally assisted delayed fluorescence (TADF) OLED structures, which increased the internal quantum

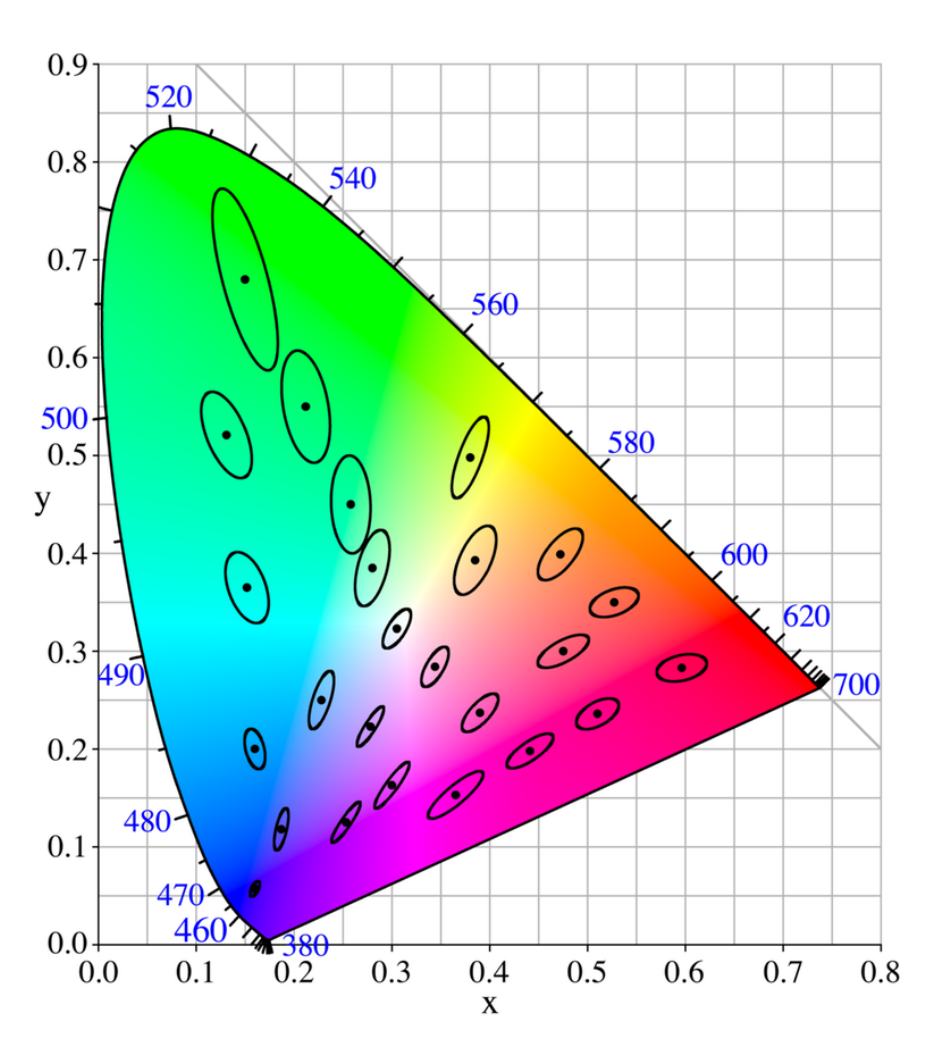


**Figure 2.2** MacAdam ellipses plotted on the Cie coordinates (the ellipses are ten times magnified)

efficiency (IQE) to 100% have been proposed in 2012 to solve the efficiency problem [69]. M. Frobel et al. introduce color tunable OLED in 2017. A blue and yellow emitting units were combined by the authors. The authors ensure that OLEDs have a wide range of colors on the color space determined by the CIE. The light emitted from a light source and the light perceived by the human eye are quite different from each other. It is the anatomical structure of the human eye and the way information is processed in the brain that makes this difference. The first researches on the light absorption property of the human eye were made in the 1930s. As a result of these studies, curves called the CIE graphic, and showing the sensitivity of the human eye against wavelengths were obtained. In 1942, David MacAdam, a color scientist, investigated whether each point on the CIE graphic actually represents a different color. He ran a series of tests and showed that instead of a single color represented by a dot on the graph, it can be represented by an ellipse surrounding that point, resulting in the MacAdam ellipse, as shown in Figure 2.2. For example, a white-radiating color is ideally positioned at a specific CIE point (chromaticity coordinates are x = 0.333, and y = 0.333). However, around these coordinates there is a very large area that can be defined as white light.

The flexible structure of organic semiconductor materials, as can be seen from the Figure 2.3, easy to obtain and to produce in large quantities has opened up new application areas especially in organic electronics. The development of organic semiconductors has found application opportunities in many fields such as photo-voltaic cells, sensors, photo-detectors, transistors, memory storage devices, organic electro-luminescent devices [70–74]. OLEDs are the leading devices that attract the most attention and investment in this new area.

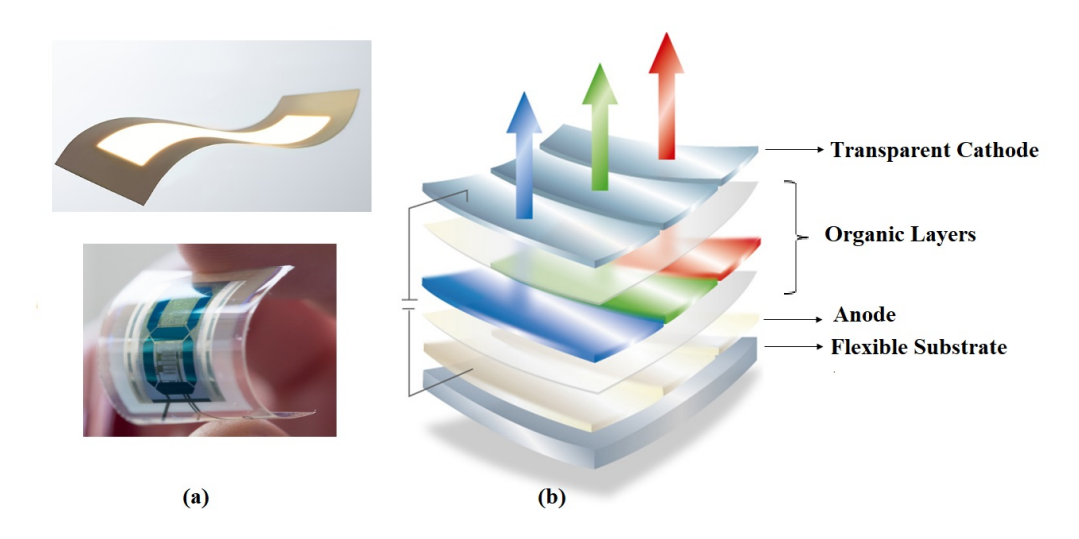


**Figure 2.3** (a) Flexible organic device examples [75, 76] (b) cross section view of flexible devices

The OLED market forecasts show that the expected value will be reached over \$52 billion by 2023 [77]. OLEDs have enormous potential, and their use in smartphones and tablets, wearables, and automotive markets will continue to grow in the near future.

## 2.1.1 Basic Structure and Operation Principles of OLEDs

A typical OLED device consists of several thin layers of organic semiconductor material between two conductive electrodes, as shown in Figure 2.4. An OLED consists of the following layers: rigid or flexible substrate material (can be glass or polymer foil), anode, hole injection layer (HIL), hole transport layer (HTL), electron blocking layer (EBL), emissive layer (EML), hole blocking layer (HBL), electron transport layer (ETL), electron injection layer (EIL) and finally cathode. The total thickness of organic layers is a few hundred nanometers, and each layer has a particular purpose [78].

The operation of OLEDs is based on the phenomenon of electroluminescence. When DC voltage is applied to an OLED, with the effect of the electrical field, holes and electrons, migrate from the electrodes into the EML until they meet each other. Thanks to the radiative recombination of the exciton (bound couple of holes and electrons) electrical energy is directly converted to light in this layer [79]. The blocking layers are used to reduce leakage currents and improve OLED's efficiency by restricting electrons to the emissive layer. One of the main problems with organic materials is that they

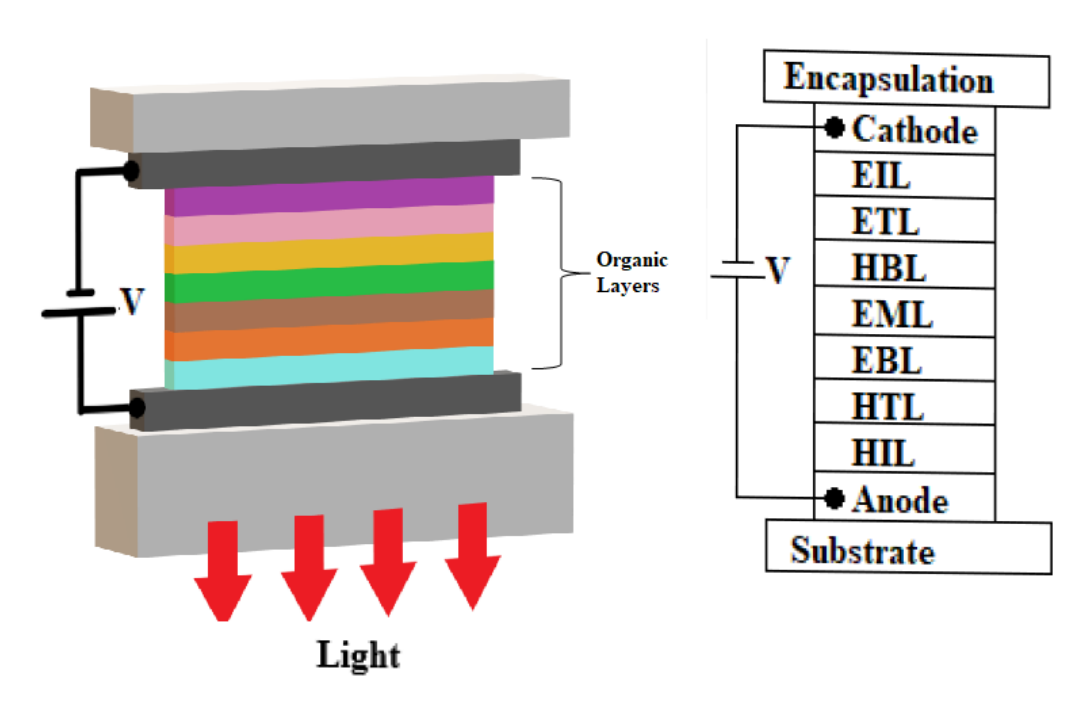


Figure 2.4 Typical multi-layer oled structure

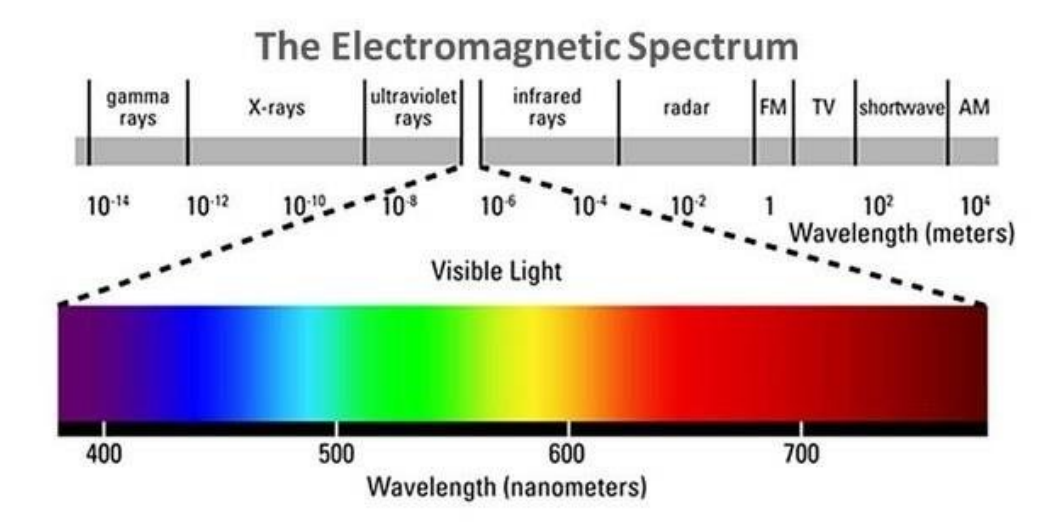


Figure 2.5 The visible light spectrum

are extremely sensitive to external factors such as humidity and temperature. An encapsulation layer is used to protect the device against these external influences and to ensure the required lifetime. Indium-tin-oxide (ITO) is used as a transparent, conductive oxide since the generated light in the device must be emitted through the glass substrate. Many researchers have proposed different structures in order to improve OLEDs' efficiency and lifetime [25, 26]. When voltage is applied to the electrodes of an OLED, the device emits a specific color according to the energy band gap of active organic materials in its structure. Although it is possible to change the energy band gaps of inorganic materials by doping various materials that will create impurities, they are not at the desired level. However, the energy band gaps of organic semiconductors can be controlled within the desired range by adding different groups to the organic structure to be obtained by chemical synthesis. In this way, it is possible to obtain all colors in the visible spectrum, given in the Figure 2.5, by varying the energy band range of these materials. The color is determined by the wavelength of light, which is associated with frequency and energy. Table 2.1 lists the ranges of these different colors.

**Table 2.1** Wavelengths of the visible spectrum

Color	Wavelength (nm)
Violet	380 - 450
Blue	450 — 485
Cyan	485 — 500
Green	500 — 565
Yellow	565 – 590
Orange	590 – 625
Red	625 – 740

OLEDs can be classified by basically three different structures according to the light emitting direction of the device: top-emitting, bottom-emitting, and transparent configuration. These device configurations are illustrated in Figure 2.6. In transparent configuration the light is emitted from both sides of the device [80]. The transparent configuration significantly increases the contrast, and rendering the viewing of screens in direct sunlight much simpler [81]. The OLED samples have been used throughout this thesis are built in bottom-emitting configuration. This means that the device uses transparent electrode which is located directly on top of a transparent substrate, through which the generated light is out-coupled.

#### 2.1.2 Energy Levels and Quantum Efficiency

The holes are transmitted from the positive electrode to the HOMO excited state of the HTL substance when the voltage is applied between two OLED electrodes, whereas the electrons are transmitted from the cathode to the LUMO energy level of the ETL material. In general, the HOMO energy level corresponds to the valence band of the material while the LUMO energy level corresponds to the conductivity band of the material. Therefore, inter molecular interaction affects the width of the valence and conductivity bands and, consequently, the conductivity properties of the material. When the electron is stimulated from the HOMO level to the LUMO level, an exciton is created. When the exciton is electronically formed, electrons and holes begin to be injected into the organic semiconductor. Thus, electrons convert the energy into light by relaxation of energy state. Excitons can be classified to two types of energy levels, as singlet and triplet. The recombining charges are approximately 75% triplet exciton and 25% singlet exciton, according to the spin statistics [82].

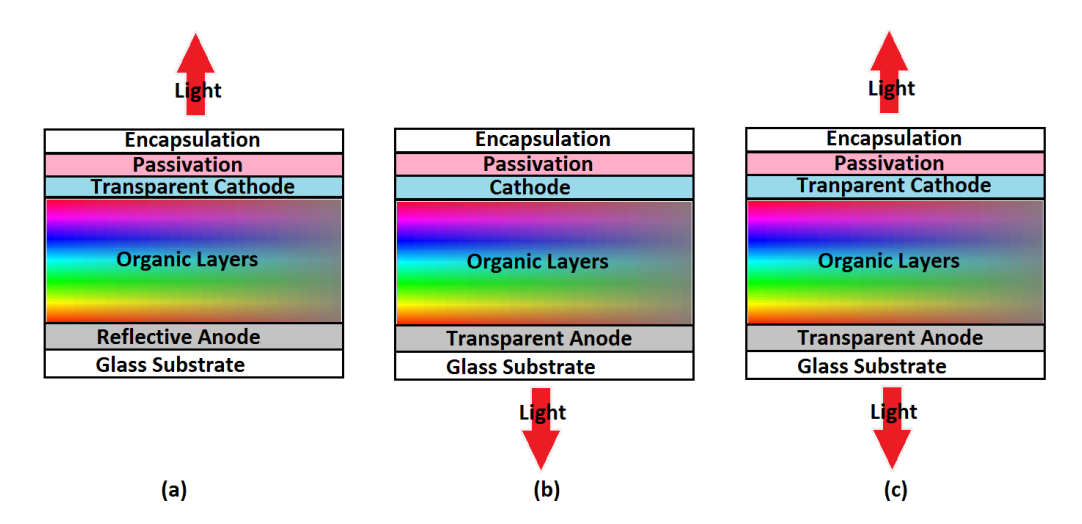


**Figure 2.6** Different types of oled structures: (a) top-emitting (b) bottom-emitting (c) transparent configuration

The operation processes and energy levels of a forward biased OLED are illustrated in Figure 2.7. The operating principle of OLEDs can be explained in brief as follow:

- 1. Charge Injection: The holes and electrons(charge carriers) are injected into the organic layers.
- 2. Charge Transportation: Charge carriers are transported to the emitter layer.
- 3. Excitation: Electron-hole pair is described as an exciton.
- 4. Light Out-coupling: Exciton creates a photon. As a result, the photon is emitted out of the OLED through one or both of the electrodes.

The external quantum efficiency (EQE) is a concept commonly used in the characterization of OLED devices. The proportion of the amount of photons received from the organic semiconductor to the amount of inserted electron-hole pairs is generally known as EQE. The efficiency of the emission inside the OLED is defined as internal quantum efficiency (IQE). The EQE definition is given as [83]:

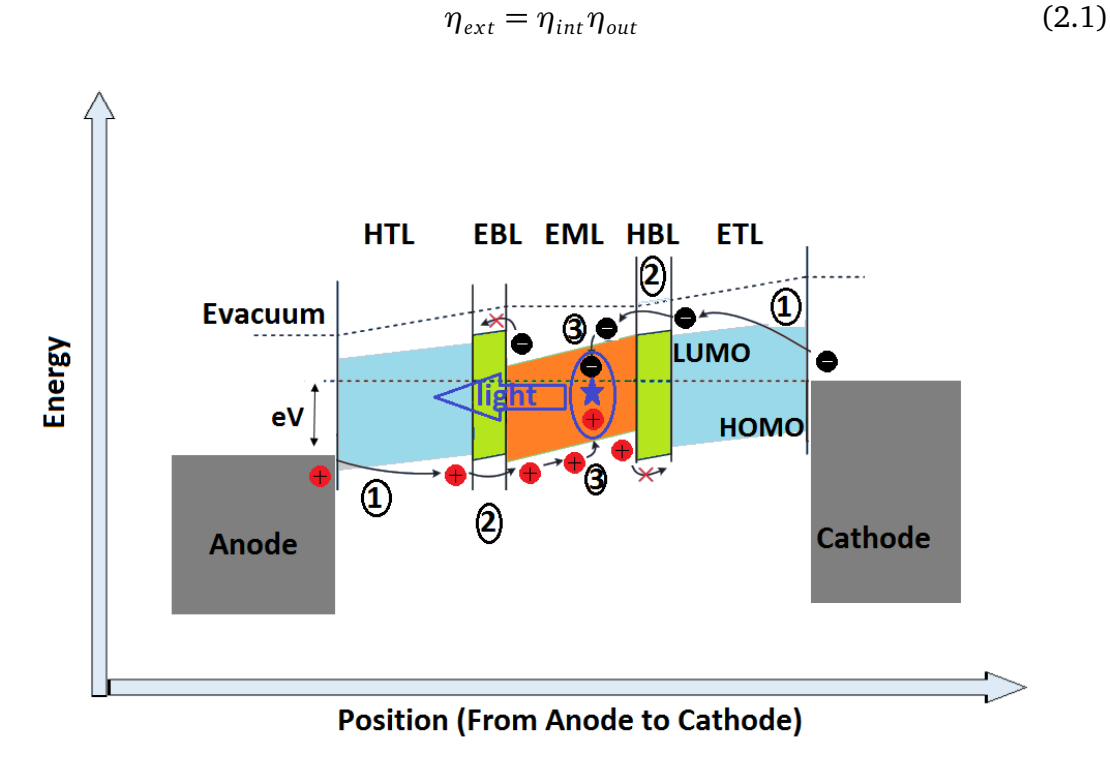


**Figure 2.7** Energy levels and light out-coupling process: (1) charge injection (2) charge transportation (3) recombination

$$\eta_{int} = \gamma \eta_{ST} \Phi_P \tag{2.2}$$

Where  $\eta_{ext}$  and  $\eta_{int}$  represent the EQE and IQE,  $\eta_{out}$  is the out-coupling efficiency,  $\gamma$  is the charge carrier balance,  $\eta_{ST}$  and  $\Phi_P$  are depend on the molecule properties and described as spin factor (the fraction of spin-allowed excitons) and the photo-luminescence efficiency of the emitter, respectively. The IQE varies depending on whether the emitter type used in the device is fluorescent or phosphorescent. A typical fluorescent material can only emit from the singlet exciton. Therefore, the maximum theoretical IQE is limited to 25% [84]. Phosphorescent emitters can emit from both singlet and triplet excitation. In recent years triplet harvesting approach has been extensively studied to overcome the problem of low efficiency [85, 86].

#### 2.1.3 Degradation Mechanisms of OLEDs

In the harsh environment of automotive exterior lighting, the performance of OLEDs can be influenced by many factors. It is generally known that long-term operation of OLEDs degrades their electrical and optical properties. External or internal factors can cause the degradation mechanisms. The most common factors leading to external degradation are the effects of oxygen and water, as well as the heat and direct sunlight. While the diffusion of oxygen leads to the oxidation, water is causing the delamination of the electrode [87]. When driving OLEDs, the generated heat at the hot spots also acts as a source of degradation. The heat can be reduced by increasing the conductivity of organic layers by doping, using additional layers to improve load injection, or using spreader layers with low recombination losses [88]. However, these methods can only reduce the heat by a small amount. The photo-degradation of OLEDs due to exposure to visible and near-ultraviolet light is reported in [89]. In this study, while the ITO polymer interface is defined as the interface where photo-degradation took place, it is revealed that most of each layer is insensitive to irradiation with the sunlight. The radiation of sun is partially absorbed in the automotive lamp and causes additional heat load.

On the other hand, the internal degradation depends strongly on the material properties the OLED stack. The cathode metal that is used in contact with the EIL, the morphological stability of the HTL or the used material-specific chemical reactions can cause the internal degradation of OLEDs [90, 91]. The drop in the luminance is the primary indicator of degradation. Different ways of luminance degradation have been reported. One type is called the "dark spot" degradation, which leads to local non-emitting spots [92]. Increasing dark spots will inevitably cover almost the entire

surface of the OLED, and it can reduce the electroluminescence of the system [93]. The other one is the total failure of the device in which a sudden drop in the luminance occurs. The most common reason for this effect is the shortcuts between the anode and cathode [94]. Another type is the internal degradation that comes with a steady decrease in the luminous efficacy [95]. Therefore, the most critical challenges for OLEDs in the automotive lighting system are lifetime and reliability.

#### 2.1.4 Comparison Between LEDs and OLEDs

The use of LEDs in replacement of incandescent bulbs offers some advantages to the automotive sector, such as high luminous efficiency, long lifetime, and low power consumption and quick response time [96]. After LEDs have become standard for the most of car manufacturers, particularly in Europe where daytime running lights are mandatory in many countries, the use of OLED technology is now the next step of automotive lighting design. The OLEDs can offer the same efficiency advantages while offering additional benefits. OLEDs are also defined as the concept of electro-luminescence, as with traditional LEDs.

In contrast to point-sourced LEDs, OLEDs glow entire regions at a significant brightness level, their light reaches such a new state of homogeneity, and the strength of light could be lightened uniformly. OLED-based automotive rear lighting system needs no extra optical components such as reflectors, or light guides, which makes OLED units more efficient. Thanks to OLED's larger light emitting surface areas, OLEDs are distinguished from conventional counterparts in getting relatively low thermal resistivity and being less sensitive to the ambient temperature. Therefore, in many situations they do not require heat sinks because OLEDs are cooled passively by heat convection and radiation from both surfaces. This means that the OLED based rear lamps are smaller than in traditional tail lights. Table 2.2 shows the comparison of typical thermal resistance values of some AEC-Q LEDs that perform the position function in the rear stop lamp and OLED.

**Table 2.2** Comparison of thermal resistance

Type	Manufacturer	Part number	Thermal resistance ( ${}^{\circ}C/W$ )
LED	Osram	LRG6SP	35
LED	Seoul Semi.	SZR05A0A	15,1
LED	Samsung	SPMRD13435	60
LED	Lumileds	Signalsure 75	45
LED	Everlight	A09K-SR1501H	50
OLED	Osram	CMW30	0,34
OLED	Lumiotec	LTS-10015	0,59

## 2.2 Automotive Exterior Lighting

It is impossible to imagine a car without exterior headlamps and taillights as driving an automobile at night without these now-obligatory parts. Automotive exterior lighting is not always what it is today. As time went by, technology evolved, and automotive lighting became compulsory in all countries around the globe, which reduced the risk of accidents. The first automobile headlamps were based on acetylene and gasoline officially introduced during the 1880s, close to the old gas-lamps. A breakthrough in automotive lighting technology first emerged in the invention of fluorescent light sources. The discovery of the semiconductor LED is the further development. This invention enabled the illumination of various colors with a highly effective and usable lighting devices. Efficient lighting and display has become one of the most important problems in the automotive industry. In illumination and visualization technology, this has resulted in numerous philosophies. A new concept of nano-structured materials for such applications is provided by organic semiconductors.

A typical automotive rear lamp system based on SSL technology generally consists of an optical system (outer lenses and reflectors), an electrical system (PCB) and a mechanical system (connection cables, screws, housing, etc.) as shown in Figure 2.8. Maximum temperature includes the temperature rise in the housing caused by self-heating within an enclosed lamp, as shown in the following figure. Heat sinks are also commonly used to keep the junction temperature within the prescribed limits in the real applications. There are basically five main functions in a typical rear stop lamp: position, stop, reverse, turn and fog.

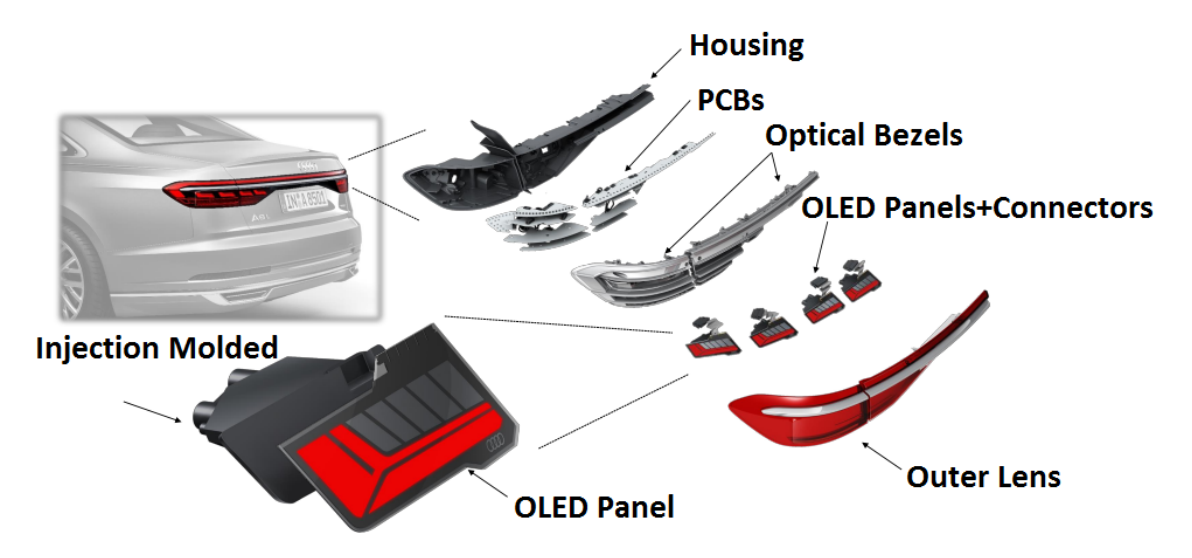


**Figure 2.8** Oled-based rear lamp components: mechanical, optical, and electrical systems (adapted from [97])

**Table 2.3** The Sae requirements for the rear lamp functions [98, 99]

Function	Color	Usage time (h)	Min. intensity (cd)
Position	Red	2000	2
Stop	Red	720	80
Reverse	White	40	80
Turn	Amber	160	80
Fog	Red	8	80

The lifetime of a rear lamp mainly depends on the lamp usage during the life of the vehicle. The signal and lighting equipment in the rear lamp must meet legal requirements for the color temperature and the lifetime. The colors of OLED based rear lamps should be designed to be compatible with the SAE (Society of Automotive Engineers) International standards. For instance, position or stop function must be emitted from the device in the red color spectrum with a minimum wavelength of 610 *nm* according to the SAE J578: Color Specification Standard. The SAE J2938: LED Light Sources Tests and Requirements Standard provides the average usage time for each function of the rear lamp as summarized in Table 2.3.

Automotive lamp design can be summed up in the following phases:

- Input and regulations specifications pertaining to packaging design, topology, and model parameters,
- Identification of eligible vehicle parts associated with electrical, photonic or mechanical requirements,
- Determination of the topology of the driver (linear regulator, buck converter, boost controller etc. ).

#### 2.2.1 Automotive Requirements

Automotive exterior lighting is one of the most challenging applications in terms of harsh environmental conditions. Automotive applications, unlike other consumer sectors, have stringent criteria and a lot of tight requirements that are expressed in industry guidelines and purchase specifications. Those specifications are wide temperature ( $-40^{\circ}C$  to  $125^{\circ}C$ ) range, operation voltage range (8 V-16V), ability to withstand chemicals, reverse polarity, humidity, electrostatic discharge (ESD), electromagnetic compatibility and interference (EMC, EMI), as well as reliability requirements are demanded by original equipment manufacturers.

The vehicle voltage varies from 8 V to 16 V, and by the vehicle battery that will supply

this voltage, it has to operate under harsh temperature conditions that may be in a desert or arctic region where the vehicle can be used. The automotive industry also requires the following extraordinary conditions; inverted or constant double battery voltage  $(-12 \ V \text{ or } +24 \ V)$ , jump-start situations, load-dump issue which happens when the battery is detached from the generator, and different voltage intermittent voltage conditions. A worst case is 28 V for 2 minutes. When the battery terminal is abruptly removed while the generator supplies current, the load-dump situation happens. This issue may last as long as a few seconds and can easily reach a hundred volt, however nowadays numerous producers have centralized clamping circuits, thus that parts should endure the voltage levels up to a hundred volts. In addition to higher voltage prerequisites, crank mechanism triggers lower voltage that need assurance for the worst-case scenario. A reverse polarity condition occurs when the battery line is connected to ground and the ground line to the battery supply. During the module handling and installation or when the vehicle has low battery the driver may connect cables incorrectly then the reverse polarity results. The necessity of safety and protection circuits such as open and short circuit protection, over and under voltage protection required by the standards or OEMs in the automotive industry can be provided with discrete circuit elements or integrated circuits (ICs) containing all of them. The lifetime of the component used in automotive environment must also be checked by inspection to meet the target life and guaranteed specifications of the vehicle manufacturer, which may be fifteen years or 300000 km [100]. Reliability of OLED has a great importance for the automotive rear lamps. Throughout the lamp lifetime, OLEDs experience electrical and different types of environmental stresses such as humidity and temperature.

Generally, automotive certification specifications are expressed in tests like the AEC-Q100 series for ICs from the Automotive Electronic Council, although stricter standards and even more testing could be needed by individual automotive vendors and car manufacturers. The three significant effects are the air temperature, power source and disturbance at the automobile lamp's seating system. While strict descriptions are given for these variables, such as the ISO16750 – 2 for the environmental stability norm, the ISO / DIS 12346 – 2007 for the electrical testing standard, and the AEC-Q100 – 1 for the mechanical stress requirements, these available norms can be at danger because of both the disparity between the motor and alternator in whole vehicles and the complexity and uncertainty that may occur between the vehicle, the human and the road being traveled.

#### 2.2.2 OLEDs in Automotive Lighting

The automotive lighting market is one of the most attractive markets for OLEDs, and they can be the next technological development after the LED technology. Like the point-source LED sister technology, the light is emitted as a function of the current through the device. OLED's current-voltage behavior is very similar to LEDs. However, the multi-layer organic structure and the bigger light emitting area produce a huge capacitive behavior with respect to their inorganic counterparts [13]. Some of the world's most well-known automobile manufacturers have developed vehicle designs that implement OLEDs in their rear stop lamps, as shown in Figure 2.9. The first OLED based tail lamp is used in 2016 [101]. With 15 glass-based non-bendable OLEDs per rear lamp and a brightness of  $1200 \ cd/m^2$ , the brightness levels are suitable for performing the position function.

Nowadays, due to the increasing safety requirements in the automotive industry, the car manufacturers require more and more complex and reliable electronics systems. Most automotive rear lamps are considered as safety devices and shall conform to the regulatory specifications pertaining to the color intensity regarding European Economic Commission (ECE-R128) and light emission (ECE R19). In addition, most automotive lamps have both minimum and maximum photo-metric light intensity level prerequisites for specific angles. Combined functions of the lamp also require an intensity ratio, as well. For instance, the intensity ratio between a stop function and position function in the tail lamp must be distinguishable by the human eye. OLEDs that are used in the automotive market complies with the above regulations of ECE, and they are suitable for realizing the position/stop light function (the dominant wavelength for red light must be minimum of 610 nm according to the ECE) in the rear lamp. Further innovative and technical moves are predicted to be the innovation of relatively high intensity level OLEDs for the implementation of various functions such as position indicators, center high-mounted brake light (CHMSL) or front lamp daytime running lights (DRL).

OLEDs have the potential to contribute significantly to our automotive lifestyles thanks to their dynamic functionality created by segmentation. These segments can be controlled separately, thus providing different "welcome home" and "leaving home" scenarios. Compared to other traditional lighting sources, with their unique physical structure to be bent into any conceivable shape and optical characteristics, some of the advantages[102] of OLED for automotive industry are:

- Good visibility, segmentation, and transparency (mirror-view in off-state),
- Shape freedom (bendable, flexible structures),



**Figure 2.9** Oled-based automotive tail lamps: (a) Bmw m4 [101], (b) Mercedes s-class coupe [104], (c)Audi a8 [105], and (d)Tt rs coupe [106]

- Allowing for 3D and depth effects,
- High uniformity.

OLEDs with these properties are superior to LEDs in automotive rear lamps. On the other hand temperature stability and mass production cost problems require further developments. Revenue for automotive lighting systems is expected to reach \$ 37.2 billion in 2023, and 85% of it will be coming from SSL technology [103]. The distribution of expected revenue is illustrated in Figure 2.10.

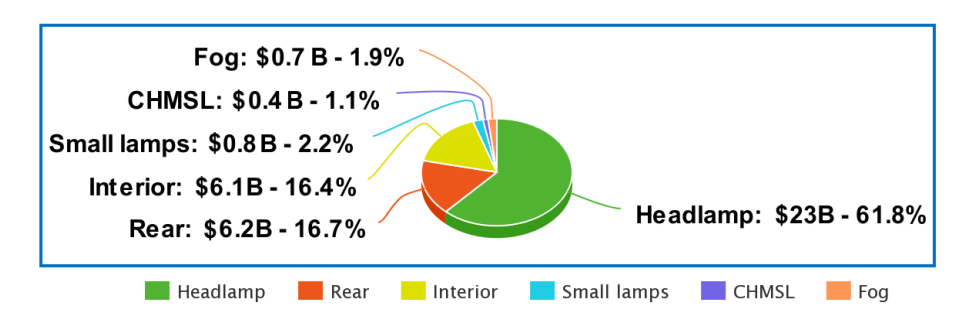


**Figure 2.10** Automotive lighting market forecast for 2023 (adapted from [103])

#### 2.2.3 Driving Methods: Current/ Voltage Mode

When powering OLED, it is essential to drive it with the current and not with the voltage. At [107] this is stated and experimentally proved that the relation between luminance and current is quasi-linear, which is not proportional to the operation voltage. This means that a small variation of the operation voltage will result in significantly high changes in the luminous output. The current-luminance characteristic is much more flat at the nominal operating point. As it is already mentioned, OLEDs have considerable parasitic capacitance due to its large emitting surface area. This parasitic capacitance can cause current spikes if a step voltage is applied. These spikes may damage device or reduce lifetime of OLED. Therefore, pulse width modulation (PWM) technique is also not recommended [108].

A single OLED cannot provide sufficient light output to implement lamp functions, a large array of OLED string consisting of series connected OLEDs can be used in a typical stop lamp. Serial connected OLED strings are the optimum option to get ideal current matching. As long as the current through all of the OLEDs is the same, they will have the same brightness. A constant current source automatically adjusts the output voltage to keep the output current stable and therefore the light output is constant. Another advantage is that the constant current driver does not cause any single OLED in the string to be over-driven and thus ensures that they have a long operation lifetime. Therefore, current controlled mode is the best solution for driving OLED devices. A constant current power supply with 125 *mA* is used in this study to avoid exceeding the current limit.

When the driver must control several OLEDs in series, conventional DC-DC converters are commonly used in vehicles. However, these bulky and heavy converters have the disadvantages of high EMI noise and large output ripple, due to use of big inductors and capacitors, because their size varies with the switching frequency [109]. Another solution to drive OLED lamps is to use linear drivers. They provide a simpler control and do not require electromagnetic interference (EMI) filters. However, their power dissipation can become excessive for higher power applications. The specific AEC-Q linear OLED drivers are currently not available on the market but typical AEC-Q linear LED drivers, which act like linear current sources, (such as Infineon TLD1313, ON Semiconductor NCV7680, Elmos E522.83, Texas Instruments TPS92830) can be used for driving OLEDs. The output currents of these drivers can be easily adjusted with one resistor. For the harsh automotive environments, several protection circuits such as under/over voltage, reverse polarity, over-current, short circuit and over temperature protection are already integrated into these ICs to prevent device failure under faulty conditions. As a result, a single linear AEC-Q LED/ OLED driver can cover the all

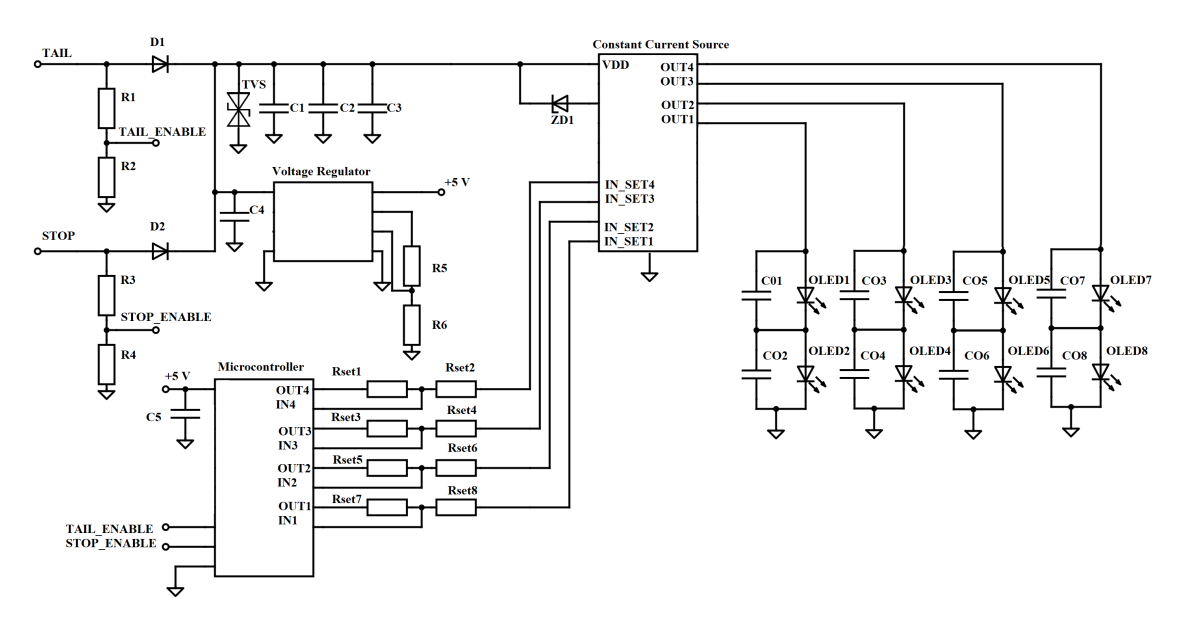


**Figure 2.11** A typical circuit schematic diagram of a multi-segment oled-based tail lamp

requirements of automotive applications.

A typical schematic of stop/tail function for OLED based rear lamp is given in Figure 2.11. Low-frequency ripple will be seen as flicker on the light output, so the current fluctuation on any power supply design should be taken in account. Parallel connected capacitance for each OLED device can be placed or the parasitic capacitance of OLED can be used as the output filter as it suggested at [110]. Dimming the light output between different brightness levels is a common requirement for exterior lighting. For example, stop / tail functions or low beam / high beam headlights are bi-level lighting. As shown in Figure 2.11 different functions with brighter and normal light output can use the same OLEDs. With different resistance values  $(R_{set1} \dots R_{set8})$ , the micro-controller can adjust the output current at two different levels via constant current source. From standard operation, the vehicle battery spectrum ranges from 8 V to 16 V (traditionally 13 V) to load the 12.6 V battery at operating temperatures from  $-40^{\circ}C$  to  $+125^{\circ}C$  and includes extreme circumstances such as reverse battery, constant double battery voltage, jump start situations to failure situations. To protect the circuit from these voltage transients and supply noise, transient-voltage-suppression (TVS) diode and parallel-connected capacitors (C1-C3) should be used.

## EXPERIMENTAL MEASUREMENTS

In this chapter, a brief information is given about the OLED samples used in electrical and optical tests. Afterwards, the measurement setup and environmental test conditions used for characterization and creating the OLED model are introduced.

## 3.1 The OLED Sample

During the experimental studies, OLED samples that are actively used in the rear stop lamp of BMW M4 [101] have been subjected to various tests. The OLED sample with red-emitting color is attached to a glass substrate having an approximate size of  $33 \times 80 \ mm^2$ . The device structure is shown in Figure 3.1. It is used to perform the position and stop functions on the OLED-based rear lamp.

Four AEC-Q OLED samples have been used to extract model parameters, characterization, and verify the reliability of the OLEDs. The samples are RoHS compliant with bottom-emitter technology. Interconnections have been made by flex PCB with the connectors. In this study, these OLED samples have been tested under electrical stress.

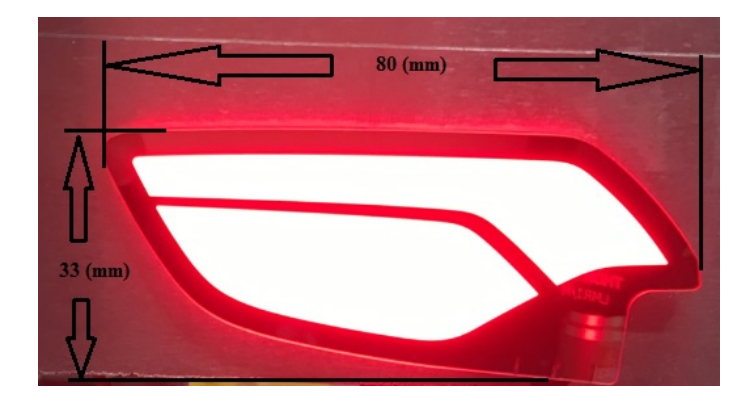


Figure 3.1 Photograph of the investigated oled sample

### 3.2 Test Setup

The device characteristics of interest are optical (luminance and dominant wavelength), and electrical (I-V characteristics, parasitic capacitance, threshold voltage shifting) performances before and after the aging process. The following parameters are observed during the experiments: threshold voltage, dominant wavelength and spectral shape, impedance, luminance, and intrinsic capacitance.

OLEDs are extremely sensitive to the temperature, and the lifetime of OLEDs decrease with an increase in junction temperature [45]. Therefore, the junction temperature should be considered during the design phases. For many automotive rear lamp applications, heat sinks are used to keep the junction temperature within prescribed limits [111], [112]. In order to exclude temperature effects from this work and and investigate the effects of pure electrical stress, the setup is located in a temperature-controlled room (at an ambient temperature of  $25^{\circ}C$  and 50% - 60% humidity rate) and covered with a closed black colored foam to prevent light leaks, as shown in Figure 3.2.

In order to keep the OLED device at the constant junction temperature, OLED is mounted on heat-sinks by thermally conductive tapes. Thermoelectric coolers (TECs) have also been mounted between two heat-sinks to transfer the heat from the OLED's back surface to the heat-sink, as shown in Figure 3.3. The average panel temperature of the OLED is  $30.4^{\circ}C$ .

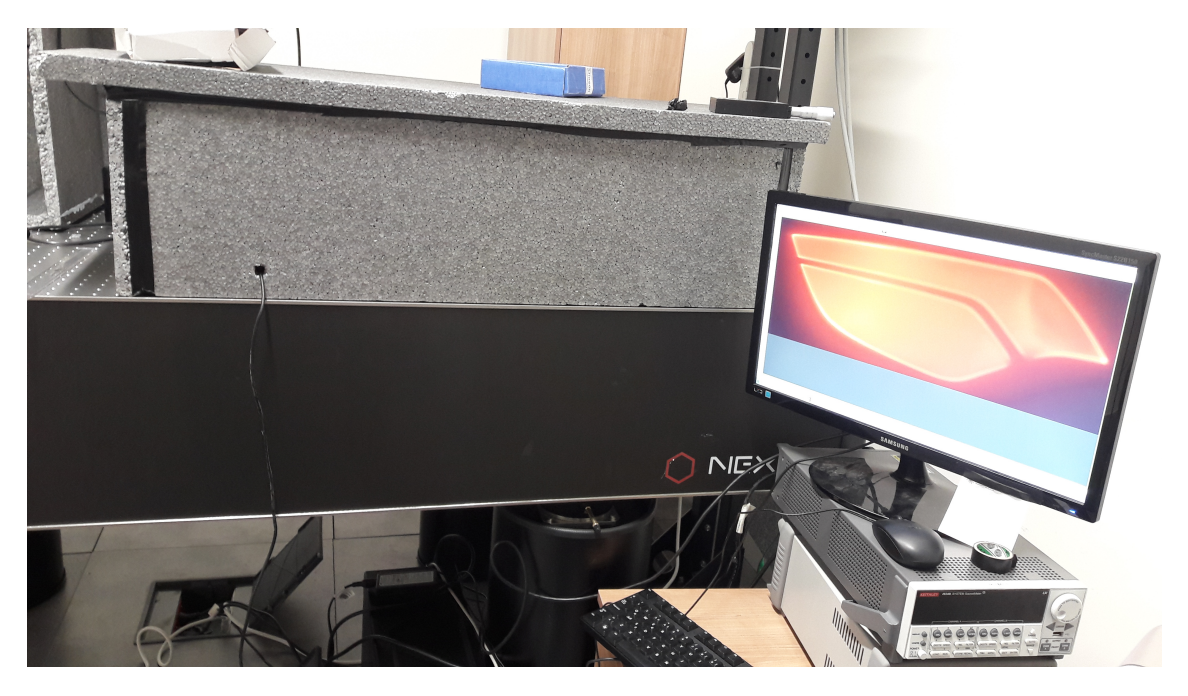


Figure 3.2 The test setup covered with black foam block

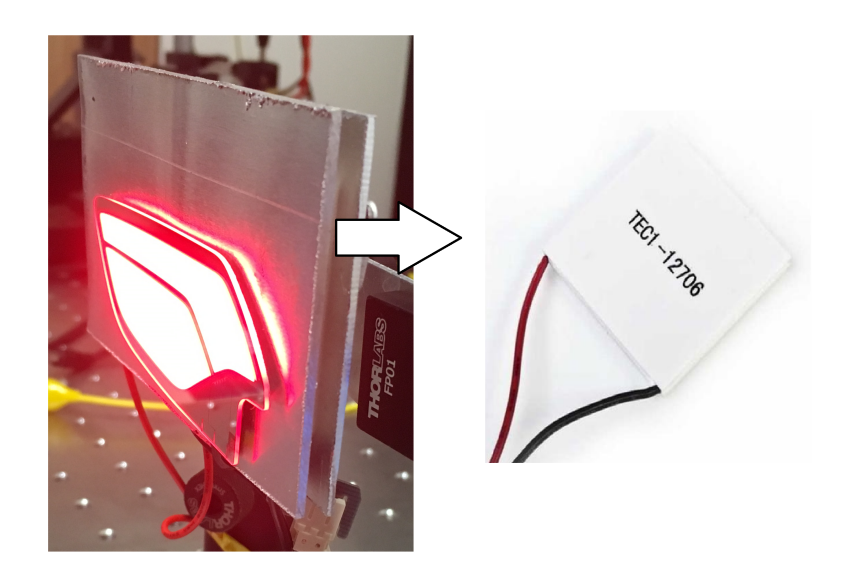


Figure 3.3 The heat-sinks and thermoelectric cooler

In the earlier studies [59],[56] luminance degradation has been continuously monitored and identified as an aging precursor for OLEDs, to estimate remaining lifetime. In this study, all of the above OLED parameters affected by electrical stress are investigated based on the data collected in the measurement set-up, as shown in Figure 3.4.

#### The setup consists of:

- 1. CMOS camera (Thorlabs DCC1545M-GL),
- 2. Imaging lens (Thorlabs LA1131, F = 50mm),
- 3. Spectrometer (Thorlabs CCS175/M) that is coupled into the fiber (Thorlabs FTO30),
- 4. The OLED sample mounted on thermoelectric cooler (TEC1-12706) and heat-sinks,
- 5. Keithley 2634B source meter unit (SMU).

The Thorlabs post products have been used in order to mount OLED-holder on the basement. An output of the Keithley 2634*B* SMU is used in current source mode and 125 *mA* constant current is applied to stress the devices. Another output of the SMU is utilized for the I-V measurements. The OLED images are mapped by the imaging lens onto the CMOS camera, and relative light intensity measurements are automated by the MATLAB scripts. The spectral shape and dominant wavelength are measured using

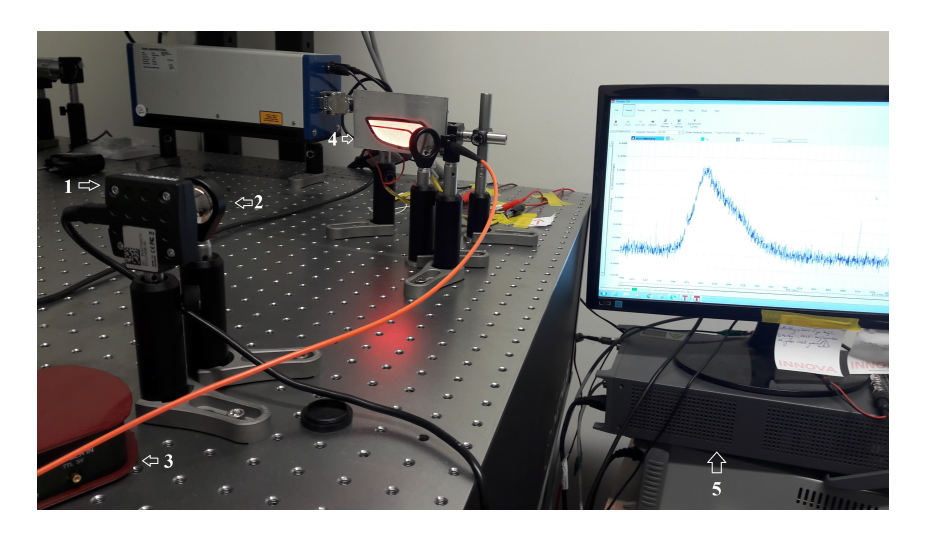


**Figure 3.4** The experimental test setup: (1) cmos camera, (2) imaging lens, (3) spectrometer, (4) the oled under test, (5) source-meter unit

the spectrometer. The capacitance-voltage (C-V) and capacitance-frequency (C-f) measurements have been completed on the Agilent B1500A semiconductor device analyzer.

# 4 CHARACTERIZATION AND MODELLING OF THE OLED DEVICE

In this chapter, to understand the operation of the OLED sample, main electrical and optical characteristics of the device are presented. Subsequently, by extracting model parameters, a SPICE compatible OLED model is introduced. Finally, simulation results of the proposed model are experimentally verified with the test results.

## 4.1 Electrical and Optical Characterization

This section describes the main electrical and optical characteristics of the sample device. The forward and reverse voltage-current, complex impedance, capacitance-voltage, capacitance-frequency, spectral shape, and chromatically coordinates are examined.

All measurements were carried out under an ambient condition of  $25^{\circ}C$  and 50%-60% humidity rate. The purpose of this experiment is to detect the effects of purely electrical stress. Thanks to heat-sinks and TECs, the average panel temperature of the OLED is measured as  $30.4^{\circ}C$  on a weekly basis, using an infrared thermometer. In order to accelerate the degradation of the OLED, more than  $\sim 25\%$  of the nominal current density is applied. Measurements were performed at regular intervals. The Illuminating Engineering Society's (IES) LM-80-08: Measuring Lumen Maintenance of LED Light Sources [IES 2008], prescribes an approved method for long-term measurement of LED packages. LM-80-08 requires that the chromaticity shift be measured throughout the test procedure, which must last a minimum of 6000 hours. The device ran at a constant current of 125~mA for continuous operation of 7040 hours at the ambient temperature and humidity. The test setup also is fullfilled the ISO 16750-2 DC reverse voltage standard. The test setup is completed by complying to these two standards.

In the first measurement, the forward current-voltage (I - V) characteristic of the

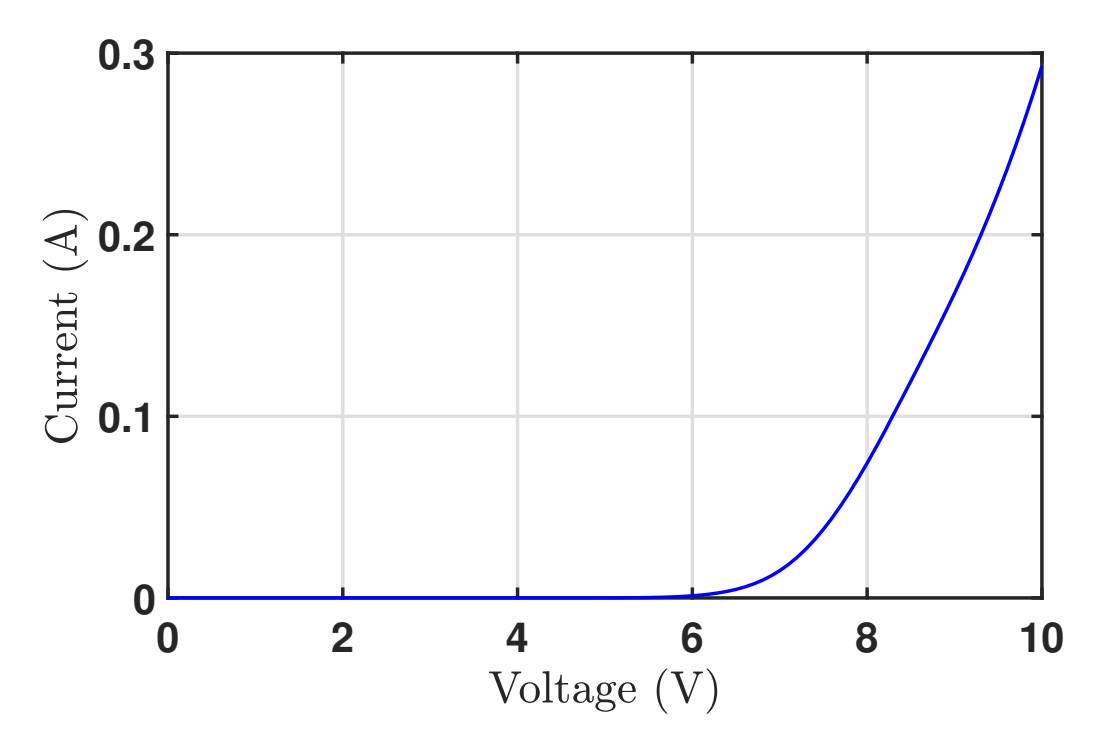


Figure 4.1 The forward current-voltage characteristic of the oled sample

OLED sample is observed. DC voltage, which is swept between 0 V -10 V, is applied to the electrodes while the current through the OLED is measured. The forward characteristic is given in Figure 4.1.

The threshold voltage,  $V_{th}$ , is an important parameter for characterizing the operation of OLEDs. In general it is the voltage at which the OLED begins to function in a useful manner (i.e. emits light). However, this definition must be very carefully specified so that the  $V_{th}$  for a given OLED is the same regardless of the equipment being used for measurement. Also,  $V_{th}$  should reflect the device physics of the OLED and should not depend on OLED parasitic.

The voltage at which brightness is detected is a poor definition for threshold voltage since it depends on the detection threshold of the light measuring equipment. This definition for  $V_{th}$  requires that the optical detector used in measurement be precisely calibrated. In this thesis, current–voltage values around light emitting operation range are carefully observed. The operation voltage and current points around the threshold voltage are given in Table 4.1. We observe a rapid increase in the current starts at a voltage around 4.2 V, which corresponds to the threshold voltage ( $V_{th}$ ).

During maintenance or service, the battery of the car is typically detached and reconnected. There is a probability of connecting the wires to the wrong terminals of the battery. In case of a reverse polarity condition, there could be significant damage

**Table 4.1** Operation points of the oled sample

Voltage (V)	Current (A)
3.8	$7.4905 \times 10^{-7}$
3.9	$7.651 \times 10^{-7}$
4	$7.826 \times 10^{-7}$
4.1	$7.969 \times 10^{-7}$
4.2	$1.275 \times 10^{-6}$
4.3	$1.754 \times 10^{-6}$
4.4	$2.805 \times 10^{-6}$
4.5	$4.6305 \times 10^{-6}$

to the electronic components. In order to experience breakdown for a semiconductor devices, a significant amount of reverse current should pass through it, which can cause a permanent destruction. The amount of this current depends on how well the semiconductor can convert the applied reverse voltage into current. Hence, the more conductive (in other words highly doped) the semiconductor becomes, the lower will be the reverse breakdown voltage of the diode. This is because even a smaller reverse voltage can yield a significant reverse current, enough to reach the breakdown limits. However, for an organic semiconductor, the conductivity is low; so, it is expected to have a large reverse breakdown voltage. In fact, the reverse voltage is not destructive to the OLED sample until the breakdown voltage at 32.2 *V* is reached, as shown in Figure 4.2.

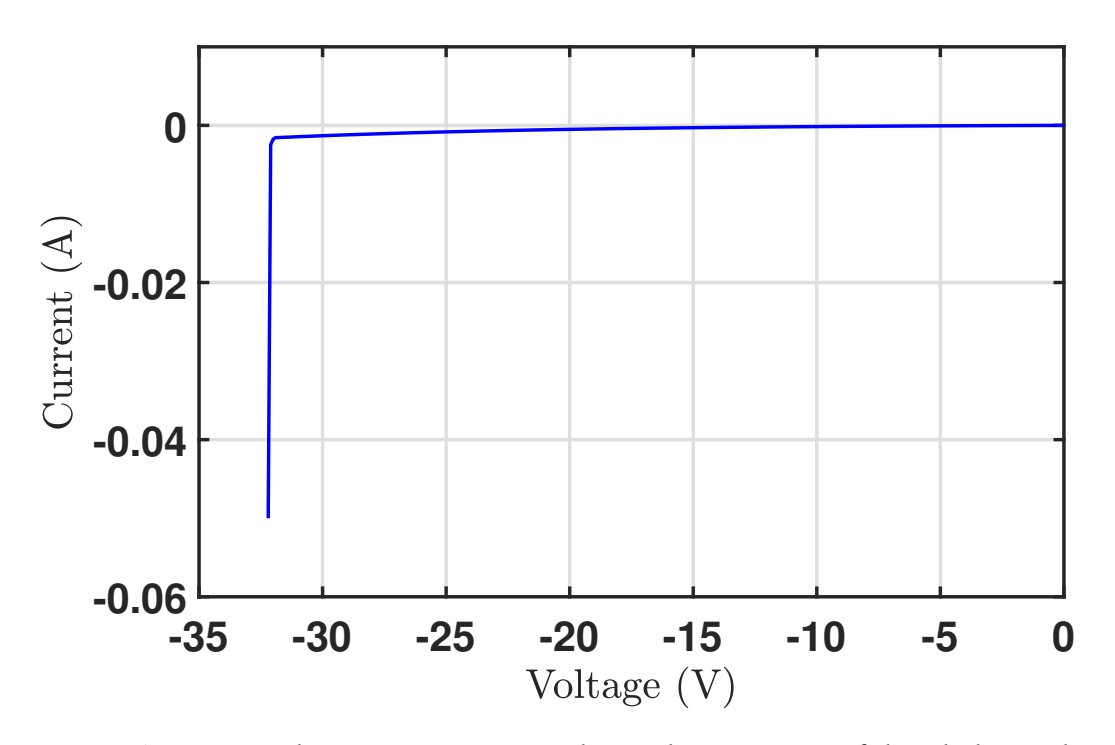


Figure 4.2 The reverse current-voltage characteristic of the oled sample

**Table 4.2** The Iso 16750 - 2:2012 reverse voltage parameters [113]

Nominal voltage (V)	Test voltage (V)
12	-14
24	-28

Due to the automotive operation standards, OLEDs are sometimes subject to reverse bias potentials, which they should properly withstand. We have observed that the reverse bias is not destructive until the breakdown voltage, and the OLED can resume its operation once it is again forward biased.

Regarding "ISO 16750 - 2: 2010 Road vehicles — Environmental conditions and testing for electrical and electronic equipment Part 2: Electrical loads" standard, for the system with  $12\ V$  battery, the DUT (device under test) must be able to withstand the reverse voltage of  $-14\ V$ . For the system with  $24\ V$  battery, the DUT must be able to withstand the reverse voltage of  $-28\ V$ . In order to facilitate the implementation of the model in SPICE simulations, the model should continuously provide the entire current-voltage relationship.

In the automotive environment, the DUT must be able to withstand the reverse voltage specified by the ISO 16750-2:2012 standard, as shown in Table 4.2. Therefore, the reverse-bias is critical to be captured by a SPICE model especially for automotive applications, even though OLEDs do not emit light in that operating region.

The IS method is used to examine the impedance of the OLED sample. A small sinusoidal AC voltage of 30 mV is superimposed on a DC bias voltage varying in the range from -3 V to 8 V with a step voltage of 0.1 V. The complex impedance and phase response are given in Figure 4.3. There are several equivalent representations of the impedance obtained by the impedance spectroscopy. In this study, C - V and C - f are investigated. In forward bias condition, the capacitance is increased by the effect of the majority charge carrier injection into the organic layers. At very low bias voltages, the organic semiconductor layers are completely depleted and the capacitance is almost constant, and does not depend on the operating voltage. In this range, the OLED space charge capacitance is dominant at reverse biasing, equal to the  $C_{geo}$  and expressed in the following equation:

$$C_{geo} = \frac{\varepsilon_0 \varepsilon_r A}{d} \tag{4.1}$$

where  $\epsilon_0$  is the permittivity of free space (8.8542 × 10<sup>-12</sup> F/m),  $\epsilon_r$  is the relative dielectric constant (3.5 for many organic semiconductors), A is the active area of the

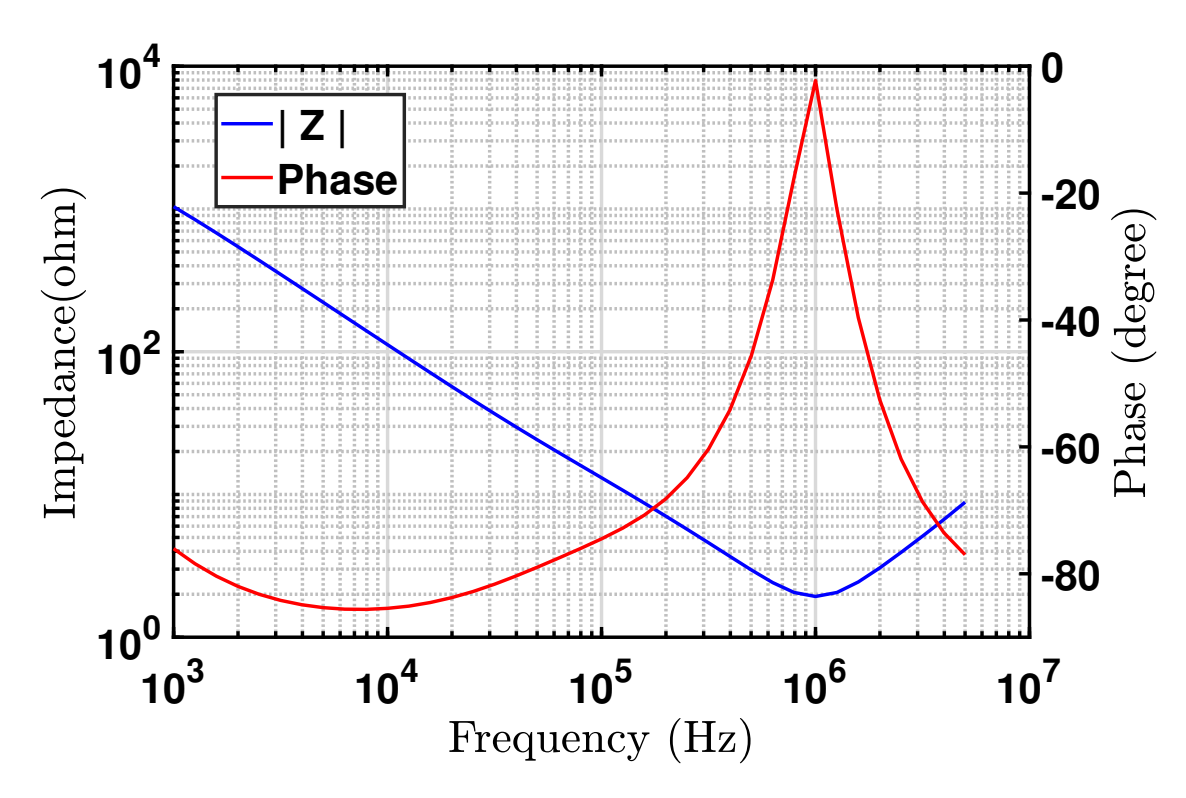


Figure 4.3 The impedance and phase response of the oled sample

device, and *d* is the thickness of the organic layers.

The measured capacitance of the OLED sample varies with operation frequency and biasing voltage, as shown in Figure 4.4 and 4.5 respectively. The capacitance stays nearly constant till a knee point where the charge injection begins, around 4 V (at the built-in voltage  $V_{bi}$ ). This carrier injection causes a sharp increase in the OLED capacitance, due to the effect of the diffusion capacitance ( $C_D$ ).

For the larger voltage values above the threshold voltage, a significant injection of electron and holes happens. As a result, radiative recombination occurs in the emissive layer, the capacitance reaches the maximum value and afterward, it decreases the OLED capacitance.

At higher frequencies, the behavior becomes a bit inductive, as shown in Figure 4.5. Negative capacitance is observed at higher frequencies. When the imaginary part of the impedance is positive, this implies inductance behavior. The observed negative capacitance, as an inductance can be caused by wiring in the test set-up or even by the electron injection [114], [115].

Electroluminescence measurements are obtained using a power supply and a fiber optic system. The increase in the radiation intensity of the OLED against both the

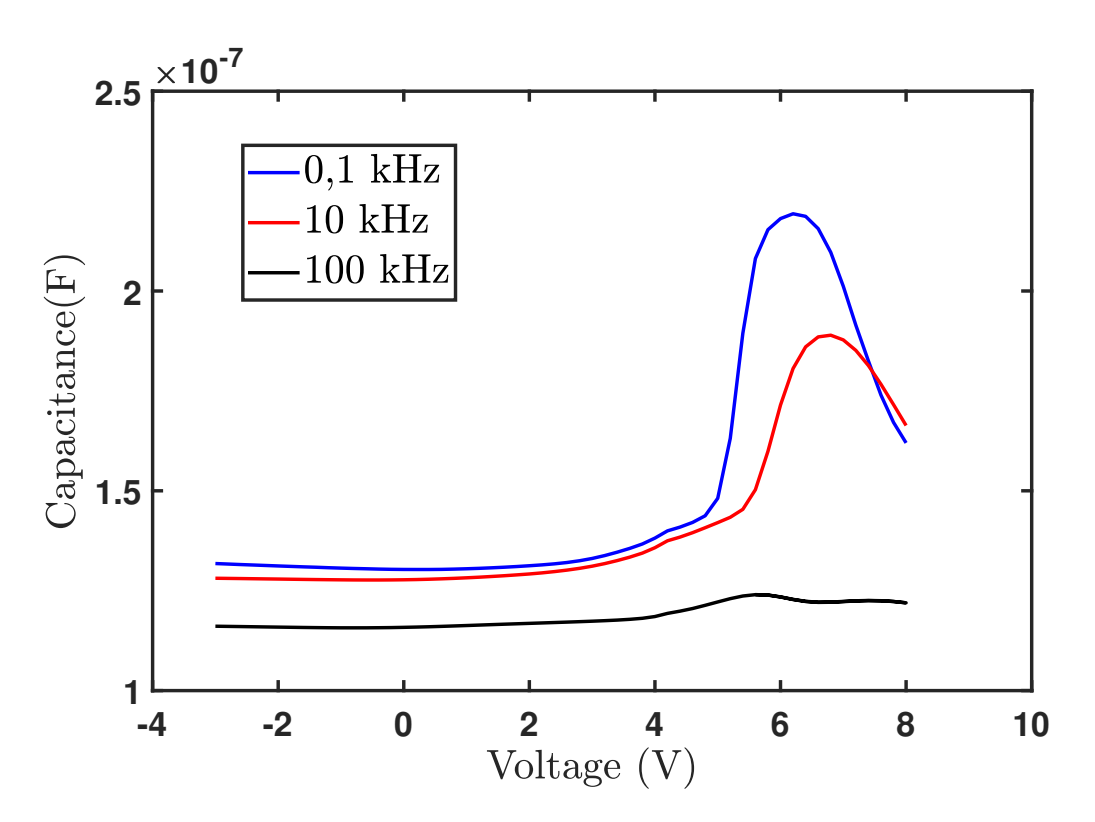
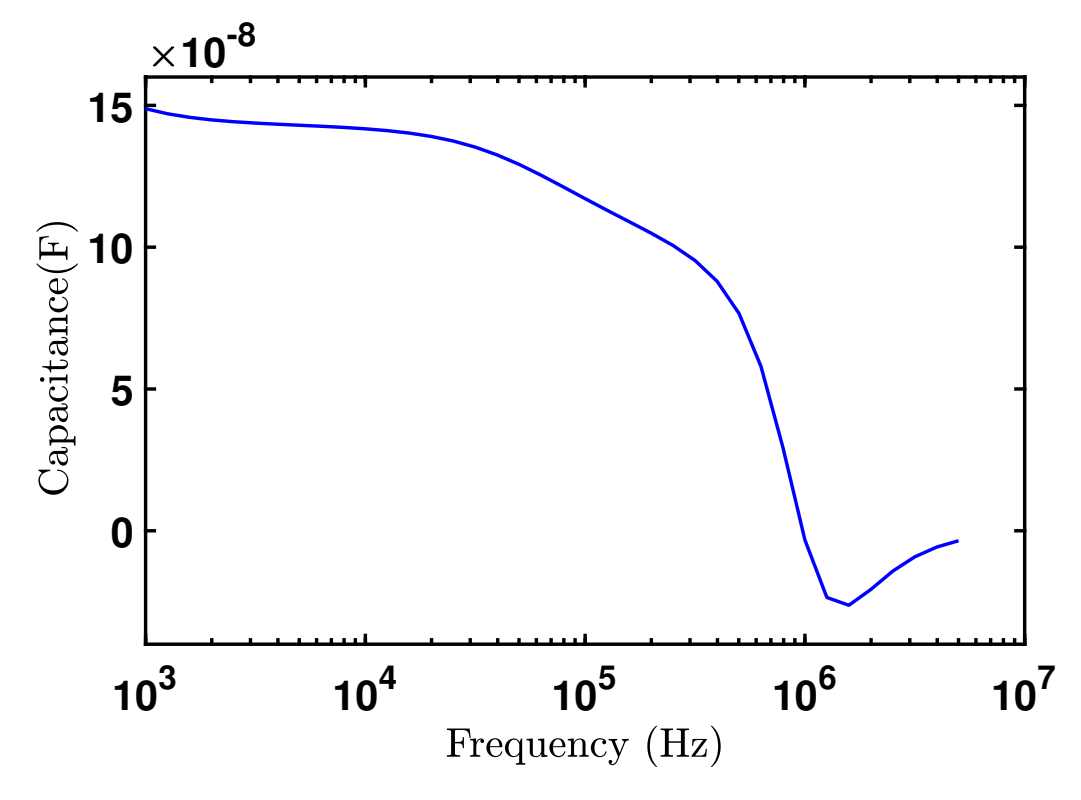


Figure 4.4 Capacitance versus applied voltage for the different frequencies



**Figure 4.5** Capacitance-frequency characteristic of the oled sample under 5 V bias condition

applied current and the applied voltage, together with the spectral range of the light are determined. The structure of the spectral curves at different biasing voltages should be the same indicating the device is operating properly. Typically, integrated sphere and spectrometer have been used for the optical characterization of OLEDs. In this thesis, an alternative low cost method based on image processing and Thorlabs CMOS camera that is relatively inexpensive has been proposed to observe the decrease in luminous intensity. The proposed method has been applied and tested on 7040 hours of test data taken over the OLED sample and has been observed that it works successfully.

Optical measurements are all carried out at room temperature in radiance mode with the spectrometer CCS175/M and CMOS camera. The light intensity, normalized by MATLAB to its initial value, is the parameter used to determine the lifetime of the OLED. The entire spectrum, as well as the dominant wavelength ( $\lambda_{dom} = 640.93 \ nm$ ) are measured, as shown in Figure 4.6.

Determination of color coordinates is important in terms of determining what the light emitted by OLEDs corresponds to which numerical value according to the standard. In order to determine the color coordinates known as the CIE index, the light emitted by the OLED in operation is measured with a spectrometer with color analysis and

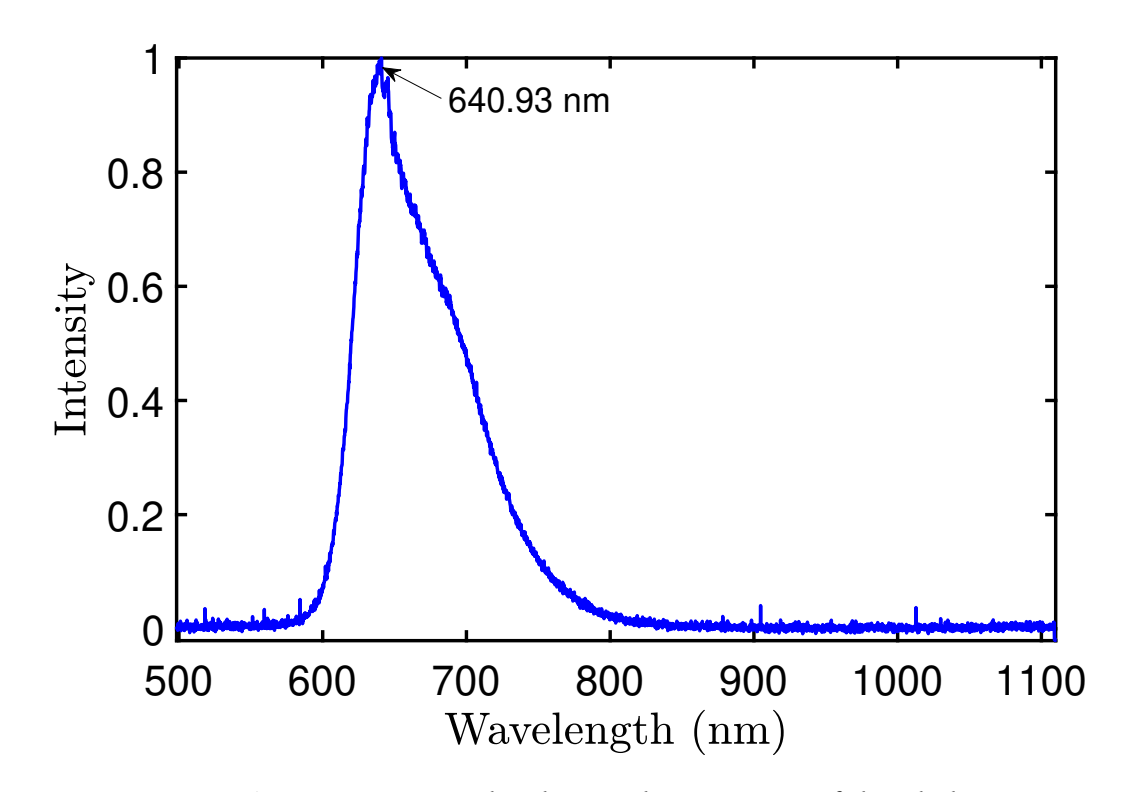


Figure 4.6 Spectral radiance characteristic of the oled

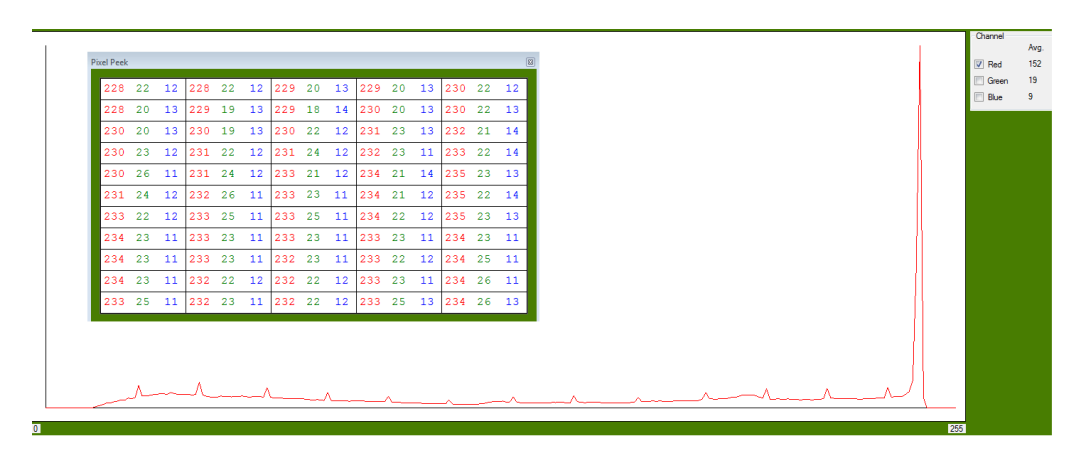


Figure 4.7 Pixel values and histogram of the oled

the x and y values are calculated as follow: x = 0.72, y = 0.28. In order to reduce the noise in spectra signal, a Gaussian filter has been applied to the original spectrum data. Histogram and pixel values of the red color emitting OLED sample are shown in Figure 4.7. Table 4.3 lists the main electrical and optical performance parameters of the sample device.

**Table 4.3** The main characteristics of the oled sample

Parameter	Value	Unit
Rated voltage	4.2	V
Rated current	$1.275 \cdot 10^{-6}$	A
Threshold voltage	4.2	V
Breakdown voltage	32.2	V
Device area	2640	$mm^2$
Dominant wavelength	640.93	nm
Chromaticity coordinates <i>x</i>	0.72	_
Chromaticity coordinates y	0.28	_

# 4.2 The Proposed Model

The typical single diode-based model [61] has the advantage of simplicity, but it suffers from the accuracy. Some SPICE compatible electrical OLED models [19],[62] only take into account the forward current-voltage behavior but reverse characteristic or capacitance behavior are not included. Some others [13], [38] include capacitance behavior as well but assuming that the OLED's intrinsic capacitance has a constant value and is not voltage-dependent. As discussed later, this assumption is not able to represent the device dynamics. The proposed electrical model is presented in Figure 4.8.

In the forward current-voltage characteristic, three main operation regions

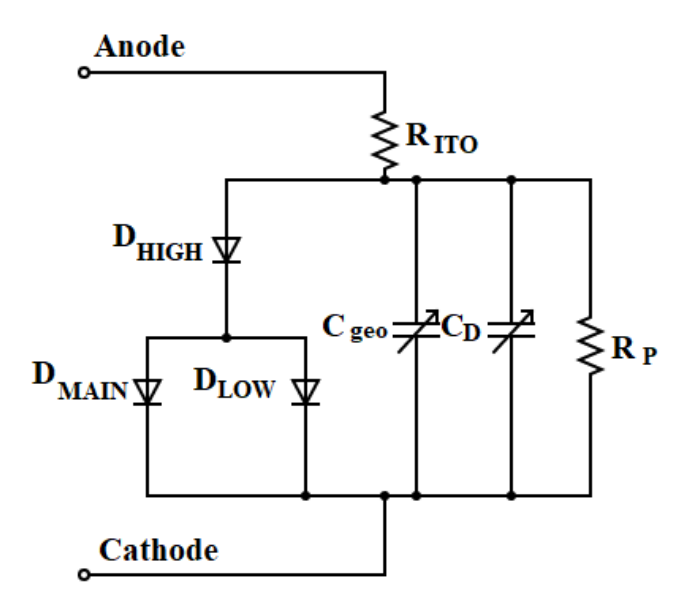


Figure 4.8 The proposed oled model

corresponding to the different slopes are observed. For the forward bias, this characteristic is distinguished as regions I-III to obtain an accurate model. The proposed electrical model consists of electrode resistance ( $R_{ITO}$ ) and leakage resistance ( $R_p$ ), geometric and diffusion capacitance ( $C_{geo}$  and  $C_D$ ), three diodes for forward and reverse regions.

## 4.3 Parameter Extraction and Modeling Results

The leakage resistance is particularly effective in the region I where the OLED's voltage is smaller than the threshold voltage. At very low operation voltages, there is a small leakage current limited by  $R_p$  when the OLED is OFF. To extract the parameter  $R_p$ , different data points are taken from the low injection region of the I-V curve. The inverse slope of I-V plot in the low injection region is estimated for the leakage resistance  $(R_p)$  by employing a linear regression method.

At low operation voltage due to depletion-recombination effects in the region I, the current is represented by  $D_{LOW}$ . The threshold voltage can be measured as the voltage value corresponding to the sudden change of the slope in the transition from the region I to II. The transition from the region I to region II can be seen from Table 4.1. We observe a rapid increase in the current starting at a voltage around 4.2 V at the intersection of the region I and II, which corresponds to the threshold voltage  $(V_{th})$ .  $D_{MAIN}$  models the current behavior in the middle region.

As the current-voltage curve begins to follow a concave shape in the linear scale, the characteristic switches from the region II to III. The high injection represents the

luminance operation region when the device starts to emit light.  $D_{HIGH}$  represents the behavior at high injection region. At higher current levels greater than 170 mA in region III, the voltage drop across the series resistance  $R_{ITO}$  becomes dominant.  $R_{ITO}$  is determined in region III by the same procedure as the leakage resistance. Neglecting high current effects, i.e.  $R_{ITO} = 0$  and the OLED's current-voltage characteristic in active region can be modeled by the Shockley general diode equation as given below [116]:

$$I_{D} = I_{S}(exp(\frac{V_{D}}{nV_{T}}) - 1)$$
(4.2)

where  $I_S$  is the saturation (leakage) current, n is an empirical ideality factor,  $V_T$  is the thermal voltage which is approximately 26 mV at room temperature. If we apply logarithmic transform and neglect the term -1 in equation (1) we obtain the following equation:

$$log(I_D) = log(I_S) + \frac{V_D}{nV_T} log(e)$$
(4.3)

This is an equation of the type of y = mx + b; thus we can calculate the slope and y-intersection of the fitted line. The model parameters  $I_S$  and n are calculated from each individual diode range using these equations. Figure 4.9 shows the measured and simulated data with the proposed model for the forward I - V characteristic of the OLED device, in both the linear and semi-logarithmic scale.

Based on the semi-logarithmic I-V plot, it can be observed that the model results deviate from the experimental outcomes below 2 V. In the proposed model, the leakage resistance (off-state) is assumed to be constant, instead of a function of current or voltage. The term -1 in the equation (4.2) is directly ignored by the logarithmic transformation, which may lead to an increase in the relative error with the low voltage injection. Note that this region is far from the nominal operating voltage/current for the lighting applications. Nevertheless, since the current levels are already below micro-ampere levels, the overall accuracy of the proposed model is hardly affected by that error. By recognizing the typical operation voltage range of the lighting applications, there is a general agreement between the measured and simulated results, with a maximum relative error of 5.82% and the mean relative error of 1.51%.

For the SPICE model, reverse current-voltage characteristic is modelled by the following parameters:  $I_s$  which is constant, the breakdown voltage, specified as parameter BV, and with the current at breakdown voltage of IBV. Until the

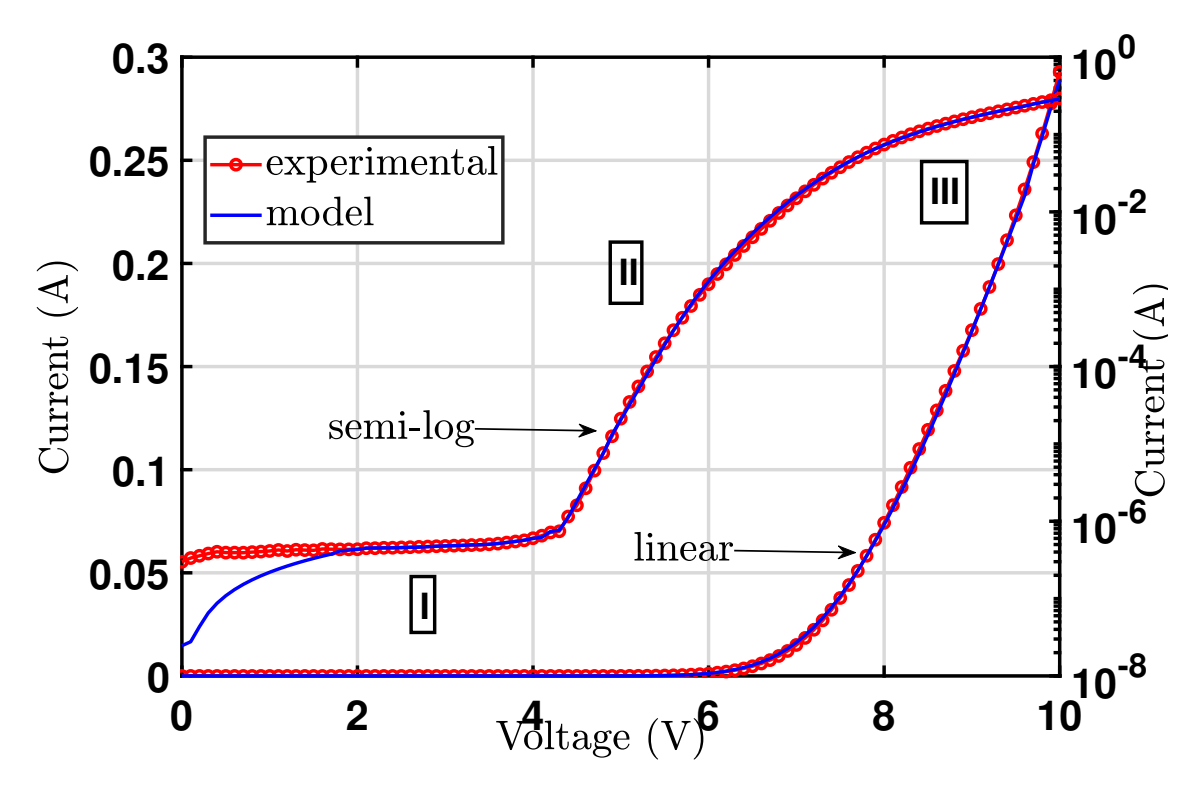


Figure 4.9 The forward I-V characteristic plotted in linear and semi-logarithmic scale

breakdown voltage (32.2 *V*), the reverse bias is not destructive. As shown in the Figure 4.10, taken from the Agilent B1500A semiconductor device analyzer, it can be observed that after reverse bias, the OLED can resume its operation once it is again forward biased.

When the device is applied to the reverse bias breakdown voltage, however, the OLED could get damaged. We have also observed the hard breakdown characteristic at the breakdown voltage for the sample. This process is irreversible, and the device does not work anymore. The current after a breakdown is modelled with the following equation:

$$I_{OLED} = -I_S(exp - (\frac{BV + V_{OLED}}{V_T}) - 1 + \frac{BV}{V_T})$$
 (4.4)

The reverse I-V characteristic is shown in Figure 4.11 with maximum relative error of 14.48% and the mean relative error of 6.16%. Impedance characteristics can be used to characterize electronic circuits, components.

Impedance spectroscopy [43] is used to analyze the intrinsic capacitance as a function of frequency and operation voltage. The geometric capacitance is modeled by SPICE with the parameters CJ0,  $V_J$ , M, and FC [116].

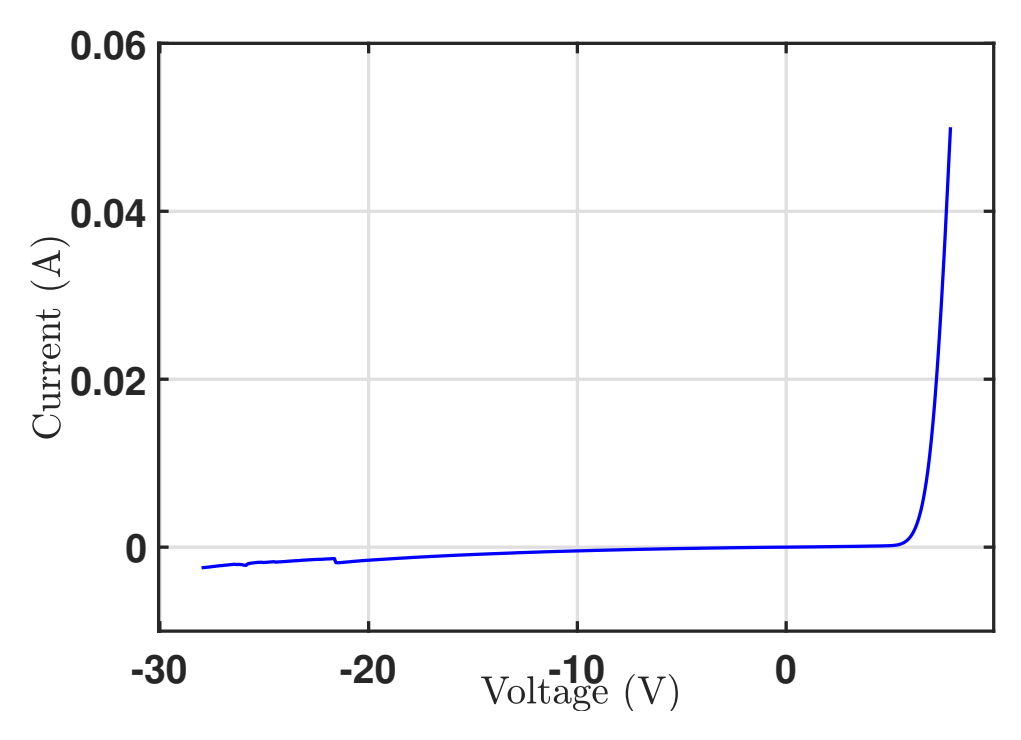
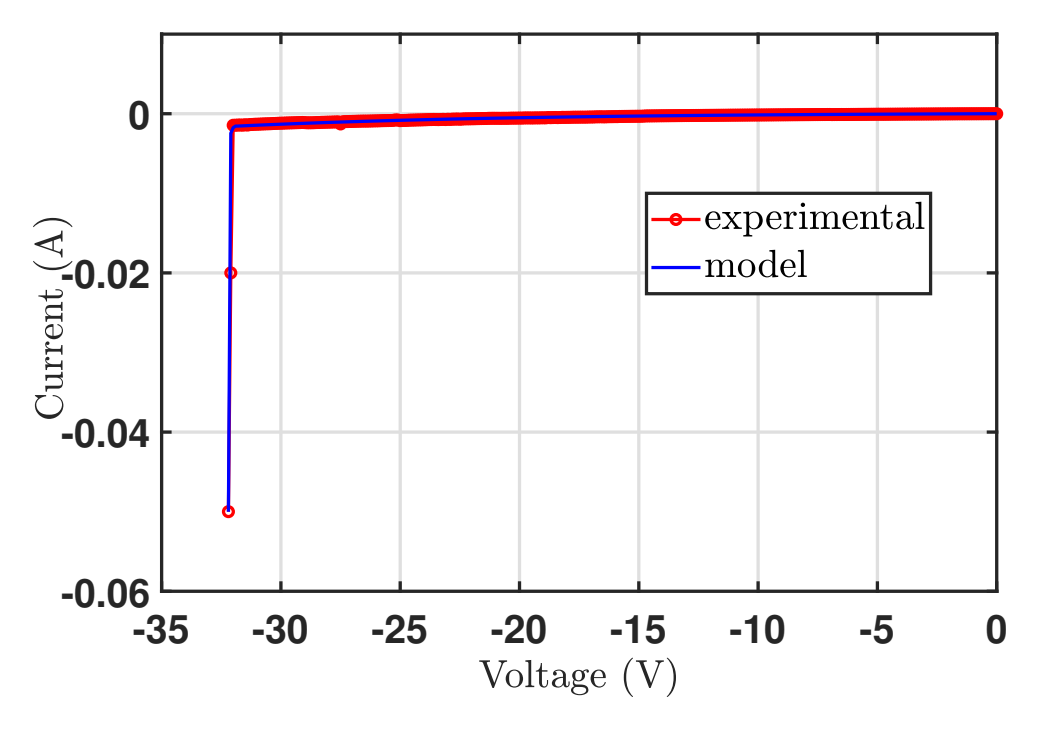


Figure 4.10 Reverse voltage characteristic of the oled shows that the reverse voltage is not destructive until the  $V_{b\nu}$ 



**Figure 4.11** Comparison of the simulated and measured reverse voltage characteristics

Two regions of C - V operation describe the capacitive behavior as given below:

• For 
$$V_{OLED} < FC \cdot V_J$$
 
$$C_{geo} = CJ0(1 - \frac{V_{OLED}}{V_J})^{-M} \tag{4.5}$$

• For  $V_{OLED} \ge FC \cdot V_J$ 

$$C_{geo} = \frac{CJ0}{(1 - FC)^{M+1}} (1 - FC(M+1) + \frac{MV_{OLED}}{V_J})$$
(4.6)

Taking the natural logarithm of 4.5 yields:

$$ln(C_{geo}) = ln(CJ0) - M \cdot ln(1 - \frac{V_{OLED}}{V_J})$$
 (4.7)

This is the equation of a straight line of y = mx + b. The parameter CJO is the zero-bias junction capacitance and the built-in potential  $V_j$  models the slope of the junction capacitance versus voltage characteristics curve in the forward region.

The parameter M is a grading exponent that is used to change the slope of C - V curve at reverse biasing. The parameter FC is set to the default value of 0.5. Diffusion capacitance is modeled by the forward transit time parameter (TT) and the conductance  $(g_{OLED})$  of the OLED as follow:

$$C_D = TT \cdot g_{OLED} \tag{4.8}$$

$$g_{OLED} = \frac{\delta i_{OLED}}{\delta \nu_{OLED}} \tag{4.9}$$

where  $\delta i_{OLED}$  represents a change in the OLED current caused by a small change in the OLED voltage  $\delta v_{OLED}$  at a specific point. The transit time parameter is measured from pulsed voltage time-delay measurements at 6.2 V corresponding to the peak value of the capacity.

The capacitance versus voltage characteristic curves (at  $0.1 \ kHz$ ) for simulated and experimental data are shown in Figure 4.12 with maximum relative error of 17.67% and the mean relative error of 4.21%.

In this study, C - V and C - f are investigated. The complex impedance ( $Z_{OLED}$ ) consisting of a capacitor ( $C_{OLED}$ ) and a resistor ( $R_p$ ) in parallel connected with a series

resistance  $(R_{ITO})$  is given by:

$$C_{OLED} = C_{geo} + C_D (4.10)$$

$$Z_{OLED} = R_{ITO} + \frac{R_p - jwR_p^2 C_{OLED}}{1 + w^2 R_p^2 C_{OLED}^2}$$
(4.11)

$$Re\{Z_{OLED}\} = R_{ITO} + \frac{R_p}{1 + w^2 R_p^2 C_{OLED}^2}$$
 (4.12)

$$Im\{Z_{OLED}\} = -\frac{R_p^2 C_p^2 w}{1 + w^2 R_p^2 C_{OLED}^2}$$
 (4.13)

$$\theta = tan^{-1} \left( \frac{Im\{Z_{OLED}\}}{Re\{Z_{OLED}\}} \right) \tag{4.14}$$

The results of the SPICE model's capacitance values show a similarity to the capacitance of measurement data, especially in the reverse–bias and low voltage-bias regions. However, the capacitance calculated near  $V_J$  tends to approach inaccurate values.

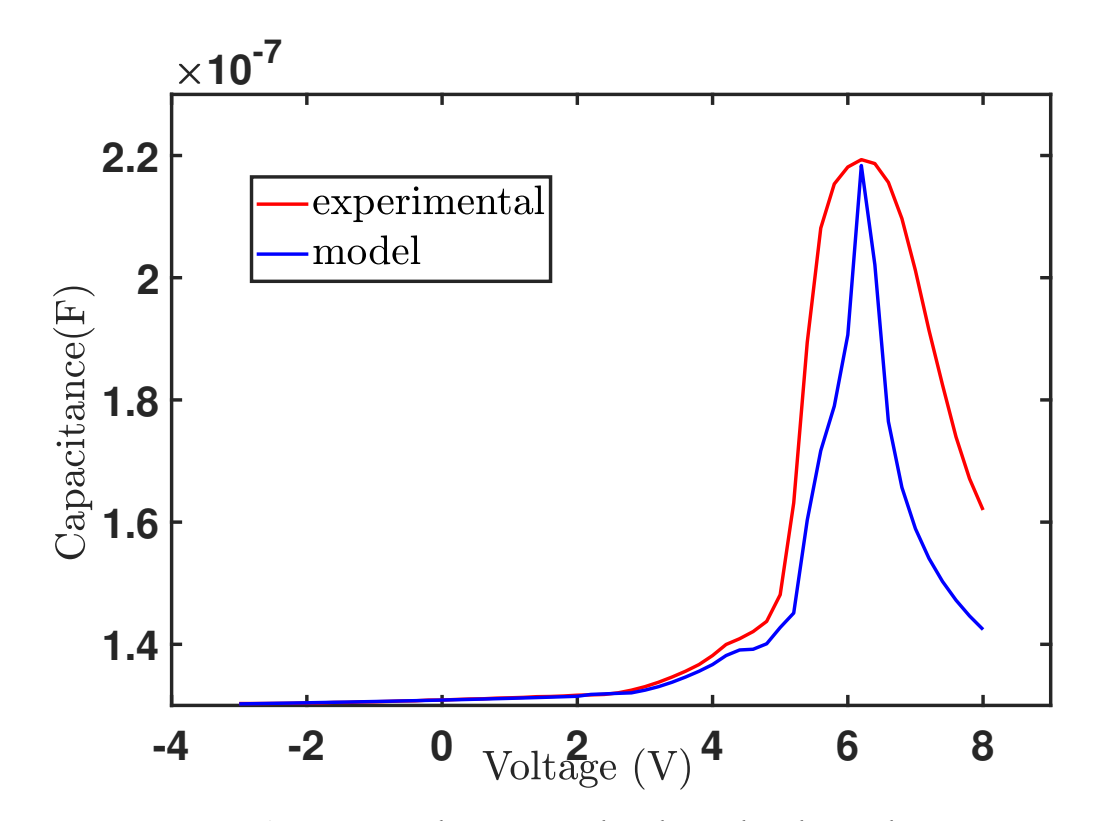


Figure 4.12 The measured and simulated C-V plots

**Table 4.4** The model parameters

Parameter	Description		Value
$R_p$	Leakage resistance	$k\Omega$	73.37
$R_{ITO}$	Electrode resistance	Ω	5.12
$n_{LOW}$	Emission coefficient for $D_{LOW}$	-	1542
$I_{s_{LOW}}$	Saturation current for $D_{LOW}$	Α	$8.631 \times 10^{-6}$
$n_{MAIN}$	Emission coefficient for $D_{MAIN}$	-	8.089
$I_{s_{MAIN}}$	Saturation current for $D_{MAIN}$	Α	$819.6 \times 10^{-15}$
$n_{HIGH}$	Emission coefficient for $D_{HIGH}$	-	7.5
$I_{s_{HIGH}}$	Saturation current for $D_{HIGH}$	Α	$1.504 \times 10^{-3}$
FC	Forward capacitance coefficient	-	0.5
TT	Forward transit time	ns	1
CJ0	Zero-bias junction capacitance	F	$1.308 \times 10^{-7}$
$V_J$	Built-in potential	V	4.3
M	Junction capacitance grading exponent	-	0.00123
BV	Reverse breakdown voltage	V	32.2
IBV	Current at reverse breakdown	A	$49.8 \times 10^{-3}$

The diffusion capacitance behavior has a proportional increase in capacitance with current since the transit time parameter is assumed to be constant in the proposed model. For the real behavior, however, TT is known to decrease at higher voltage levels ( $TT = L^2/(\mu \times V_{DC})$ ), where L is the thickness of the active layers,  $\mu$  is the mobility) [117].

Thus, the capacitance behavior typically deviates from the experimental behavior. The calculated SPICE parameters for the proposed model of the OLED are given in Table 4.4.

As a result, the simulated and measurement results are in close agreement within the acceptable error rates. Different types of OLED models including electrical, optical, and thermal can be found in the literature. Based on the electrical models in the literature, some models incorrectly assume the parasitic capacitance of OLED as constant.

Some models are only analytical and not compatible with SPICE simulators. And the reverse polarization characteristic of OLED, which is an important feature for automotive applications, is not included in these models. The proposed model is compared with other electrical models along with their features in Table 4.5 for the comparative study.

 Table 4.5 Comparison of the proposed oled model with the previously reported models

Ref.	Complexity	Components	SPICE Model	Capacitive Behavior	Reverse Characteristic	Accuracy
[13]	High	3 diodes, 4 resistors, 2 capacitances, 2 voltage sources	No	Included with fixed values	Not incl.	Error = 6.1%
[17]	High	Analytical model	No	Not incl.	Not incl.	Not specified
[19]	High	Analytical model	No	Not incl.	Not incl.	Not specified
[20]	High	Analytical model	No	Not incl.	Not incl.	Not specified
[27]	High	1 diode, 2 resistors, 1 capacitance	Yes	Included with fixed value	Not incl.	Not specified
[28]	Low	2 resistors, 1 capacitance	No	Included with variable values	Not incl.	Not specified
[31]	Low	2 resistors, 1 capacitance	No	Included with fixed value	Not incl.	Not specified
[33]	High	2 diodes, 2 resistors, 1 capacitance	Yes	Included with fixed value	Not incl.	Error < 8%
[38]	Low	1 diode, 1 capacitance, 2 resistors, 1 variable resistor, 1 voltage source	No	Included with fixed value	Not incl.	Error = 11%
[40]	Low	3 resistors, 2 capacitance	No	Included with fixed value	Not incl.	Not specified
[47]	Low	2 piece-wise linear voltage sources, 1 inductor, 1 resistor	No	Included with look-up table	Not incl.	Error < 2%
[48]	High	Analytical model	No	Not incl.	Not incl.	Error = 4.2%
[49]	High	1 diode, 1 dependent voltage source, 3 resistors, 1 capacitance	No	Not incl.	Not incl.	Error = 13.56%
[62]	Low	1 diode, 1 variable resistor, 1 voltage source	Yes	Not incl.	Not incl.	Not specified
[118]	Low	2 diodes, 1 voltage source	Yes	Not incl.	Not incl.	Not specified
[119]	Low	1 diode, 2 fixed, and 1 variable resistors, 1 capacitance	Yes	Included with fixed value	Not incl.	<i>Error</i> = 3.82%
This study	High	3 diodes, 2 resistors, 2 variable capacitances	Yes	Included with variable values	Included	$Err_{fwd} = 1.5\% \ Err_{rev} = 6.16\%$

# 4.4 Application Circuit: OLED Based Stop/Tail Light

A typical rear lamp has five functions including tail light, brake (stop) light, turn signal, fog and reverse light. Brake lights and tail lights are red and installed in all vehicles. When the vehicle headlights are turned on, power is normally fed to the taillight circuits. And for many automobiles, the same set of LEDs / OLEDs illuminate both tail lights and brake lights.

The light source must therefore operate at two different brightness levels: full brightness for braking, and lower level of that brightness (dimmed) for the tail lights. It is possible to dim the light source in two ways: analog dimming and digital dimming with pulse-width modulation. Analog dimming adjusts the light output only by changing the DC current on the string while PWM dimming has the same effect by changing the duty-cycle of a fixed current in the string such that the average string current is changed effectively. Some of applications require a wide-range of brightness control, spurring a demand for products that offer PWM-based brightness control. However, automotive tail/stop light control demands only two different brightness level.

In this study, it is assumed that the tail and stop functions consist of six OLED panels and the same four set of them will be used for the both functions. A model file and schematic symbol of the OLED sample are created in ORCAD Pspice v16.6 for the simulations, as shown in Figure 4.13.

The application circuit is designed as a complete solution for an automotive tail lamp. The application circuit includes reverse battery, over- voltage, short circuit, and ESD protection. The designed circuit can operate over the full range of automotive battery conditions  $(8-16\ V)$ . The circuit is designed to be compliant with the radiated and conducted-emissions automotive EMI standards. All active and passive components are chosen as AEC-Qualified products.

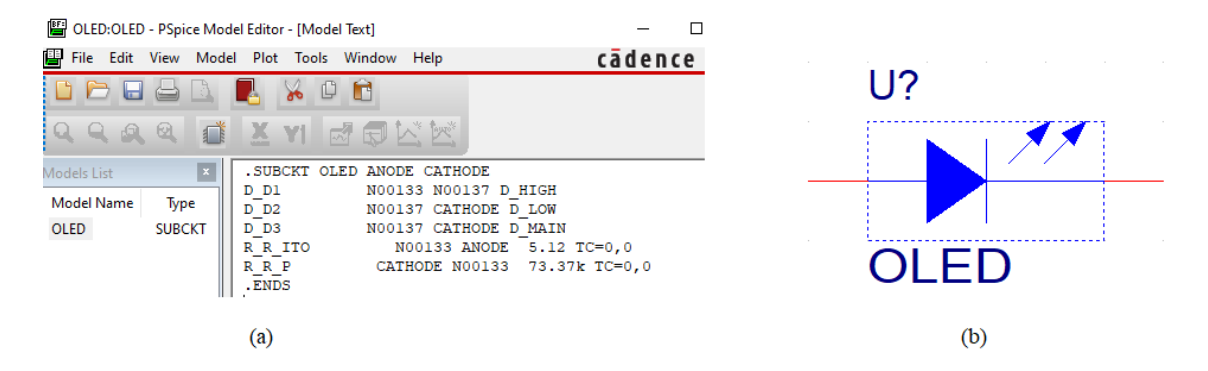


Figure 4.13 (a) The model card and (b) schematic symbol of the oled sample

The functions of tail light and brake light are controlled by the Infineon TLD2314EL which is a three channel high side driver AEC-Q IC. It is assumed that six OLED panels are driven at  $\approx 30$  mA when the tail function is active. And, when the stop signal is high (while breaking), the four OLED panels are driven at  $\approx 120$  mA. The designed application circuit is given Figure 4.14.

The output current of each channel can be adjusted independently. The current adjustment can be done by placing a low power resistor( $R_{SET}$ ) at the  $IN_{SETx}$  pin to ground. The output current of the channel can be calculated using the formula below:

$$I_{out} = \frac{k}{R_{SET}} \tag{4.15}$$

The typical value of the gain factor k is 750, and it can be in the range of 645 – 855 [120]. The output current is adjustable via external low power resistor and it is possible to connect PTC resistor for over temperature protection. This is the key to develop a tail/stop light circuit that increase the light intensity as the brakes are applied. The output current is transferred through parallel resistors.

The schematic of the application circuit is given in Figure 4.14. The supply inputs for stop and tail lights are connected to the circuit through diodes D1 and D2. These diodes provide protection against any reverse voltages that might be present on the vehicle supply bus. U1 and U2 are transient-voltage-suppressors (TVS) and placed to save the circuit from the sudden spikes in voltage or current. The TVS devices are placed in parallel to the circuit to protect the electronic components from over-voltage.

The input filter capacitors C1-C8 bypass any noise spikes that may be present on the power supply line. Low frequency noise requires larger electrolytic capacitors, while high frequency power supply noise is reduced with low inductance surface mount ceramic capacitors. As the frequency increase, the impedance will start to rise due to the equivalent series inductance (ESL) of the capacitor. The location and width of the resonance frequency vary with capacitor construction, dielectric and capacitance value. This is why different values of capacitors are connected in parallel with the supply lines. The self-resonant frequency of the capacitor is expressed in the following equation:

$$f_{resonance} = \frac{1}{2\pi\sqrt{ESL \cdot C}} \tag{4.16}$$

For EMI improvement, R4, C9 - C16 are placed. The driver IC has open-load and

short-circuit to ground diagnosis feature. The diagnosis enables (DEN) pin is used to activate or deactivate the device internal diagnosis functions. As per the manufacturer recommendation, a zener diode (D3) is connected between DEN pin and supply line.

When only tail signal is active,  $IN_{SET1-3}$  pins see 25  $k\Omega$  resistance. When the stop signal is active, the Q1 transistor decrease the resistance seen by  $IN_{SET1-2}$  pins. Thus, the current of U9-U12 increases, and the brake lamp provides more brightness. The components used in the circuit are listed in the in Table 4.6.

As can be seen from the simulation results in Figure 4.15, each time the brake signal comes, the currents of four OLED strings increases to 120 *mA*. In tail mode operation, OLED strings are driven at 30 *mA*.

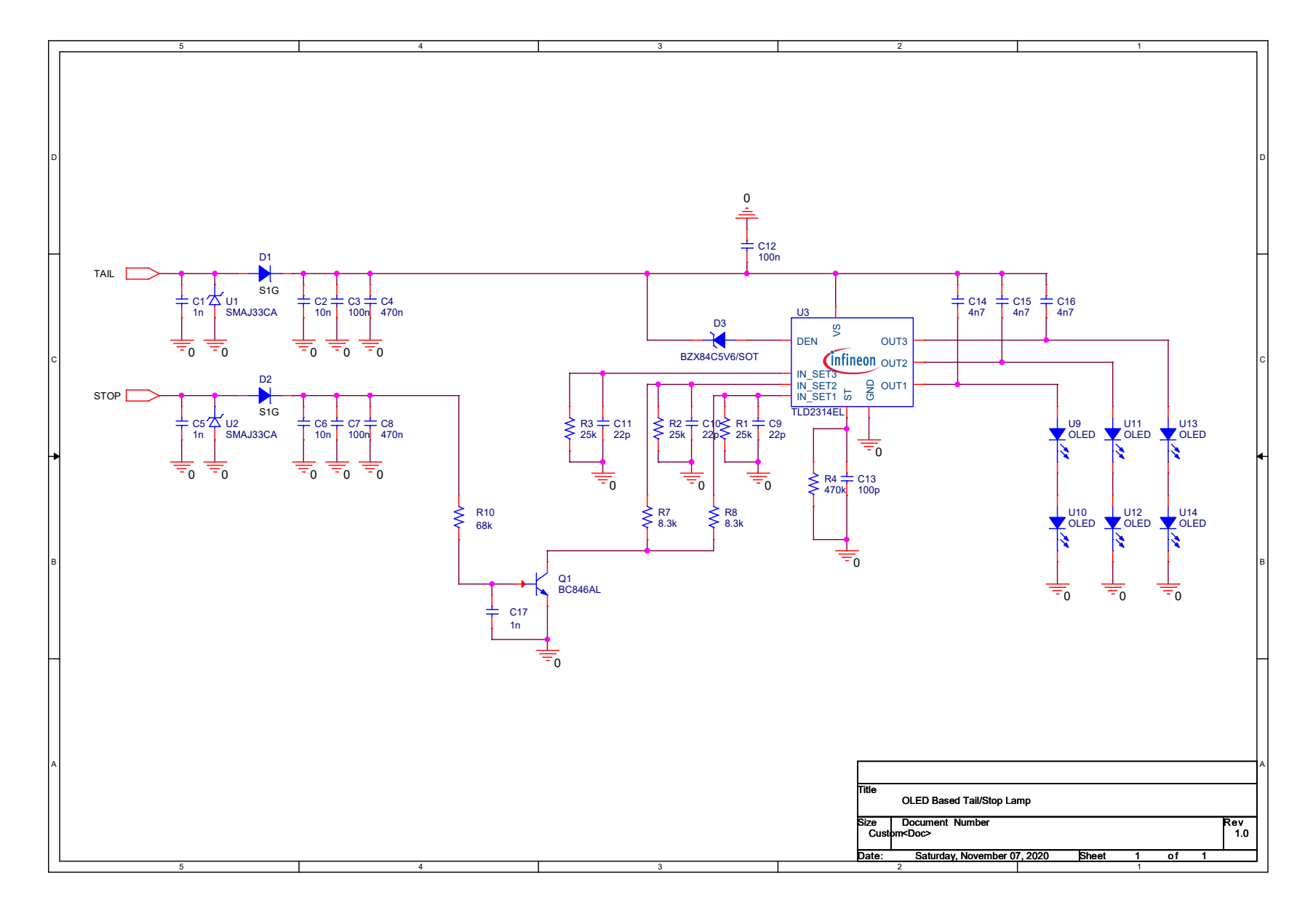


**Figure 4.14** The schematic view of the application circuit: tail/stop light

**Table 4.6** The bill of material (bom) of the application circuit

Designator	Quantity	Description	Value	Package	Manufacturer part number
C9-C11	3	Surface mount multi-layer ceramic chip capacitors X7R dielectric	22 pF	0603	C0603C220K5RACAUTO
C13	1	Surface mount multi-layer ceramic chip capacitors <i>X7R</i> dielectric	100 <i>pF</i>	0402	C0402C101J5RACAUTO
C1, C5, C17	3	Surface mount multi-layer ceramic chip capacitors <i>X7R</i> dielectric		0603	C0603C102J5RACAUTO
C14 - C16	3	Surface mount multi-layer ceramic chip capacitors <i>X7R</i> dielectric		0603	C0603C472K5RACAUTO
C2, C6	2	Surface mount multi-layer ceramic chip capacitors <i>X7R</i> dielectric	10 nF	0603	C0603C103J5RACAUTO
C3, C7, C12	3	Surface mount multi-layer ceramic chip capacitors <i>X7R</i> dielectric	100 nF	0603	C0603C104J5RACAUTO
C4, C8	2	Surface mount multi-layer ceramic chip capacitors X7R dielectric	470 nF	0805	C0805C474K5RACAUTO
R7,R8	2	Standard thick film chip resistors	$8.25 k\Omega$	1210	CRCW12108K25FKEA
R1-R3	3	Standard thick film chip resistors	$25 k\Omega$	1210	<i>ERJ — U</i> 14 <i>F</i> 2051 <i>U</i>
R10	1	Standard thick film chip resistors	$68 k\Omega$	0805	<i>ERJ — P</i> 06 <i>F</i> 6802 <i>V</i>
R4	1	Standard thick film chip resistors	$470 k\Omega$	0805	RCS0805470KJNEA
U1,U2	2	Transient voltage suppression diodes	400 W	DO-214AC	SMAJ33CA
D1,D2	2	General-purpose rectifiers	400 V	SMA	S1G
Q1	1	65 V, 100 mA NPN general-purpose transistors	65 V	SOT23	BC846
D3	1	Zener Voltage Regulators	5.6 V	SOT23	SZBZX84C5V6ET1G
U9 - U14	6	OLED device	-	-	-

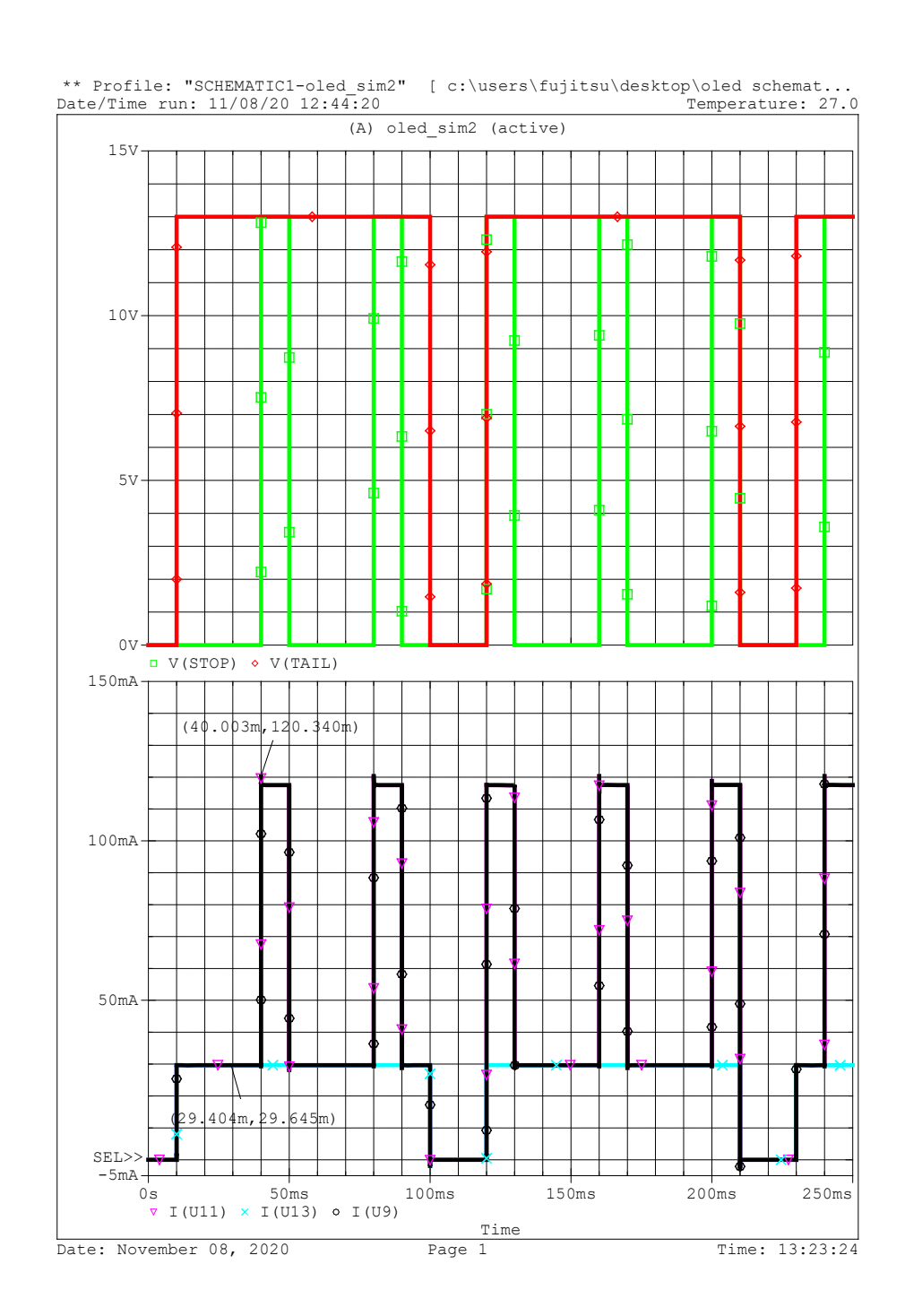


Figure 4.15 The simulation result of the application circuit

#### EFFECTS OF THE ELECTRICAL STRESS

This chapter is dedicated to the electrical stress effects. Degradation on the electrical and optical properties of the sample device are analyzed in this chapter.

### 5.1 Aging on Electrical and Optical Characteristics on the OLED

As mentioned earlier, when OLEDs are operating in harsh conditions some electrical and optical device properties degrade over operation time. The major type of degradation during operation, which can be observed quite easily is the decay of luminance.

Typically, integrated sphere and spectrometer have been used for the optical characterization of OLEDs. Figure 5.1 demonstrates the typical test setup for luminous degradation measurements. In this study, an alternative low-cost method based on CMOS camera and image processing has been used to observe the luinance degredation. The relative luminance data are taken over the OLED sample for 7040 hours and observed that it performs successfully.

The pixel intensity formulation in MPEG and JPEG algorithms according to ITU-R BT.601 standard is given in 5.1. The variables  $E_R$ ,  $E_G$ ,  $E_B$  in 5.1 represent red, green and blue components, respectively and  $E_Y$  is the luminance signal.

$$E_Y = \begin{bmatrix} 0.299 & 0.587 & 0.114 \end{bmatrix} \begin{bmatrix} E_R \\ E_G \\ E_B \end{bmatrix}$$
 (5.1)

Binarization and thresholding processes have been used to detect OLED's contour. Only the OLED part of the image is selected in the images taken from the CMOS camera. The brightness value of the pixels in the selected image is calculated and normalized for each image using the above formula. Using this method, an integrated

sphere is not required to measure the relative luminance. After the luminance values are normalized for 7040 - hours of data, the change in relative luminance is shown in the upper right corner of Figure 5.2.

The double-exponential model is used to describe the performance degradation of the OLED [122]. The luminance degradation is defined as:

$$l(t) = a \cdot e^{-\alpha_1 t} + b \cdot e^{-\alpha_2 t} \tag{5.2}$$

Where a=6.44, b=93.42 are the constants;  $\alpha_1=0.033$ ,  $\alpha_2=7.56\times 10^{-6}$  that present the initial and long-term degradation parameters according to time (t). The double-exponential model traces the experimental data accurately, as shown in Figure 5.2.

We have also observed that there is no deterioration in spectral shape during the test period. Dark spot degradation phenomena is not observed. These results show that



Figure 5.1 A typical light measurement equipment [121]

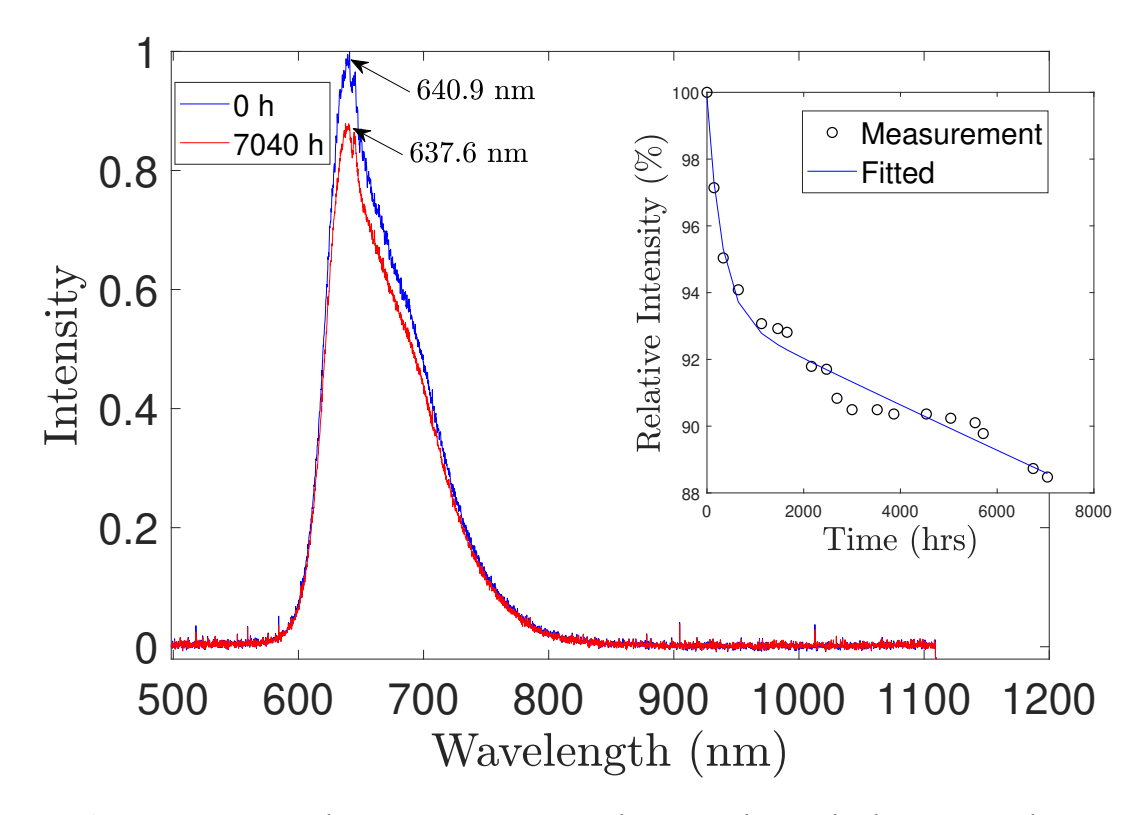
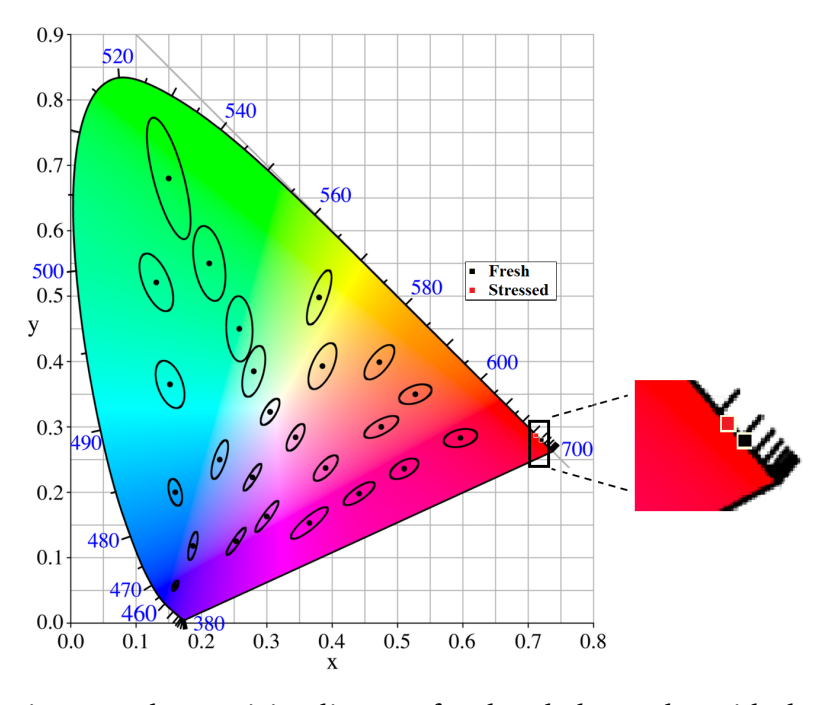


Figure 5.2 Spectral emission variation (the inset shows the luminance decay)



**Figure 5.3** Cie 1931 chromaticity diagram for the oled samples with the MacAdam ellipses (ten times magnified)

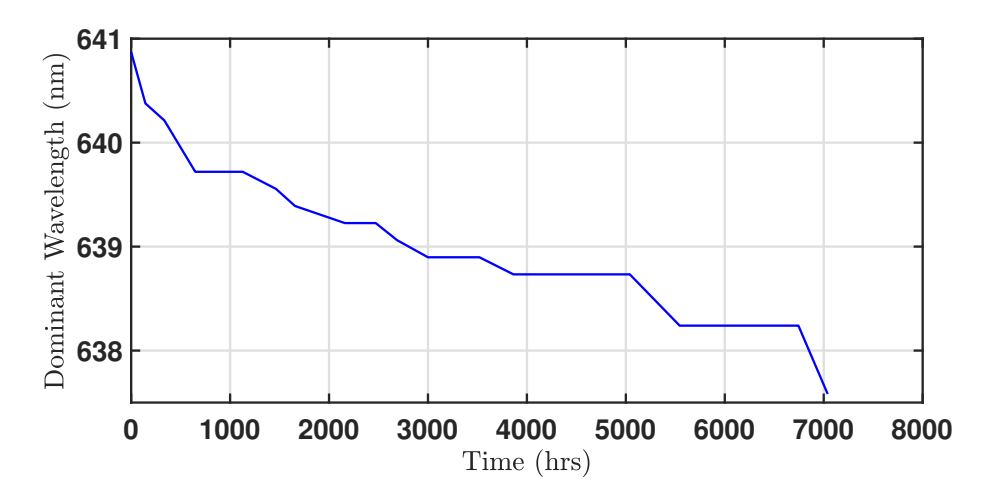


Figure 5.4 Dominant wavelength variation

the AEC-Q OLED sample used in accordance with the quality regulations required by the automotive industry has a higher quality level of encapsulation layer than other samples of industrial standards. We have mapped the wavelength shift of the stressed (x = 0.71, y = 0.29) sample, as opposed to the fresh sample (x = 0.72, y = 0.28) on the color gamut chart, as shown in the Figure 5.3. The observed shift is well within the MacAdam ellipses radii of  $\approx 5$  nm around red tones (right bottom corner of the gamut), which could not be differentiated by the human eye. When the dominant wavelength variation is examined, as shown in Figure 5.4, a subtle change is observed in the aged sample. We observe 3.29 nm shift in the dominant wavelength, which is still in the red color spectrum and will cause a slight color shift in the stop lamp. As shown in Figure 5.5, the impedance and phase characteristics show a significant change before and after stress.

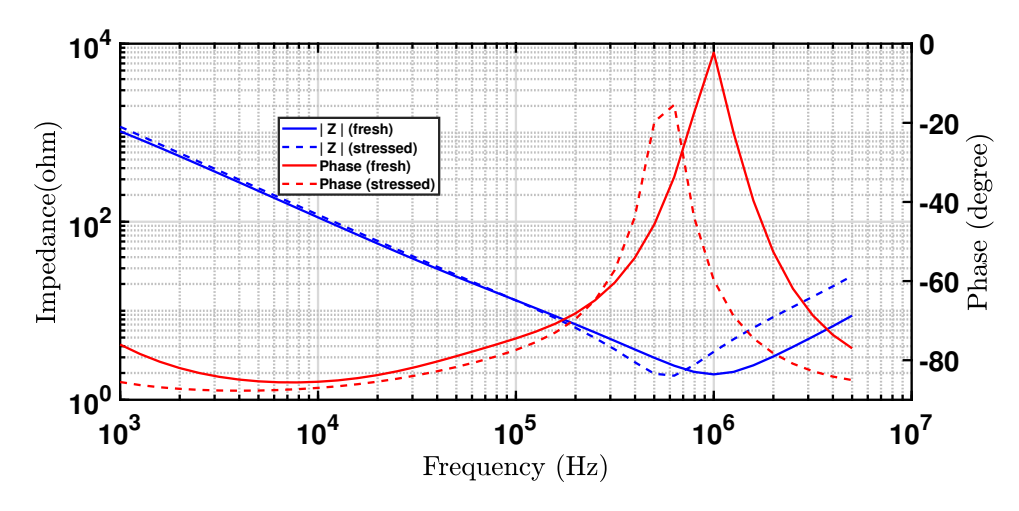


Figure 5.5 Impedance characteristic change before and after electrical stress

It is noted in Figure 5.5 that zero-bias capacitance values decrease from  $1.31 \times 10^{-7} \ F$  to  $1.29 \times 10^{-7} \ F$  (the accuracy:  $\pm 0.1\%$ ). On the contrary,  $R_{ITO} + R_P$  values increase from 73.37  $k\Omega$  to 75.17  $k\Omega$  (the accuracy:  $\pm 0.03\%$ ). The change is much clearer in the current-voltage characteristics versus time plot, as shown in Figure 5.6. With the effect of increasing OLED resistance, the threshold voltage shifts from 4.2 V to 5.25 V.

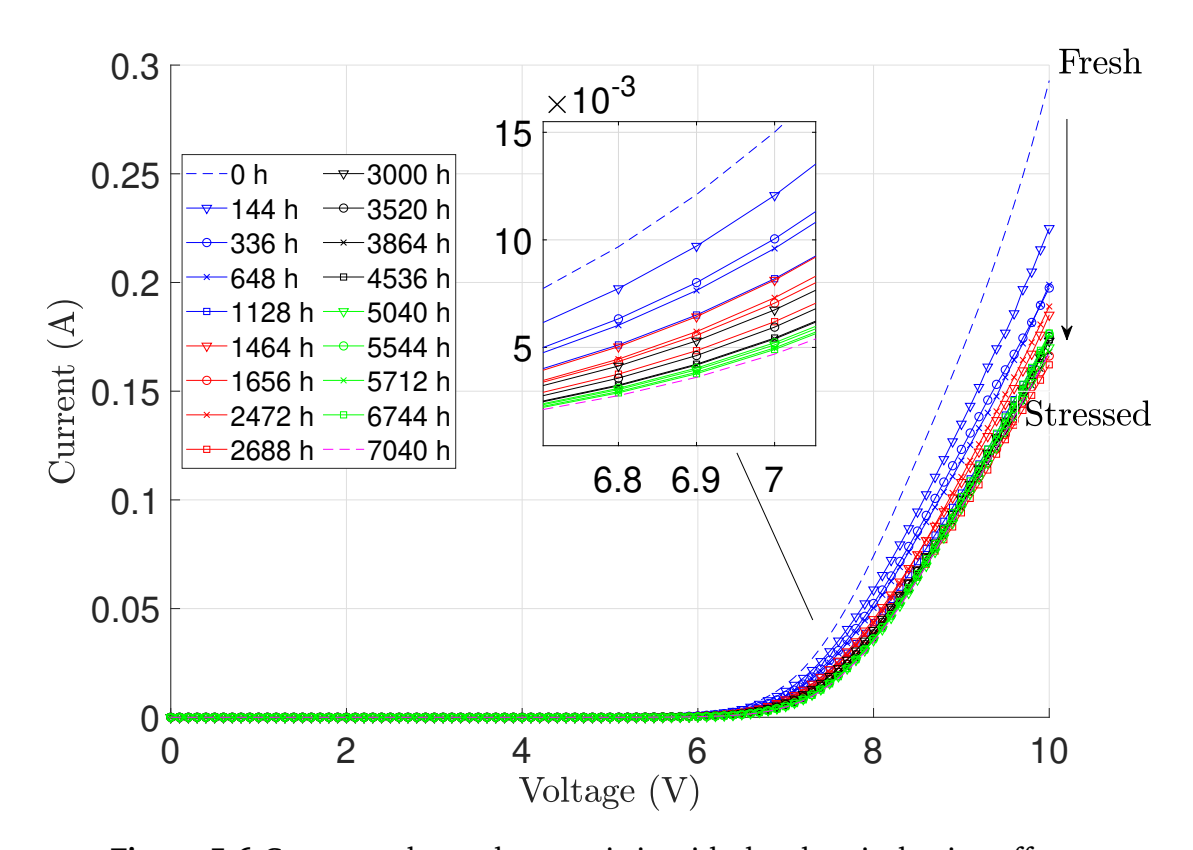


Figure 5.6 Current-voltage characteristic with the electrical aging effect

# RESULTS AND DISCUSSION

The recent development in OLEDs has brought new possibilities for the lighting industry. The automotive lighting market is one of the most attractive markets for OLEDs, and it is expected to be the next technological development after the LED technology. They are especially well suited for totally uniform, smooth illumination, and bendable, flexible luminous displays. At the moment, it is too expensive to apply this technology extensively. However, further development possibly allows the realization of extensive automotive lighting solutions with OLEDs in the long or medium term.

In the harsh environment of the automotive exterior lighting, the performance of OLEDs can be influenced by many factors. Therefore, the most important challenges for OLEDs in the automotive lighting system are lifetime and reliability. With the increasing demand for illumination flux for the automotive rear lighting system, electrical, optical, and thermal behaviors of OLEDs are crucial for the lifetime and reliability of the system. In order to design reliable circuits and predict the lifetime of OLEDs, accurate modeling and characterization of OLEDs are required. Many different types of OLED models may be found in the literature. Some models are analytical and not compatible with SPICE simulators [17, 19, 20]. Some SPICE compatible electrical OLED models take into account only the forward bias region, but do not include the reverse bias characteristic and dynamic capacitance behavior of the OLED [62, 118]. Some others include capacitance behavior as well but assuming that the OLED's intrinsic capacitance has a constant value and is not-voltage dependent which is not able to represent the device dynamics [27, 31, 33, 38, 40]. In a rear stop lamp, OLEDs are sometimes subject to reverse bias potentials. During maintenance or service, the battery of the vehicle is typically detached and reconnected. There is a probability of connecting the wires to the wrong terminals of the battery. In case of a reverse polarity condition, there could be significant damage to the electronic components. Due to automotive qualification requirements such as "ISO 16750-2:2010 Road vehicles-Environmental conditions and testing for electrical and electronic equipment Part 2:

Electrical loads", OLEDs must properly withstand the reverse voltage. The reverse bias characteristic of OLEDs is critical to be captured by an electrical model especially for the automotive applications even though the OLED does not emit light in that region. The reverse bias characteristic is not taken into account in any of these models.

In this thesis, a new SPICE compatible OLED model is proposed to fill this gap in the literature. Reasonable accuracy between the modeled and measured results is achieved. The proposed model not only simulates the forward characteristic of the OLED, but also the reverse characteristic and dynamic capacitive behavior have been successfully included in the model. This proposed model can be integrated into any SPICE simulator without any numerical difficulties. In order to validate the proposed model, an application circuit that realizes the position and stop functions for an OLED-based rear stop lamp has been designed, as a real-case scenario. For many automobiles, the same set of light sources illuminate both tail lights and stop lights. Thus, the light sources (LEDs or OLEDs) must operate at two different brightness levels. In the designed application circuit, six OLEDs are driven at 30 mA for the tail function, and when the stop signal is high (while breaking), the four OLED panels are driven at 120 mA.

We have further investigated the reliability of the OLED sample. During the usage of a vehicle life, the tail lamp is exposed to disruptive factors: electrical and mechanical stress, environmental effects such as humidity and temperature. In order to evaluate the OLED reliability, we apply the electrical stress on the AEC-Q OLED under an ambient condition of  $25^{\circ}C$  and 50%-60% humidity rate. The Illuminating Engineering Society's (IES) LM-80-08: Measuring Lumen Maintenance of LED Light Sources [IES 2008] requires that the chromaticity shift be measured throughout the test procedure, which must last a minimum of 6000 hours. The device is aged at a constant current of 125 mA for continuous operation of 7040 hours.

The main measure of aging throughout the lifetime of OLED devices is the luminance decay at a given bias voltage or current which is characterized by simple luminance measurement. However, such a simple measurement is not adequate to examine the degradation mechanism in OLED devices. Therefore, we have observed several optical and electrical characteristics including the current-voltage curves, spectral shape, chromatically coordinates, dominant wavelength, capacitance and complex impedance before and after the electrical stress. The optical properties of the OLED sample are characterized by a low-cost test setup with the aid of a CMOS camera, spectrometer, and optical lenses. An image processing-based algorithm has been developed to examine the relative light intensity. The degradation in the electrical properties of the OLED sample is observed by employing the impedance spectroscopy.

The luminance decay result shows that the curve does not fit the well-known stretched or exponential decay models meaning that the initial degradation rate is higher than the degradation rate in the mid or later states of operation. However, we have not observed a rapid luminance decline in the initial stages under constant electrical stress. Dark spot degradation phenomena is not observed. These results show that the AEC-Q OLED sample used in accordance with the quality regulations required by the automotive industry has a higher quality level of encapsulation layer than other samples of industrial standard. With constant current stress over 7000 - hours, luminance decay (12%), threshold voltage variation (1.05 V), and dominant wavelength shifting (3.29 nm) are observed. The chromaticity coordinates are shifted from (x = 0.72, y = 0.28) pairs to (x = 0.71, y = 0.29). We have also observed the shift is well within the MacAdam ellipses radii of  $\approx 5 nm$  around red tones, which could not be differentiated by the human eye.

The following changes in the complex impedance are noticed: the zero-bias capacitance value decreases from  $1.31 \times 10^{-7} \, F$  to  $1.29 \times 10^{-7} \, F$ . The OLED's resistance  $(R_{ITO} + R_P)$  value increases from  $73.37 \, k\Omega$  to  $75.17 \, k\Omega$ . Since the change in  $R_{ITO}$  is too small 5, 12  $\Omega$  before stress and 4.96  $\Omega$  after stress, the pure electrical stress has changed the recombination properties in the emissive layer of device. This change in the OLED's resistance causes a rightward shift in current-voltage characteristics. We also observe that the reverse voltage is not destructive to our OLED until the breakdown voltage at  $-32.2 \, V$  is reached, and the OLED can resume its operation once it is again forward biased. We have observed the hard breakdown characteristic at the breakdown voltage for the sample, this is irreversible and the device does not work any more. Furthermore, the pure electrical stress does not affect the spectral shape during the test period.

The basic contributions of the thesis and their significance for theory and practice can be summarized as follows:

- The OLED samples are electrically and optically characterized. In order to characterize and extract model parameters, a specific test setup developed.
- The proposed model smoothly provides the whole current-voltage relation (the forward and reverse characteristics), and also dynamic capacitive behaviour is included the model.
- The model is SPICE compatible and can be integrated into any SPICE simulator without any numerical difficulties.
- The suggested model has also been verified with the experimental outcomes.

The strong agreement between the theoretical and observed results have shown that the method used in this thesis provides adequate precision for the continuous, transient, and AC simulations needed to develop an OLED based schematics.

• We demonstrate that threshold voltage variation, dominant wavelength shifting, and luminance decay are observed with stress time whereas spectral shape were not affected by electrical stress.

Future research can focus on the aging model. With more OLED samples, statistical data can be collected by performing aging tests under different environmental conditions. The proposed model and aging results can be used by application engineers to accurately predict the electrical and luminous performance of OLED systems before manufacturing to save time and cost.

- [1] D. Vij, *Luminescence of solids*. Springer Science & Business Media, 2012.
- [2] D. R. Gamota, P. Brazis, K. Kalyanasundaram, J. Zhang, *Printed organic and molecular electronics*. Springer Science & Business Media, 2013.
- [3] C. W. Tang, S. A. VanSlyke, "Organic electroluminescent diodes," *Applied physics letters*, vol. 51, no. 12, pp. 913–915, 1987.
- [4] G. Lu, "Research on high-resolution color oled display technology," in 2010 International Conference on Optoelectronics and Image Processing, IEEE, vol. 2, 2010, pp. 233–235.
- [5] M. Zhao, H. Zhang, X. Chen, Y. Chen, C. J. Xue, "Online oled dynamic voltage scaling for video streaming applications on mobile devices," in *Proceedings of the Ninth IEEE/ACM/IFIP International Conference on Hardware/Software Codesign and System Synthesis*, IEEE Press, 2013, p. 9.
- [6] W. Hong, S. Lim, S. Ko, Y. G. Kim, "Oled-embedded antennas for 2.4 ghz wi-fi and bluetooth applications," in *2017 IEEE International Symposium on Antennas and Propagation & USNC/URSI National Radio Science Meeting*, IEEE, 2017, pp. 2551–2552.
- [7] H. Chen, Z. Xu, "Oled panel radiation pattern and its impact on vlc channel characteristics," *IEEE Photonics Journal*, vol. 10, no. 2, pp. 1–10, 2017.
- [8] F. So, J. Kido, P. Burrows, "Organic light-emitting devices for solid-state lighting," *MRS bulletin*, vol. 33, no. 7, pp. 663–669, 2008.
- [9] J. Y. Tan, P. J. Ker, K. Lau, M. Hannan, S. G. H. Tang, "Applications of photonics in agriculture sector: A review," *Molecules*, vol. 24, no. 10, p. 2025, 2019.
- [10] K. Akedo, A. Miura, H. Fujikawa, Y. Taga, "Flexible oleds for automobiles using sinx/cnx: H multi-layer barrier films and epoxy substrates," *Journal of Photopolymer Science and Technology*, vol. 19, no. 2, pp. 203–208, 2006.
- [11] A. Kraus, N. Benter, H. Boerner, "Oled technology and its possible use in automotive applications," SAE Technical Paper, Tech. Rep., 2007.
- [12] J. Chen, C. T. Liu, "Technology advances in flexible displays and substrates," *Ieee Access*, vol. 1, pp. 150–158, 2013.
- [13] V. C. Bender, N. D. Barth, F. B. Mendes, R. A. Pinto, J. M. Alonso, T. B. Marchesan, "Modeling and characterization of organic light-emitting diodes including capacitance effect," *IEEE Transactions on Electron Devices*, vol. 62, no. 10, pp. 3314–3321, 2015.
- [14] Huawei. (2019). "Huawei mate x, 5g smartphone, foldable design," [Online]. Available: https://consumer.huawei.com/en/phones/mate-x/(visited on 10/26/2019).

- [15] T. Pilgrim. (2019). "Oleds could boost vertical farm efficiency by 20 per cent," [Online]. Available: https://www.brunel.ac.uk/news-and-events/news/articles/OLEDs-could-boost-vertical-farm-efficiency-by-20-per-cent (visited on 10/26/2019).
- [16] LG. (2019). "Oled tvs: Ultra slim lg 4k oled tvs," [Online]. Available: https://www.lg.com/uk/oled-tvs (visited on 10/26/2019).
- [17] C. Pinot, H. Cloarec, J.-C. Martinez, T. Maindron, D. Vaufrey, C. Prat, H. Doyeux, G. Haas, Y. Bonnassieux, "P-157: Electrical modeling and numerical simulation of doped multilayer organic light-emitting diodes (oleds)," in *SID Symposium Digest of Technical Papers*, Wiley Online Library, vol. 38, 2007, pp. 792–795.
- [18] R. Yang, X. Cao, "Thermal and nonthermal factors affecting the lifetime of blue phosphorescent organic light-emitting diodes," *IEEE Transactions on electron devices*, vol. 65, no. 8, pp. 3300–3304, 2018.
- [19] L. Zhang, L. Wang, W.-J. Wu, M. Chan, "Modeling current–voltage characteristics of bilayer organic light-emitting diodes," *IEEE Transactions on Electron Devices*, vol. 66, no. 1, pp. 139–145, 2018.
- [20] E. Kollár, L. Pohl, A. Poppe, Z. Kohári, "Nonlinear electro-thermal and light output modeling and simulation of oleds," *Periodica Polytechnica Electrical Engineering and Computer Science*, vol. 58, no. 2, pp. 43–53, 2014.
- [21] P. D. Keir, "Fabrication and characterization of actfel devices," 1999.
- [22] Y. Chen, D. Krupka, "Limitation imposed by field clamping on the efficiency of high-field ac electroluminescence in thin films," *Journal of Applied Physics*, vol. 43, no. 10, pp. 4089–4096, 1972.
- [23] R. Liguori, A. Rubino, A. Botta, S. Pragliola, "Blue and white oleds with highly stereoregular polymers," in *2017 International Semiconductor Conference (CAS)*, IEEE, 2017, pp. 79–82.
- [24] J. S. Park, J. H. Seo, J. R. Koo, B. M. Seo, K. H. Lee, J. K. Park, S. S. Yoon, Y. K. Kim, "High-efficiency and color stable deep-blue organic light-emitting diodes," in *2010 3rd International Nanoelectronics Conference (INEC)*, IEEE, 2010, pp. 726–727.
- [25] K.-H. Seol, Y. I. Kim, S. Park, H. Nam, "Simultaneous emission ac-oled pixel circuit for extended lifetime of oled display," *IEEE Journal of the Electron Devices Society*, vol. 6, pp. 835–840, 2018.
- [26] S.-K. Hong, J.-H. Sim, I.-G. Seo, K.-C. Kim, S.-I. Bae, H.-Y. Lee, N.-Y. Lee, J. Jang, "New pixel design on emitting area for high resolution active-matrix organic light-emitting diode displays," *Journal of Display Technology*, vol. 6, no. 12, pp. 601–606, 2010.
- [27] J. P. Bender, "Spice modeling of actfel devices and oleds," M.S. thesis, Oregon State University, USA, 2000.
- [28] J.-H. Ahn, D.-H. Chung, S.-W. Hur, J.-U. Lee, M.-J. Song, W.-J. Lee, T.-W. Kim, "Equivalent-circuit analysis of organic light-emitting diodes using frequency-dependent response of *ito/alq\_3/al* device," in *Proceedings of the Korean Institute of Electrical and Electronic Material Engineers Conference*, 2004, pp. 5–8.

- [29] N. D. Barth, V. C. Bender, T. B. Marchesan, "An analysis of frequency response on oled for lighting applications," in *2017 IEEE Industry Applications Society Annual Meeting*, IEEE, 2017, pp. 1–5.
- [30] J. Kowal, D. Hente, D. U. Sauer, "Model parameterization of nonlinear devices using impedance spectroscopy," *IEEE Transactions on Instrumentation and Measurement*, vol. 58, no. 7, pp. 2343–2350, 2009.
- [31] B. Wei, K. Furukawa, J. Amagai, M. Ichikawa, T. Koyama, Y. Taniguchi, "A dynamic model for injection and transport of charge carriers in pulsed organic light-emitting diodes," *Semiconductor science and technology*, vol. 19, no. 5, p. L56, 2004.
- [32] J. C. Scott, P. J. Brock, J. R. Salem, S. Ramos, G. G. Malliaras, S. A. Carter, L. Bozano, "Charge transport processes in organic light-emitting devices," *Synthetic Metals*, vol. 111, pp. 289–293, 2000.
- [33] S. X. Zong, C. N. Li, C. H. Lv, G. H. Xie, Y. Zhao, S. Y. Liu, "Equivalent circuit model of top-emitting oled for the designing of oled-on-silicon microdisplay," in *Advanced Materials Research*, Trans Tech Publ, vol. 383, 2012, pp. 7037–7042.
- [34] J. Kanicki, S.-J. Lee, Y. Hong, C.-C. Su, "Optoelectronic properties of poly (fluorene) co-polymer light-emitting devices on a plastic substrate," *Journal of the Society for Information Display*, vol. 13, no. 12, pp. 993–1002, 2005.
- [35] J. Drechsel, M. Pfeiffer, X. Zhou, A. Nollau, K. Leo, "Organic mip-diodes by p-doping of amorphous wide-gap semiconductors: Cv and impedance spectroscopy," *Synthetic metals*, vol. 127, no. 1-3, pp. 201–205, 2002.
- [36] W.-Y. Wong, C.-L. Ho, "Functional metallophosphors for effective charge carrier injection/transport: New robust oled materials with emerging applications," *Journal of Materials Chemistry*, vol. 19, no. 26, pp. 4457–4482, 2009.
- [37] S. Nowy, W. Ren, A. Elschner, W. Lövenich, W. Brütting, "Impedance spectroscopy as a probe for the degradation of organic light-emitting diodes," *Journal of Applied Physics*, vol. 107, no. 5, p. 054501, 2010.
- [38] D. Buso, S. Bhosle, Y. Liu, M. Ternisien, C. Renaud, Y. Chen, "Oled electrical equivalent device for driver topology design," *IEEE Transactions on Industry Applications*, vol. 50, no. 2, pp. 1459–1468, 2013.
- [39] S. Nowy, W. Ren, J. Wagner, J. A. Weber, W. Brütting, "Impedance spectroscopy of organic hetero-layer oleds as a probe for charge carrier injection and device degradation," in *Organic Light Emitting Materials and Devices XIII*, International Society for Optics and Photonics, vol. 7415, 2009, 74150G.
- [40] A. Alchaddoud, G. Ibrahem, L. Canale, G. Zissis, "Impedance spectroscopy and evolution of the equivalent electrical circuit model for large area organic light emitting diodes aged under stress," in 2018 IEEE International Conference on Environment and Electrical Engineering and 2018 IEEE Industrial and Commercial Power Systems Europe (EEEIC/I&CPS Europe), IEEE, 2018, pp. 1–4.

- [41] P. Chulkin, O. Vybornyi, M. Lapkowski, P. Skabara, P. Data, "Impedance spectroscopy of oleds as a tool for estimating mobility and the concentration of charge carriers in transport layers," *Journal of Materials Chemistry C*, vol. 6, no. 5, pp. 1008–1014, 2018.
- [42] S. Nowy, "Understanding losses in oleds: Optical device simulation and electrical characterization using impedance spectroscopy," *Inst. Phys., Univ. Augsburg*, 2010.
- [43] G. W. Lee, H. Kim, J. Park, J.-I. Shim, D.-S. Shin, "Investigation of luminance degradation in organic light-emitting diodes by impedance spectroscopy," *IEEE Photonics Technology Letters*, vol. 30, no. 13, pp. 1183–1185, 2018.
- [44] A. Poppe, L. Pohl, E. Kollr, Z. Kohári, H. Lifka, C. Tanase, "Methodology for thermal and electrical characterization of large area oleds," in *2009 25th Annual IEEE Semiconductor Thermal Measurement and Management Symposium*, IEEE, 2009, pp. 38–44.
- [45] A. Cester, D. Bari, J. Framarin, N. Wrachien, G. Meneghesso, S. Xia, V. Adamovich, J. Brown, "Thermal and electrical stress effects of electrical and optical characteristics of alq3/npd oled," *Microelectronics Reliability*, vol. 50, no. 9-11, pp. 1866–1870, 2010.
- [46] R. Fan, X. Zhang, Z. Tu, "Influence of ambient temperature on oled lifetime and uniformity based on modified equivalent lifetime detection," *Journal of the Society for Information Display*, vol. 27, no. 10, pp. 597–607, 2019.
- [47] R.-L. Lin, J.-Y. Tsai, D. Buso, G. Zissis, "Oled equivalent circuit model with temperature coefficient and intrinsic capacitor," *IEEE Transactions on Industry Applications*, vol. 52, no. 1, pp. 493–501, 2015.
- [48] H.-T. Chen, W. C. Choy, S. Hui, "Characterization, modeling, and analysis of organic light-emitting diodes with different structures," *IEEE transactions on power electronics*, vol. 31, no. 1, pp. 581–592, 2015.
- [49] V. C. Bender, N. D. Barth, R. A. Pinto, J. M. Alonso, T. B. Marchesan, "Scale-photo-electro-thermal model for organic light-emitting diodes," *IET Optoelectronics*, vol. 10, no. 3, pp. 100–110, 2016.
- [50] H. Pang, L. Michalski, M. S. Weaver, R. Ma, J. J. Brown, "Thermal behavior and indirect life test of large-area oled lighting panels," *Journal of Solid State Lighting*, vol. 1, no. 1, p. 7, 2014.
- [51] E. F. Schubert, T. Gessmann, J. K. Kim, "Light emitting diodes," *Kirk-Othmer Encyclopedia of Chemical Technology*, 2000.
- [52] F. Salameh, A. Al Haddad, A. Picot, L. Canale, G. Zissis, M. Chabert, P. Maussion, "Modeling the luminance degradation of oleds using design of experiments," *IEEE Transactions on Industry Applications*, vol. 55, no. 6, pp. 6548–6558, 2019.
- [53] A. Güney, M. B. Yelten, O. Ferhanoğlu, N. Kahraman, "Experimental and modeling studies of automotive-qualified oleds under electrical stress," *Microelectronics Reliability*, vol. 111, p. 113 704, 2020.
- [54] H. Kim, H. Shin, J. Park, Y. Choi, J. Park, "Statistical modeling and reliability prediction for transient luminance degradation of flexible oleds," in *2018 IEEE International Reliability Physics Symposium (IRPS)*, IEEE, 2018, pp. 3C–7.

- [55] M. E. Miller, J. Gerhardt, H. Yoo, T. Akhavan, "Model for assessing organic light-emitting diode display lifetime across applications," *Journal of the Society for Information Display*, vol. 28, no. 7, pp. 629–640, 2020.
- [56] K. Choi, J. Lee, J. Park, "Nonlinear mixed model and reliability prediction for oled luminance degradation," in 2019 IEEE International Reliability Physics Symposium (IRPS), IEEE, 2019, pp. 1–4.
- [57] R. Fan, X. Zhang, Z. Tu, "Luminance compensation and optimization to delay oled degradation based on equivalent lifetime detection," *IEEE Journal of the Electron Devices Society*, vol. 8, pp. 626–634, 2020.
- [58] M. Ishii, "Luminance decay mechanisms in organic light-emitting diodes," *R&D Rev. Toyota CRDL*, vol. 38, pp. 55–60, 2003.
- [59] J. Zhang, W. Li, G. Cheng, X. Chen, H. Wu, M.-H. H. Shen, "Life prediction of oled for constant-stress accelerated degradation tests using luminance decaying model," *Journal of Luminescence*, vol. 154, pp. 491–495, 2014.
- [60] C. Féry, B. Racine, D. Vaufrey, H. Doyeux, S. Cinà, "Physical mechanism responsible for the stretched exponential decay behavior of aging organic light-emitting diodes," *Applied Physics Letters*, vol. 87, no. 21, p. 213502, 2005.
- [61] C. Pinot, "Modélisation des diodes électroluminescentes organiques multicouches dopées. application à de nouvelles architectures.," Ph.D. dissertation, Ecole Polytechnique, 2008.
- [62] Y. Li, J.-W. Lee, B.-S. Lee, C.-S. Lu, W.-H. Chen, "A novel spice compatible current model for oled circuit simulation," in *Technical Proceedings of the 2005 NSTI Nanotechnology Conference and Trade Show*, vol. 3, 2005, pp. 103–106.
- [63] A. De Almeida, B. Santos, B. Paolo, M. Quicheron, "Solid state lighting review–potential and challenges in europe," *Renewable and Sustainable Energy Reviews*, vol. 34, pp. 30–48, 2014.
- [64] R. Pode, "Organic light emitting diode devices: An energy efficient solid state lighting for applications," *Renewable and Sustainable Energy Reviews*, vol. 133, p. 110 043, 2020.
- [65] H. J. Round, "Light-emitting diodes hit the centenary milestone," *World*, vol. 19, p. 309, 1907.
- [66] I. L. Azevedo, M. G. Morgan, F. Morgan, "The transition to solid-state lighting," *Proceedings of the IEEE*, vol. 97, no. 3, pp. 481–510, 2009.
- [67] J. Spindler, M. Kondakova, M. Boroson, M. Büchel, J. Eser, J. Knipping, "84-1: Invited paper: Advances in high efficacy and flexible oled lighting," in *SID Symposium Digest of Technical Papers*, Wiley Online Library, vol. 49, 2018, pp. 1135–1138.
- [68] P. Destruel, P. Jolinat, R. Clergereaux, J. Farenc, "Pressure dependence of electrical and optical characteristics of alq 3 based organic electroluminescent diodes," *Journal of applied physics*, vol. 85, no. 1, pp. 397–400, 1999.
- [69] H. Uoyama, K. Goushi, K. Shizu, H. Nomura, C. Adachi, "Highly efficient organic light-emitting diodes from delayed fluorescence," *Nature*, vol. 492, no. 7428, pp. 234–238, 2012.

- [70] J. D. Myers, J. Xue, "Organic semiconductors and their applications in photovoltaic devices," *Polymer Reviews*, vol. 52, no. 1, pp. 1–37, 2012.
- [71] H. Matsui, Y. Takeda, S. Tokito, "Flexible and printed organic transistors: From materials to integrated circuits," *Organic Electronics*, vol. 75, p. 105 432, 2019.
- [72] D. A. Bernards, R. M. Owens, G. G. Malliaras, "Organic semiconductors in sensor applications," 2008.
- [73] M. Guan, L. Li, G. Cao, Y. Zhang, B. Wang, X. Chu, Z. Zhu, Y. Zeng, "Organic light-emitting diodes with integrated inorganic photo detector for near-infrared optical up-conversion," *Organic Electronics*, vol. 12, no. 12, pp. 2090–2094, 2011.
- [74] Y. Yu, Q. Ma, H. Ling, W. Li, R. Ju, L. Bian, N. Shi, Y. Qian, M. Yi, L. Xie, *et al.*, "Small-molecule-based organic field-effect transistor for nonvolatile memory and artificial synapse," *Advanced Functional Materials*, vol. 29, no. 50, p. 1904 602, 2019.
- [75] S. Chemical. (2020). "Sumitomo chemical's polymer oled lighting." Accessed: 2020-08-07, [Online]. Available: https://www.sumitomo-chem.co.jp/english/pled/about/.
- [76] Cal-OS. (2020). "California organic semiconductors inc." Accessed: 2020-08-07, [Online]. Available: http://www.cal-os.com/.
- [77] R. Young, "Oleds expected to gain ground as lcd investment slows," *Information Display*, vol. 35, no. 3, pp. 24–29, 2019.
- [78] A. Alchaddoud, L. Canale, G. Ibrahem, G. Zissis, "Photometric and electrical characterizations of large-area oleds aged under thermal and electrical stresses," *IEEE Transactions on Industry Applications*, vol. 55, no. 1, pp. 991–995, 2018.
- [79] E. Cantatore, "Applications of organic and printed electronics," *A Technology-Enabled Revolution, Springer*, 2013.
- [80] M.-G. Song, K.-S. Kim, H. I. Yang, S. K. Kim, J.-H. Kim, C.-W. Han, H.-C. Choi, R. Pode, J. H. Kwon, "Highly reliable and transparent al doped ag cathode fabricated using thermal evaporation for transparent oled applications," *Organic Electronics*, vol. 76, p. 105 418, 2020.
- [81] I. Lee, S. Kim, J. Y. Park, S. Kim, H. W. Cho, J. Ham, S. Gim, K. Kim, K. Hong, J.-L. Lee, "Symmetrical emission transparent organic light-emitting diodes with ultrathin ag electrodes," *IEEE Photonics Journal*, vol. 10, no. 3, pp. 1–10, 2018.
- [82] H. Yersin, "Triplet emitters for oled applications. mechanisms of exciton trapping and control of emission properties," in *Transition metal and rare earth compounds*, Springer, 2004, pp. 1–26.
- [83] D. D. S. Pereira, A. P. Monkman, "Methods of analysis of organic light emitting diodes," *Display and Imaging*, vol. 2, pp. 323–337, 2017.
- [84] M. Koden, *OLED displays and lighting*. John Wiley & Sons, 2016.

- [85] H. Soofi, M. Jabbari, "Efficiency enhancement in thermally activated delayed fluorescence organic light-emitting devices by controlling the doping concentration in the emissive layer," *IEEE Transactions on Electron Devices*, vol. 66, no. 8, pp. 3425–3432, 2019.
- [86] H. W. Bae, G. W. Kim, R. Lampande, J. H. Park, I. J. Ko, H. J. Yu, C. Y. Lee, J. H. Kwon, "Efficiency enhancement in fluorescent deep-blue oleds by boosting singlet exciton generation through triplet fusion and charge recombination rate," *Organic Electronics*, vol. 70, pp. 1–6, 2019.
- [87] M. Schaer, F. Nüesch, D. Berner, W. Leo, L. Zuppiroli, "Water vapor and oxygen degradation mechanisms in organic light emitting diodes," *Advanced Functional Materials*, vol. 11, no. 2, pp. 116–121, 2001.
- [88] P. Tyagi, R. Srivastava, L. I. Giri, S. Tuli, C. Lee, "Degradation of organic light emitting diode: Heat related issues and solutions," *Synthetic Metals*, vol. 216, pp. 40–50, 2016.
- [89] H. Heil, G. Andress, R. Schmechel, H. Von Seggern, J. Steiger, K. Bonrad, R. Sprengard, "Sunlight stability of organic light-emitting diodes," *Journal of applied physics*, vol. 97, no. 12, p. 124501, 2005.
- [90] S. Stolz, Y. Zhang, U. Lemmer, G. Hernandez-Sosa, H. Aziz, "Degradation mechanisms in organic light-emitting diodes with polyethylenimine as a solution-processed electron injection layer," *ACS applied materials & interfaces*, vol. 9, no. 3, pp. 2776–2785, 2017.
- [91] H. Aziz, Z. D. Popovic, N.-X. Hu, A.-M. Hor, G. Xu, "Degradation mechanism of small molecule-based organic light-emitting devices," *Science*, vol. 283, no. 5409, pp. 1900–1902, 1999.
- [92] S. F. Lim, W. Wang, S. J. Chua, "Understanding dark spot formation and growth in organic light-emitting devices by controlling pinhole size and shape," *Advanced Functional Materials*, vol. 12, no. 8, pp. 513–518, 2002.
- [93] R. Phatak, T. Tsui, H. Aziz, "Dependence of dark spot growth on cathode/organic interfacial adhesion in organic light emitting devices," *Journal of Applied Physics*, vol. 111, no. 5, p. 054512, 2012.
- [94] L. Ke, S.-J. Chua, K. Zhang, N. Yakovlev, "Degradation and failure of organic light-emitting devices," *Applied Physics Letters*, vol. 80, no. 12, pp. 2195–2197, 2002.
- [95] Z. D. Popovic, H. Aziz, "Reliability and degradation of small molecule-based organic light-emitting devices (oleds)," *IEEE Journal of selected topics in quantum electronics*, vol. 8, no. 2, pp. 362–371, 2002.
- [96] Y. Wang, J. M. Alonso, X. Ruan, "A review of led drivers and related technologies," *IEEE Transactions on industrial electronics*, vol. 64, no. 7, pp. 5754–5765, 2017.
- [97] W. Thomas, "Oled lighting in automotive applications," in *Solid-State Lighting*, Optical Society of America, 2016, SSW3C–2.
- [98] "Color Specification," SAE-Society of Automotive Engineers, Warrendale, PA, USA, Standard, Feb. 2019.

- [99] "LED Light Sources Tests and Requirements," SAE-Society of Automotive Engineers, Warrendale, PA, USA, Standard, Sep. 2017.
- [100] B. Schoettle, M. Sivak, Y. Fujiyama, "Leds and power consumption of exterior automotive lighting: Implications for gasoline and electric vehicles," 2008.
- [101] V. Vollmer M.; Schwegler, "The world's first serial oled tail lamp as a milestone for developing a brilliant future of automotive lamps," *Vehicle and Infrastructure Safety Improvement in Adverse Conditions and Night Driving (Vision)*, vol. 4, no. 1, 2016.
- [102] T. Trojak, N. Guebel, "The oled technology: Possibilities, advantages, challenges," *Vehicle and Infrastructure Safety Improvement in Adverse Conditions and Night Driving (Vision), Paris*, 2014.
- [103] Y. Developpement, "Automotive lighting: Technology, industry and market trends," Tech. Rep., 2018.
- [104] Mercedes. (2019). "Oled tech for revamped mercedes s-class coupe and cabrio," [Online]. Available: https://mercedesblog.com/oled-tech-for-revamped-mercedes-s-class-coupe-and-cabrio/ (visited on 10/17/2019).
- [105] M. Kruppa, W. Thomas, W. Huhn, "An oled taillight revolution: From point light sources to segmented area light sources," *Information Display*, vol. 35, no. 4, pp. 14–18, 2019.
- [106] Audi. (2019). "Audi tt rs coupé and roadster matrix oled technology," [Online]. Available: https://www.audi-technology-portal.de/en/electrics-electronics/lighting-technology/audi-tt-rs-coupe-and-roadster-matrix-oled-technology (visited on 10/17/2019).
- [107] A. Pollock, H. Pollock, C. Pollock, "High efficiency led power supply," *IEEE Journal of Emerging and Selected Topics in Power Electronics*, vol. 3, no. 3, pp. 617–623, 2015.
- [108] Osram. (2019). "User guideline for operation of oleds with electronic driver systems." Accessed: 2019-09-07, [Online]. Available: https://www.osram.com/media/resource/HIRES/503914/606738/anleitung-ansteuerung-oled-gb.pdf.
- [109] J. Jacobs, D. Hente, E. Waffenschmidt, "Drivers for oleds," in *2007 IEEE Industry Applications Annual Meeting*, IEEE, 2007, pp. 1147–1152.
- [110] F. Palaiogiannis, "Gan enabled oled driver for automotive lighting application," M.S. thesis, Dept. Electrical Sustainable Energy., Delft Univ., Netherlands, 2015.
- [111] J. Bielecki, A. S. Jwania, F. El Khatib, T. Poorman, "Thermal considerations for led components in an automotive lamp," in *Twenty-Third Annual IEEE Semiconductor Thermal Measurement and Management Symposium*, IEEE, 2007, pp. 37–43.
- [112] G. Elger, H. Willwohl, J. Schug, "Thermal analysis of high power led subassemblies for automotive front light application," in *2012 4th Electronic System-Integration Technology Conference*, IEEE, 2012, pp. 1–8.

- [113] "Road vehicles Environmental conditions and testing for electrical and electronic equipment Part 2: Electrical loads," ISO-International Organization for Standardization, International Organization for Standardization ISO Central Secretariat, Geneva, Switzerland, Standard, Nov. 2012.
- [114] S. Sato, M. Takada, D. Kawate, M. Takata, H. Naito, "Negative capacitance of bilayer organic light-emitting diodes—its correlation with current efficiency and device lifetime," *Japanese Journal of Applied Physics*, vol. 58, no. SF, SFFA01, 2019.
- [115] J. Bisquert, G. Garcia-Belmonte, Á. Pitarch, H. J. Bolink, "Negative capacitance caused by electron injection through interfacial states in organic light-emitting diodes," *Chemical Physics Letters*, vol. 422, no. 1-3, pp. 184–191, 2006.
- [116] P. Antognetti, G. Massobrio, Semiconductor device modeling with SPICE. McGraw-Hill, Inc., 1990.
- [117] L. Zhang, H. Nakanotani, C. Adachi, "Capacitance-voltage characteristics of a 4, 4-bis [(n-carbazole) styryl] biphenyl based organic light-emitting diode: Implications for characteristic times and their distribution," *Applied Physics Letters*, vol. 103, no. 9, 162–1, 2013.
- [118] S.-G. Lee, R. Hattori, "Physics-based oled analog behavior modeling," *Journal of Information Display*, vol. 10, no. 3, pp. 101–106, 2009.
- [119] Z. Bohua, H. Ran, B. Jianhui, L. Yinxue, W. Yiqi, M. Fei, X. Guohua, Z. Zhensong, D. Huan, L. Jiajun, *et al.*, "A new oled spice model for pixel circuit simulation in oled-on-silicon microdisplay design," *Journal of Semiconductors*, vol. 33, no. 7, p. 075 007, 2012.
- [120] *3 channel high-side current source*, TLD2314EL, Rev. 1.2, Infineon Technologies AG, Apr. 2018.
- [121] I. S. O. M. GmbH. (2020). "Precise characterization of ssl light sources and leds in the lab and production." Accessed: 2020-09-07, [Online]. Available: https://www.instrumentsystems.com/en/systems/led-ssl-measurement/.
- [122] D. W. Kim, H. Oh, B. D. Youn, D. Kwon, "Bivariate lifetime model for organic light-emitting diodes," *IEEE Transactions on Industrial Electronics*, vol. 64, no. 3, pp. 2325–2334, 2016.

## **PUBLICATIONS FROM THE THESIS**

Contact Information: arda.guney@tubitak.gov.tr

## **Papers**

1. A. Güney, M. B. Yelten, O. Ferhanoğlu, N. Kahraman, "Experimental and modeling studies of automotive-qualified oleds under electrical stress," Microelectronics Reliability, vol. 111, p. 113 704, 2020